

# **Role of chromatin and DNA Damage repair pathway in Glioblastoma Multiforme**

**By**

**EKJOT KAUR**

**LIFE09201104002**

**TATA MEMORIAL CENTRE**

**MUMBAI**

*A thesis submitted to the*

*Board of Studies in Life Sciences in partial fulfilment of requirements for the Degree of*

**DOCTOR OF PHILOSOPHY**

**of**

**HOMI BHABHA NATIONAL INSTITUTE**



**February, 2017**

**Homi Bhabha National Institute**  
**Recommendations of the Viva Voce Committee**

As members of the Viva Voce Committee, we certify that we have read the dissertation prepared by Ms. Ekjot Kaur entitled "Role of chromatin and DNA damage repair pathway in Glioblastoma Multiforme" and recommend that it may be accepted as fulfilling the thesis requirement for the award of Degree of Doctor of Philosophy.

-----  
Chairman – Dr. Neelam Shirsat *Shirsat* Date: *23/2/17*

-----  
Guide/Convener – Dr. Shilpee Dutt *Shilpee Dutt* Date: *23/2/17*

-----  
Member 1 – Dr. Sanjay Gupta *Sanjay* Date: *23/2/17*

-----  
Member 2 – Dr. Prasanna Venkatraman *V. Prasanna* Date: *23/2/17*

-----  
Technical Advisor – Dr. Amit Dutt *A. Dutt* Date: *23/2/17*

-----  
Invitee – Dr. Anjali Shiras *Shiras* Date: *23/02/2017*

-----  
External Examiner – Dr. Mayurika Lahiri *Mayurika Lahiri* Date: *23<sup>rd</sup> February 2017*

Final approval and acceptance of this thesis is contingent upon the candidate's submission of the final copies of the thesis to HBNI.

I hereby certify that I have read this thesis prepared under my direction and recommend that it may be accepted as fulfilling the thesis requirement.

Date: *23/2/17*  
Place: Navi Mumbai

*Shilpee Dutt*  
*23/2/17*  
Dr. Shilpee Dutt  
Guide

## STATEMENT BY AUTHOR

This dissertation has been submitted in partial fulfilment of requirements for an advanced degree at Homi Bhabha National Institute (HBNI) and is deposited in the Library to be made available to borrowers under rules of the HBNI.

Brief quotations from this dissertation are allowable without special permission, provided that accurate acknowledgement of source is made. Requests for permission for extended quotation from or reproduction of this manuscript in whole or in part may be granted by the Competent Authority of HBNI when in his or her judgment the proposed use of the material is in the interests of scholarship. In all other instances, however, permission must be obtained from the author.



Navi Mumbai

Ekjot Kaur

Date: 23.2.2017

# DECLARATION

I, hereby declare that the investigation presented in the thesis has been carried out by me.

This work is original and has not been submitted earlier as a whole or in part for a degree / diploma at this or any other Institution / University.

Navi Mumbai



Date: 23.2.17

Ekjot Kaur

## List of Publications arising from the thesis

### Journals:

1. “Radiation-induced homotypic cell fusions of innately resistant glioblastoma cells mediate their sustained survival and recurrence”. **Kaur E**, Rajendra J, Jadhav S, Sridhar E, Goda JS, Moiyadi A and Dutt S. *Carcinogenesis*, **2015** Jun; 36(6):685-95. doi: 10.1093/carcin/bgv050.
2. “Unique spectral markers discern recurrent Glioblastoma cells from heterogeneous parent population”. **Kaur E**, Sahu A, Hole A, Rajendra J, Chaubal R, Gardi N, Dutt A, Moiyadi A, Krishna CM and Dutt S. *Sci Rep.*, **2016** May; 6, 26538. doi: 10.1038/srep26538 (2016).

### Chapters in books and lectures notes: NA

### Conferences:

- **Ekjot Kaur**, Gauri Patade, Sneha Berry and Shilpee Dutt. “Surviving Genotoxic Stress” **poster presentation** at “at XXXVI All India Cell Biology Conference -2012 and International Symposium on SARGI: 17-19th November, **2012**, Mumbai, India.
- **Ekjot Kaur**, Shailesh Jadhav, Sneha Berry, Gauri Patade and Shilpee Dutt “Polyploidy: a survival mechanism against ionizing radiation in Glioblastoma”. **Poster presentation** at “32nd Convention of Indian Association for Cancer Research Emerging Trends in Cancer research: Road to prevention & cure & International Symposium on: Infection and Cancer” (IACR-2013- February 13 -16 **2013**) under **Shri Rambhau Kulkarni and Shri Rajnikant Baxi award category**, New Delhi, India.
- **Ekjot Kaur**, Jacinth Rajendra, Shailesh Jadhav, Gauri Patade and Shilpee Dutt “Multinucleated giant cells formed by cell - cell fusion post radiation are cause of resistance and relapse in Glioblastoma”. **Oral presentation award** under Shri Sitaram Joglekar category at “33rd Annual Convention of Indian Association for Cancer Research (IACR)” 13-15,2014 February, **2014**, Kerala, India.
- **Ekjot Kaur**, Shailesh Jadhav, Aliasgar Moiyadi, Jayant S Goda and Shilpee Dutt “Radiation induced homotypic cell fusions of resistant cells form multinucleated giant cells: cause of sustained survival and recurrence in glioblastoma” **platform presentation** at “ISNOCON2015, Kochi” 26th-28th March **2015**, Kochi, India.
- **Ekjot Kaur** Jacinth Rajendra, Sanket Shah, Jyothi Nair, Ankit Khushwaha, Aliasgar Moiyadi, Shilpee Dutt, “Radiation induced Multinucleated Giant Cells: a novel therapeutic target to prevent survival and relapse of Glioblastoma” **poster presentation** during 106th Annual Meeting of American Association for Cancer Research (AACR-**2015**, April 18-22) in Philadelphia, PA, USA.

- **Ekjot Kaur**, Jyothi Nair, Ankit Kushwaha, Akshat Shetty, Anurag Srivastava, Aliasgar Moiyadi , Shilpee Dutt “A novel mechanism of homotypic cell fusion promote formation of Glioma resistance cells facilitated by NHEJ driven repair” **Selected amongst top 12 abstracts for oral presentaion** at 75<sup>th</sup> Tata Memorial Centre Platinum Jubilee Conference, 26-28th Feb **2016**, Mumbai, India.

### **Others:**

1. “Clinical implications of MTA proteins in human cancer”. **Kaur E**, Gupta S, Dutt S. *Cancer Metastasis Rev.*, **2014** Dec;33(4):1017-24. doi: 10.1007/s10555-014-9527-z.
2. “Notch Pathway Activation is Essential for Maintenance of Stem-like Cells in Early Tongue Cancer”. Upadhyay P, Nair S, **Kaur E**, Aich J, Dani P, Setunath V, Gardi N, Chandrani P, Godbole M, Sonawane K, Kanan S, Agarwal B, Kane S, Gupta S, Dutt S, and Dutt A. *Oncotarget*, **2016** July. doi: 10.18632/oncotarget.10419.

Navi Mumbai

Date: 23.2.17



Ekjot Kaur

*To my lovely family.....*

# ACKNOWLEDGEMENTS

It is aptly said that “*a shared journey lights the way*” and thus, I would like to take this opportunity to thank all the people who embarked on this journey of constant challenges with me and made it a cherishable one.

First and foremost, I would be like to express my deepest gratitude to my mentor Dr. Shilpee Dutt for her constant guidance and motivation throughout my stint as a graduate student. I appreciate for all her enthusiastic discussions that made my Ph.D. experience more productive and stimulating. Her invaluable support over these five years not only related to research but also academically and emotionally, has allowed me to grow as a research scientist.

The excellent research infrastructure at ACTREC provided a very conducive environment for my research work for which I would like to sincerely thank Dr. Rajiv Sarin (Ex-Director, ACTREC), Dr. Surekha Zingde (Ex-Deputy Director, ACTREC) and Dr. S.V. Chiplunkar (Director, ACTREC). I would also like to thank Department of Biotechnology (DBT) for funding the project and ACTREC for my fellowship. I am also grateful to the Homi Bhabha National Institute (HBNI) and Tata Memorial Centre (TMC) for proving me with the financial assistance to present my work at an international platform.

I would like to extend my gratitude to my thesis committee members: Dr. Neelam Shirsat (Chairperson, ACTREC), Dr. Sanjay Gupta (ACTREC), Dr. Prasanna Venkatraman (ACTREC), Dr. Anjali Shiras (Invitee, NCCS) and also to my ex-Chairperson Dr. G.B. Maru for their critical and insightful comments.

I would also express my special appreciation to Dr. Amit Dutt (Technical Advisor, ACTREC) for his advice and precious support throughout my thesis that incited me to widen my research from various perspectives. The several interactions I had with him during laboratory meetings as well as other laboratory events have helped me in opening up my horizon of thoughts as a researcher.

I am grateful to all my clinical collaborators Dr. Alisgar Moiyadi (ACTREC), Dr. Epari Sridhar (ACTREC) and Dr. Prakash Shetty (ACTREC) for providing us with the GBM tumour samples and the histological diagnosis. I am thankful to Dr. Jayant Sastri Goda (ACTREC) for his immense support in getting the patient clinical details and follow-up data. I would especially like to thank Dr. Rakesh Jalali (Tata Memorial Hospital) for his continuous encouragement for me to present my work at various conferences and his enthusiasm towards my work. I wish to thank Dr. Murali Chilakapati (ACTREC) who allowed to explore and understand the Raman spectroscopic technique helping to me to add another feather in my cap. During my work, I was also provided with the opportunity of working with an eminent and charismatic scientist Professor Indraneel Mitra (ACTREC) whose approach towards science has been highly motivating. I am thankful to Dr. Sagar Sengupta (NII) for providing us with the RPA32 antibody for our important experiments.

I am extremely grateful to all the patients for agreeing to be a part of this study and making it possible.

I would like to thank Mr. Dandekar for his proficient assistance in the common instrument facility. I'm grateful to the staff in microscopy, flow cytometry, sequencing, IT, library, steno-pool, administration and accounts for their constant help and support. A special thanks to the security staff member Mr. Kadam for his love, care for me and especially for his delicious food.

The members of the Shilpee Dutt and Amit Dutt laboratory have contributed immensely to my personal and professional growth. The group has been a source of friendships as well as successful collaboration. I am grateful to Smita, Ganesh and Deepak for their excellent technical help. I thank Priya, Gauri and Madhur for their help during the initial years of my PhD. I would like to thank Rohan, Nilesh, Pawan and Pratik for their support in different aspects of my work. I'm appreciative of the tremendous help provided by Sneha, Priti, Ankit, Swati, Akshat, Ankita, Rashmi and Monissa. I thank Jacinth, Mallika, Jyothi, Anagha, Prajish, Sameer, Mukul, Asim and Sanket for maintaining a wonderful atmosphere in the lab and making this journey a joyful one.

I am grateful to my seniors Ajit, Aditi, Hemant, Raghuram, Srikanta, Sumeer, Piyush and Madhura for their help and suggestions. I am glad that I met two of the most wonderful seniors Pallavi and Padma during different times of my PhD who guided me like a friend, heard, supported me when times were low and never made me miss home. I will always cherish the fun times we spent together.

This journey wouldn't have been so pleasant without the support of my batchmates Rasika, Divya, Prasanna, Sonali, Priyanka, Sajad, Rahul, Moqit and Qadir. We all shared memorable times together that will stay with me forever.

I am indebted to my friends outside the lab Aditi, Maulik, Dawan and Karan who patiently understood, endured my frustrations and most importantly for the long discussions we had about life. A special thanks to Chanmeet who stood by me through thick and thin and held me up from the lows of my life. His envision about my work has always made me to believe in myself more.

I am extremely grateful to my parents for all the sacrifices they endured so that I could follow my dreams, for their belief in me, the constant prayers, love and encouragement throughout these five years. I can't express how thankful I am to my sister Sarvdeep for bearing my absence and being there as a pillar of strength. I'm thankful to my brother in law Jasjit for his encouragement and most importantly to my niece Ganeev for being the reason of my happiness. A special thanks to a beautiful soul whose blessings will always be missed.

Lastly, I would to thank the almighty for his guidance and blessings that made me sail through all the difficulties. Thank You.

Ekjot Kaur

# Table of Contents

<b>Synopsis.....</b>	<b>i-xv</b>
<b>List of figures.....</b>	<b>xvi-xvii</b>
<b>List of tables.....</b>	<b>xviii</b>
<b>Abbreviations .....</b>	<b>xix-xx</b>
<b>Chapter 1: Introduction and Review of literature .....</b>	<b>1-18</b>
1.1 Glioblastoma .....	1
1.1.1 Pathology, symptoms and risk factors.....	3
1.1.2 Diagnosis, prognosis and treatment of Glioblastoma .....	4
1.1.2.1 Diagnosis .....	4
1.1.2.2 Prognosis .....	5
1.1.2.3 Standard of care.....	6
1.2 Factors responsible for tumour resistance and recurrence .....	7
1.2.1 DNA repair and cancer .....	8
1.2.2 Epigenetics, DNA repair and cancer .....	16
<b>Rationale .....</b>	<b>19</b>
<b>Specific Aims .....</b>	<b>20</b>
<b>Chapter 2: Establishment and characterization of the in vitro radiation resistant model from glioblastoma cell lines and patient samples.....</b>	<b>21-86</b>
2.1 Establishment of the in-vitro radiation resistant model .....	22
2.1.1 Introduction .....	22
2.1.2 Materials and methods .....	24
2.1.2.1 Cell culture and drug treatment.....	24
2.1.2.2 Patient samples.....	25
2.1.2.3 Cell synchronization .....	28
2.1.2.4 Trypan blue assay .....	28
2.1.2.5 Clonogenic survival assay .....	28
2.1.2.6 Propidium iodide staining .....	29
2.1.2.7 BrdU staining .....	29
2.1.2.8 CD133 staining .....	29

2.1.2.9 RNA extraction, cDNA synthesis and qPCR .....	30
2.1.2.10 $\beta$ -galactosidase activity staining .....	30
2.1.2.11 Immunofluorescence .....	30
2.1.2.12 Cell sorting based on scatter .....	31
2.1.2.13 Generation of stable cell lines .....	31
2.1.2.14 Time lapse studies .....	31
2.1.2.15 Annexin V/PI staining .....	31
2.1.2.16 Western blot analysis .....	32
2.1.2.17 Statistics .....	32
2.1.3 Results .....	32
2.1.3.1 Recapitulating radiation resistance in an in vitro cellular model developed from patient samples and cell lines. Subpopulation of Glioma cells survive lethal dose of radiation and become transiently non proliferative .....	32
2.1.3.2 Radio-resistant tumour cells are enriched with radiation induced Multinucleated Giant Cells (MNGCs) and stem cell markers .....	36
2.1.3.3 Non-apoptotic MNGCs show transient senescence and eventually resume growth to form viable mono-nucleated recurrent cells .....	40
2.1.3.4 Association of molecular, radiological and pathological parameters with patient survival in GBM.....	44
2.1.3.5 Percentage of giant cells with tumour volume significantly predict patient survival..	47
2.1.3.6 MNGCs are formed primarily by homotypic cell fusion of mono-nucleated radio-resistant cells .....	48
2.1.3.7 Cell fusion induced MNGCs give rise to relapse cells with similar ploidy .....	52
2.1.3.8 MNGCs over- express senescent associated secretory proteins (SASPs), over express anti-apoptotic genes and activate AKT to evade apoptosis .....	53
2.1.3.9 Relapse can be prevented by targeting pCdk1 (Y15) and cytokinesis.....	53
2.1.4 Discussion .....	58
2.2 Characterization of recurrent cells using Raman spectroscopy .....	62
2.2.1 Introduction.....	62
2.2.2 Materials and methods .....	64
2.2.2.1 Clinical tissues .....	64
2.2.2.2 Whole Transcriptome sequencing analysis.....	65
2.2.2.3 Raman Spectroscopy.....	65
2.2.2.3.1 Sample preparation and spectral acquisition .....	65
2.2.2.3.2 Spectral pre-processing and data analysis .....	66

2.2.3 Results .....	67
2.2.3.1 Recurrent cells have similar morphology and proliferation rate as compared to the parent population .....	67
2.2.3.2 Recurrent cells possess enhanced radiation resistance as compared to the parent population .....	69
2.2.3.3 Recurrent cells show up-regulation of survival pathways .....	70
2.2.3.4 Whole transcriptome analysis confirms recurrent cells are different from parent cells .....	71
2.2.3.5 Mean and difference spectra from Raman Spectroscopy of the parent and recurrent population reveals spectral features unique to recurrent population .....	73
2.2.3.6 Principal component analysis (PCA) identifies unique clustering of recurrent and parent cells .....	76
2.2.3.7 Principal component-linear discriminant analysis (PC-LDA) distinctly classifies the recurrent cells from parent cells .....	78
2.2.3.8 Raman spectral analysis of GBM tissues classified a population of GBM tissues differing in clinical outcome .....	79
2.2.4 Discussion .....	82
<b>Chapter 3: Identification of differential double strand break repair pathway activation and chromatin changes in radiation resistant cells .....</b>	<b>87-129</b>
3.1 Introduction .....	87
3.2 Materials and methods .....	91
3.2.1 Electron microscopy .....	91
3.2.2 Immunofluorescence .....	91
3.2.3 Alkaline comet assay .....	92
3.2.4 Histone acid extraction .....	93
3.2.5 Western blot analysis .....	94
3.2.6 RNA isolation, cDNA synthesis and Quantitative real-time RT-PCR .....	94
3.2.7 Cloning of shRNAs against SETMAR in pLKO.1-Tet-On knockdown .....	95
3.2.8 Site-Directed mutagenesis (SDM) and cloning of mutant/wild type H3.3 in pBABE vector .....	95
3.2.9 Cloning of wild type H3.3 and H3.3K36A mutant in retroviral vector pBABE .....	98
3.2.10 Retrovirus and lentivirus production, infection and drug selection .....	100
3.2.11 Transfection of NHEJ and HR vectors .....	101
3.3 Results .....	102
3.3.1 Re-appearance of $\gamma$ -H2AX observed in radiation resistant cells .....	102
3.3.2 Phosphorylation of H2AX in the resistant cells can be mediated either by ATM or ATR .....	102

3.3.3 Recurrent cells display altered ATM/ATR recruitment kinetics .....	105
3.3.4 Recurrent cells generated from radiation resistant cells show variable sensitivity towards ATM inhibitor .....	105
3.3.5 Radiation resistant cells prefer NHEJ pathway repair over HR pathway .....	107
3.3.6 Radiation resistant cells display altered chromatin architecture .....	109
3.3.7 Radiation resistant cells show over-expression of H3K36me2 and H3K4me2 modifications concomitant with the increase in its methyltransferases .....	111
3.3.8 SETMAR is required for proliferation of RR cells .....	115
3.3.9 H3K36me2 is required for retention of Ku80 and mediates the survival of RR cells .	118
3.4 Discussion .....	123
<b>Chapter 4: Summary and conclusion .....</b>	<b>128</b>
4.1 Summary .....	128
4.2 Conclusion .....	133
<b>References .....</b>	<b>134</b>
<b>Appendix I .....</b>	<b>147</b>
<b>Publications .....</b>	<b>152</b>

## **Synopsis**



## HOMI BHABHA NATIONAL INSTITUTE

### PhD Program

<b>1. Name of the Student:</b>	Ekjot Kaur
<b>2. Name of the Constituent Institution:</b>	Tata Memorial Centre, Advanced Centre for Treatment Research and Education in Cancer
<b>3. Enrolment No.:</b>	LIFE09201104002
<b>4. Title of the Thesis:</b>	Role of chromatin and DNA Damage repair pathway in Glioblastoma Multiforme
<b>5. Board of studies:</b>	Life Science

### 1. Introduction

Brain tumours accounts for 3.5% of the total tumour burden worldwide<sup>1</sup>. Out of these, Glioblastoma Grade IV (GBM) is one of most common and lethal primary brain tumours in adults, arise from glial cells and account for 50-60% of all the gliomas. These are genetically unstable, extensively angiogenic and highly infiltrative<sup>2</sup>. Current treatment modality includes maximum surgical resection followed by standard radical radiation and chemotherapy with alkylating agent Temozolomide<sup>3</sup>. Despite multi-modal therapy, the propensity for the local

recurrence increases. The recurrent cells are highly aggressive and resistant, eventually resulting into dismissal median survival time of less than a year <sup>4</sup>.

One of the major causes of the recurrence is attributed to the existence of innately resistant tumour cells that escape therapy <sup>5</sup>. Over-expression of proteins like EGFR, Survivin, MGMT and altered metabolic proteins has been reported in these GBM resistance cells<sup>6-9</sup>. Since chemo-radiation multimodal therapy for GBM works by generating DNA double strand breaks (DSB) and inducing apoptosis in tumour cells, there are reports suggesting a possible modulation of DNA DSB repair response by altering the expression of ATM, ATR and MSH6 contributing to the survival of a subpopulation of cells in this heterogeneous tumour <sup>10,11</sup>. A major determinant factor that influences the spatial-temporal accessibility of DDR proteins to the site of double-strand breaks (DSB) is the overall chromatin structure alterations<sup>12</sup>. One of the modifications, histone lysine methylation has been reported to be a key regulator of gene expression and heterochromatin function. Methylation of H3 lysine at 4 and 36 amino acids is associated with actively transcribed domains, while H3K9, H3K27 and H4K20 methylation appears to be enriched in the transcriptionally repressed regions of the chromatin<sup>13</sup>. These histone modifications also contribute to the DNA damage checkpoint by directly interacting with checkpoint components and repair proteins. For example, H3K79 methylation in mammals and budding yeast is shown to be important for localization of 53BP1 which is a DNA damage repair factor [14]. However, studies evaluating the role of chromatin dependent DDR in resistant cancer cells has not been explored.

Multinucleated and giant cells (MNGCs) are frequently seen in the late stages in various human cancers <sup>14-16</sup> formed as resultant of acytokinesis and endo-replication that eventually generate polyploid cells<sup>17,18</sup>. However, recent reports have also suggested a role of entosis or cell-in-cell structure formation and cell-cell fusion in inducing multinucleated-giant cells<sup>19,20</sup>.

A rare phenomenon in cancers, cell fusion have been implicated only in virally induced transformation of the normal cells, tumours of tendon sheath and bone, enhancing chromosomal instability and aneuploidy <sup>21-23</sup>. Some of the studies also report the multinucleated cells formation as result of radiation, though these cells so reported eventually underwent cell death by mitotic catastrophe <sup>24-26</sup>. The pre-existing MNGCs in tumours are thought to be responsible for increased resistance to therapies <sup>27,28</sup> however, the precise functional role of these cells in cancer is still not known.

## **2. Rationale**

Cancer therapy including radiation used in GBM works by causing double strand breaks (DSBs) in DNA and inducing apoptosis in cancer cells. The efficacy of DNA damage-based therapy in GBM can be modulated by DNA repair pathways. Since the physiological substrate of DNA damage repair machinery is packed into chromatin, the efficiency of DNA damage repair in a cell depends on the accessibility of these repair proteins to the damaged DNA. In this regard, histone methylations play a key role in regulating DNA repair response by directly interacting with the repair proteins. This led us to hypothesize that residual resistant GBM cells differ from the bulk tumour cells such that they alter the of DNA damage repair response by exhibiting differential chromatin modifications, either acquired during the administration of radio-therapy or innately present. These changes in chromatin structure that regulate DDR pathway efficiency and choices in turn influence the survival of residual cells post therapy. Therefore, understanding of the chromatin mediated DDR response in the resistant cells may enable in development of therapeutic strategies for specific targeting of these cells.

### **3. Key Question:**

To understand the role of chromatin and DNA damage repair pathway in glioblastoma those contribute to the survival and relapse of cells post radiation.

### **4. Specific Objectives:**

1. *Establishing the model for radiation survival from glioma cell lines and patient samples*
2. *Identifications of differential double strand break repair pathway activation in radiation surviving cancer cells or escapers.*
3. *Identify the differential changes at the chromatin level in the radiation surviving cancer cells or escapers.*

**Objective 1-** *Establishing the model for radiation survival from glioma cell lines and patient samples.*

A pre-requisite to understanding the mechanisms of resistance in residual cells is to generate a system to gain access to these cells. Therefore, we recapitulated clinical scenario of resistance in a cellular model from GBM cell lines and patient derived primary cultures. For this, we first determined the lethal dose of radiation at which ~10% of the cell survives for U87MG, SF268 and 20 patient derived primary cultures. After radiation, these cells were allowed to grow. We observed an initial burst of rapid proliferation following which more than 90% tumor cells died. However, there was a small percentage of cells that survived radiation, a halt/non-proliferative population of Radiation Resistant cells (RR). Since the Radiation resistant cells were the ones that we wanted to study we further characterized this population.

RR population of cells were distributed in all the phases of cell cycle, though there were significantly less cells in G0/G1 and higher number of cells in G2-M phase as compared to the parent untreated cells. Upon further examination of molecular players leading to non-proliferative state of these cells we found pCdk1(Y15) and p21 levels up-regulated in RR established from cell lines as well as patient samples. Since there are several reports which have demonstrated the induction of cell death via mitotic catastrophe of the damaged non-proliferative cells <sup>24,25</sup>, we examined the apoptotic markers in radiation escapers and contrary to reports, RR showed absence of apoptosis confirmed by no enhanced expression of Bax and Annexin V in these cells. Simultaneously, on investigating the expression of pro-survival genes Mcl-1, Survivin, Bcl-xL, IAPs like BIRC3 and BIRC5, high expression of Bcl-xL and BIRC3 survival genes was observed in the RR cells. Accordingly AKT pathway, one of major pathway contributing to the survival of Glioblastoma tumor cells <sup>29</sup>. That is also downstream to the many pro apoptotic genes was found to be highly activated in RE contributing to the survival of RR.

Morphological analysis using  $\beta$ -actin and nestin staining showed that ~60% of RR population was multinucleated and giant cells (MNGC's). Importantly, we demonstrate that these MNGC's were not the ones that were pre-existing in the parent samples but were radiation induced. In fact, we also, show that the percentage of giant cells in the escapers significantly influence the clinical outcome in the 20 patient sample cohort either alone or in combination with the radio-pathological parameters. Interestingly multinucleated giant cells displayed multiple spindle poles compared to the mono-nucleated cells which could lead to aberrant or aborted mitoses in MNGCs. Therefore, to confirm that MNGCs indeed divide and form relapse population we flow sorted the multinucleated, giant and mono-nucleated cells, and observed that both MNGCs and mono-nucleated cells proliferate giving rise to mono-

nucleated relapse cells. Based on the above mentioned observations, we went ahead to explore the mechanisms involved in the formation of MNGC's.

- Three possible mechanisms reported for the formation of MNGC's: 1) acytokinesis (endoreduplication), 2) entosis and 3) rare in cancer cells-cell fusions. Concomitant increase in the replication with time was not seen as determined by the percentage of cells in S phase. However, more than 4n cells were observed indicating that contribution of endo-reduplication might not be significant in MNGC formation in our system.
- Next, we explored entosis or a cell-in-cell mechanism in the formation of MNGC by staining with membrane protein N-cadherin along with H&E staining. However, in our cells, cell-in-cell structures were not observed.
- Third possibility of cell-cell fusion was examined by establishing two stable parent cells lines one expressing pEGFP and the other expressing TdRed for both the cell lines and primary cultures. The green and the red florescent cells were co-cultured in equal numbers and subjected to the lethal dose of radiation. At least 50 radiation escapers were counted in each culture and scored for yellow fluorescence (corresponding to the cell-cell fusion events). We found 68%, 56%, 62% and 61% of yellow fluorescent cells amongst the total MNGC's observed in U87MG, SF268, PS1 and PS2 respectively.

The cells formed after cell-cell fusion displayed Senescence associated  $\beta$ -galactosidase positivity along with the expression of SASP's (Senescence Associated Secretory Proteins) as observed after RNA sequencing and real time PCR validation in the escapers. Targeting formation of MNGC's by: 1) premature mitosis induction using Wee 1 kinase inhibitor and 2) inhibition of cytokinesis using Wiskostatin inhibitor. We incubated the irradiated glioma cells with 600nM of Wee1 kinase inhibitor for 24 hours post 5 days of radiation treatment. A huge amount of apoptosis was observed after 5 days of treatment. The specificity of the inhibitor was confirmed by western blot analysis using anti-Cdk1 antibody. Similarly, targeting the

cytokinesis in MNGC's using Wiskostatin also leads to cell death. However, non-radiated cells treated with Wiskostatin would also be affected.

***Objective 2: Identifications of differential double strand break DNA damage response (DDR) pathway activation in radiation surviving cancer cells or escapers (RR).***

As mentioned earlier, the survival of the cells post genotoxic stress is mediated by DNA damage repair (DDR) proteins regulated by chromatin architecture. The kinetics and sequence of recruitment of DDR proteins have a strong impact on the efficiency of DSB repair. Thus, first explored the recruitment kinetics of various DDR proteins in the escapers. While studying the kinetics of  $\gamma$ -H2AX foci formation we observed that the foci resolved within 24-48 hours post radiation. However, interesting  $\gamma$ -H2AX foci re-appeared in the escapers 6-10 days post radiation when the cells become non proliferative. These cells revealed high amount of damage as determined using alkaline comet assay. We further screened other DDR kinase proteins like pChk2, pATM and pATR. Interestingly, RR population from a few samples activated pATR-Chk1 axis of repair while the remaining activated pATM-Chk2 axis. Additionally, background levels of pATM was observed in the relapse cells in response to double strand breaks in the samples displaying ATR-Chk1 axis in the escaper cells. It could be reasoned out that the p53 status might be influencing the high amount of activation of ATR kinase rather than ATM in such samples. These results shows that the cells escaping the radiation treatment enhance DDR response, can modulate the repair by utilizing an alternative sensory kinase like ATR instead of ATM to activate the DDR signaling cascade.

The repair of the double strand breaks (DSBs) induced by any genotoxic stress can be brought about by two pathways: Non-Homologous End joining Pathway (NHEJ) and Homologous Recombination pathway (HR) depending upon the cell cycle phase and the type of structure of the broken ends of the damage. We wanted to see there is a preferential

activation of any of these repair pathway in our escapers by 1) examining the recruitment of NHEJ and HR proteins and 2) checking the expression of these proteins by western blot analysis. Importantly, we observed that higher recruitment and expression of NHEJ proteins in these resistant cells as compared to the HR proteins, suggest a preferential use of NHEJ pathway by these resistant cells. Importantly, Abrogation of NHEJ repair by DNA-Pk inhibitor NU7026, significantly reduced the survival and clonogenic ability of RR cells.

***Objective 3: Identify the differential changes at the chromatin level in the radiation surviving cells or escapers (RR).***

We first examined the gross level changes at the chromatin architecture in these RR cells using electron microscopy (EM). EM images revealed striking architectural changes in the form less condensed chromatin in the RR cells as compared to the parent cells. To explore further on these observations, we checked for the expression of Heterochromatin Protein-1 alpha (HP-1 $\alpha$ ) in these cells and observed a decreased expression of HP-1 $\alpha$  compared to the parent cells, confirming the euchromatinization of the chromatin in the RR cells.

Since histone modifications are known to be involved in aiding DDR as well as altering the chromatin architecture, we then screened for the expression of various histone modifications (methylations) namely, H3K4me<sub>2</sub>, H3K9me<sub>2</sub> and H3K36me<sub>2</sub> associated with DDR response and influencing the chromatin architecture. The expression levels of methyltransferases responsible for these modifications were also determined. The radiation resistant cells revealed higher expression of H3K4me<sub>2</sub> in 5/10 samples including cell lines (fold change ranging from 2.71-10.3), while H3K36me<sub>2</sub> showed up-regulation in both the cell lines and in 6 out 8 patient samples studied as compared to the parent cells (fold change ranging from 1.42-12.5). Additionally, these RR cells from cell lines exhibited lower levels of H3K9me<sub>2</sub> compared to the parent cells. On correlating the expression of H3K4me<sub>2</sub> and H3K36me<sub>2</sub> with the expression of SETMAR and NSD1 methyltransferases, we observed a strong

positive association between the expression of SETMAR and these modifications. Similarly, the lower expression of Suv39H2 correlated with the decreased levels of H3K9me2 modification.

Since H3K36me2 was observed to be up-regulated in 8/10 samples, we focused on understanding the relevance of the context of DDR and survival of resistant cells. For this, we first mutated the lysine residue at 36 amino acid in H3.3 to alanine, made stable cells expressing the mutant form of Histone 3.3 in a background of wild type H3. These mutant H3.3 expressing cells exhibited lower levels of H3K36me. Although possibility of methylation of endogenous H3.3 could not be ruled out, immunofluorescence assay for H3K36me2 in these mutant cells show a significant decrease in the modification, showing incorporation of the more than 80% mutant histone in these cells based on quantification of the immunofluorescence. Yet, experiments with the tagged-mutant H3.3 will be required to confirm the same. Recruitment and expression of NHEJ and HR repair proteins were then examined in the cells at different time points after radiation. Within 6-14 hours after radiation, recruitment and expression of NHEJ protein Ku80 and HR protein pBRCA1 was observed in both the cells expressing wild type H3.3 and mutant H3.3. However, at later time points, an increase in the recruitment of Ku80 along with concomitant decrease in pBRCA1 was observed till the formation of resistant cells in wild type cells. However, in the cells harbouring H3.3 mutant reduced recruitment of Ku80 protein could not be compensated by the HR pathway. Interestingly, we also observed decrease expression of Ku80 in H3.3 mutant expressing cells. To rule out the possibility of decreased expression leading to reduced recruitment of Ku80, we quantitated the western blot expression and immunofluorescence images. Even though 30% of Ku80 protein was still being expressed in the RR cells, there was absolutely no recruitment of Ku80 was seen in the Mutant H3.3 expressing RR cells, suggesting that apart from recruitment, H3K36me2 may be regulating the expression of the

Ku80 as well. Furthermore, these cells showed decreased survival capacity, eventually die off within 18-20 days of radiation.

Secondly, since SETMAR methylates H3 at lysine 36, we sought to investigate the importance of SETMAR expression in regulating the NHEJ repair response. For this, we generated stable cells expressing Tet-inducible shRNA against SETMAR. After induction with 1ug/ml of doxycycline, shRNA1 showed SETMAR knockdown efficiency of 70-80% compared to the scrambled shRNA. Upon shRNA knockdown of SETMAR in resistant cells, decreased expression of H3K36me2 and decreased recruitment of KU80 was observed in shRNA1. At 1ug/ml of doxycycline, SETMAR knockdown preventing the generation of relapse cells. Furthermore, at higher concentration (2.5 ug/ml) of doxycycline, fewer cells survived the radiation, highlighting the importance of SETMAR in the survival of GBM cells upon radiation.

## **5. Conclusions and Future Prospects:**

In this study, we show that a subpopulation of GBM cells, innately resistant to radiation, survive and were transiently arrested in G2/M phase of the cell cycle via inhibitory pCdk1(Y15). These cells however, regain their proliferative capacity to form relapse cells. During the non-proliferative phase, these cells show enrichment of multinucleated and giant cells (MNGCs). We observed that these MNGC's were not pre-existing giant cells from parent population but formed due to radiation exposure. Importantly, these MNGC's were formed as a result of non-genetic route of survival of homotypic cell-cell fusion. Further, these fused cells display damaged DNA preferentially undergoing NHEJ repair possibly facilitated by H3K36me2. This study also highlights important therapeutic windows which if targetable may enable in better prognosis of this dismissal disease. We show that pushing resistant cells prematurely into mitosis by Wee-1 kinase inhibitor (MK1775) prevents

pCdk1(Y15) mediated cell cycle arrest and relapse while treating with Wiskostatin inhibitor prevented relapse of the escapers. In conclusion, we show that that the survival residual GBM cells is a multi-factorial process that involves alteration of the DDR response facilitated by chromatin changes at the levels of histone modifications.

Future studies on identifying mechanisms involved in cell-cell fusion as well as the regulation of NHEJ repair would help in better understanding of the survival strategies adopted by these resistant GBM cells. This will further enable in the development of therapeutic strategies that will improve the prognosis and allow better management of this disease.

## **6. References:**

1. Ferlay, J., et al., *Estimates of worldwide burden of cancer in 2008: GLOBOCAN 2008*. Int J Cancer, 2010. **127**(12): p. 2893-917.
2. Adamson, C., et al., *Glioblastoma multiforme: a review of where we have been and where we are going*. Expert Opin Investig Drugs, 2009. **18**(8): p. 1061-83.
3. Stupp, R., et al., *Radiotherapy plus concomitant and adjuvant temozolomide for glioblastoma*. N Engl J Med, 2005. **352**(10): p. 987-96.
4. Berens, M.E. and A. Giese, "...those left behind." *Biology and oncology of invasive glioma cells*. Neoplasia, 1999. **1**(3): p. 208-19.
5. Inda, M.M., R. Bonavia, and J. Seoane, *Glioblastoma multiforme: a look inside its heterogeneous nature*. Cancers (Basel), 2014. **6**(1): p. 226-39.
6. Chakravarti, A., et al., *The epidermal growth factor receptor pathway mediates resistance to sequential administration of radiation and chemotherapy in primary human glioblastoma cells in a RAS-dependent manner*. Cancer Res, 2002. **62**(15): p. 4307-15.
7. Chakravarti, A., et al., *Survivin enhances radiation resistance in primary human glioblastoma cells via caspase-independent mechanisms*. Oncogene, 2004. **23**(45): p. 7494-506.
8. Kitange, G.J., et al., *Induction of MGMT expression is associated with temozolomide resistance in glioblastoma xenografts*. Neuro Oncol, 2009. **11**(3): p. 281-91.
9. Ye, F., et al., *Protective properties of radio-chemoresistant glioblastoma stem cell clones are associated with metabolic adaptation to reduced glucose dependence*. PLoS One, 2013. **8**(11): p. e80397.
10. Abdel-Fatah, T.M.A., et al., *ATM, ATR and DNA-PKcs expressions correlate to adverse clinical outcomes in epithelial ovarian cancers*. BBA Clinical, 2014. **2**: p. 10-17.
11. Mathews, L., S. Cabarcas, and W. Farrar, *DNA repair: the culprit for tumor-initiating cell survival?* Cancer and Metastasis Reviews, 2011. **30**(2): p. 185-197.

12. Rossetto, D., et al., *Epigenetic modifications in double-strand break DNA damage signaling and repair*. Clin Cancer Res, 2010. **16**(18): p. 4543-52.
13. Zhu, Q. and A.A. Wani, *Histone modifications: crucial elements for damage response and chromatin restoration*. J Cell Physiol, 2010. **223**(2): p. 283-8.
14. Sneige, N., et al., *Chemotherapy-induced histologic changes in mastectomy specimens and their potential significance*. Breast, 2001. **10**(6): p. 492-500.
15. Ariizumi, T., et al., *Multinucleation followed by an acytokinetic cell division in myxofibrosarcoma with giant cell proliferation*. J Exp Clin Cancer Res, 2009. **28**: p. 44.
16. Weihua, Z., et al., *Formation of solid tumors by a single multinucleated cancer cell*. Cancer, 2011. **117**(17): p. 4092-9.
17. Geigl, J.B., et al., *Defining 'chromosomal instability'*. Trends Genet, 2008. **24**(2): p. 64-9.
18. Holland, A.J. and D.W. Cleveland, *Boveri revisited: chromosomal instability, aneuploidy and tumorigenesis*. Nat Rev Mol Cell Biol, 2009. **10**(7): p. 478-87.
19. Krajcovic, M. and M. Overholtzer, *Mechanisms of ploidy increase in human cancers: a new role for cell cannibalism*. Cancer Res, 2012. **72**(7): p. 1596-601.
20. Brodbeck, W.G. and J.M. Anderson, *Giant cell formation and function*. Curr Opin Hematol, 2009. **16**(1): p. 53-7.
21. Duelli, D.M., et al., *A primate virus generates transformed human cells by fusion*. J Cell Biol, 2005. **171**(3): p. 493-503.
22. Hosaka, M., et al., *Giant cell formation through fusion of cells derived from a human giant cell tumor of tendon sheath*. J Orthop Sci, 2004. **9**(6): p. 581-4.
23. Nishimura, M., et al., *Cytological properties of stromal cells derived from giant cell tumor of bone (GCTSC) which can induce osteoclast formation of human blood monocytes without cell to cell contact*. J Orthop Res, 2005. **23**(5): p. 979-87.
24. Eom, Y.W., et al., *Two distinct modes of cell death induced by doxorubicin: apoptosis and cell death through mitotic catastrophe accompanied by senescence-like phenotype*. Oncogene, 2005. **24**(30): p. 4765-77.
25. Erenpreisa, J., M. Kalejs, and M.S. Cragg, *Mitotic catastrophe and endomitosis in tumour cells: an evolutionary key to a molecular solution*. Cell Biol Int, 2005. **29**(12): p. 1012-8.
26. Erenpreisa, J., et al., *Segregation of genomes in polyploid tumour cells following mitotic catastrophe*. Cell Biol Int, 2005. **29**(12): p. 1005-11.
27. Zhang, S., et al., *Generation of cancer stem-like cells through the formation of polyploid giant cancer cells*. Oncogene, 2013.
28. Barok, M., et al., *Trastuzumab-DMI causes tumour growth inhibition by mitotic catastrophe in trastuzumab-resistant breast cancer cells in vivo*. Breast Cancer Res, 2011. **13**(2): p. R46.
29. Robinson, J.P., et al., *Akt signaling is required for glioblastoma maintenance in vivo*. Am J Cancer Res, 2011. **1**(2): p. 155-167.

## **Publications in referred journals:**

### **Published Articles.**

- **Ekjot Kaur**, Jacinth Rajendra, Shailesh Jadhav, Epari Sridhar, Jayant Sastri Goda, Aliasgar Moiyadi and Shilpee Dutt. Radiation-induced homotypic cell fusions of innately resistant glioblastoma cells mediate their sustained survival and recurrence.

Carcinogenesis. 2015;36(6):685-95. doi: 10.1093/carcin/bgv050. PubMed PMID: 25863126.

- **Ekjot Kaur**, Sudeep Gupta, Shilpee Dutt. Clinical implications of MTA proteins in human cancer. *Cancer Metastasis Rev.* 2014 Dec;33(4):1017-24. doi: 10.1007/s10555-014-9527-z.

**Accepted Articles.** Not applicable

**Communicated Articles.**

- **Ekjot Kaur**, Aditi Sahu, Arti Jadhav, Jacinth Rajendra, Rohan Chaubal, Nilesh Gardi, Murali Chilakapati and Shilpee Dutt. Unique spectral markers discern recurrent Glioblastoma cells from heterogeneous parent population (*under revision*).
- **Ekjot Kaur**, Jayant Sastri Goda, Prakash Shetty, Aliasgar Moiyadi, Epari Sridhar, Abhishek Mahajan, Shilpee Dutt. ATM expression from patient derived resistant cells along with tumour volume improve prediction of GBM patient outcome (*under review*)

**Other publications.**

Pawan Upadhyay, Sudhir Nair, **Ekjot Kaur**, Jyotirmoi Aich, Prachi Dani, Vidyalakshmi Setunath, Nilesh Gardi, Pratik Chandrani, Mukul Godbole, Kavita Sonawane, Sadhana Kanan, Beamon Agarwal, Shubhada Kane, Sudeep Gupta, Shilpee Dutt, and Amit Dutt. Notch Pathway Activation is Essential for Maintenance of Stem-like Cells in Early Tongue Cancer (*under review*).

**Book Chapter:** Not applicable

**Conference abstracts**

- **Ekjot Kaur**, Gauri Patade, Sneha Berry and Shilpee Dutt. “Surviving Genotoxic Stress” **poster presentation** at “at XXXVI All India Cell Biology Conference -2012 and International Symposium on SARGI: 17-19th November, 2012, Mumbai, India.
- **Ekjot Kaur**, Shailesh Jadhav, Sneha Berry, Gauri Patade and Shilpee Dutt “Polyploidy: a survival mechanism against ionizing radiation in Glioblastoma”. **Poster presentation** at “32nd Convention of Indian Association for Cancer Research Emerging Trends in Cancer research: Road to prevention & cure & International Symposium on: Infection and Cancer” (IACR-2013- February 13 -16 2013) under **Shri Rambhau Kulkarni and Shri Rajnikant Baxi award category**, New Delhi, India.
- **Ekjot Kaur**, Jacinth Rajendra, Shailesh Jadhav, Gauri Patade and Shilpee Dutt “Multinucleated giant cells formed by cell - cell fusion post radiation are cause of resistance and relapse in Glioblastoma”. **Oral presentation award** under Shri Sitaram Joglekar category at “33rd Annual Convention of Indian Association for Cancer Research (IACR)” 13-15,2014 February, 2014, Kerala, India.
- **Ekjot Kaur**, Shailesh Jadhav, Aliasgar Moiyadi, Jayant S Goda and Shilpee Dutt “Radiation induced homotypic cell fusions of resistant cells form multinucleated giant

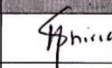
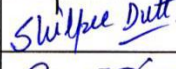
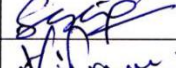
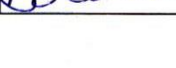
cells: cause of sustained survival and recurrence in glioblastoma” **platform presentation** at “ISNOCON2015, Kochi” 26th-28th March 2015, Kochi, India.

- **Ekjot Kaur** Jacinth Rajendra, Sanket Shah, Jyothi Nair, Ankit Khushwaha, Aliasgar Moiyadi, Shilpee Dutt, “Radiation induced Multinucleated Giant Cells: a novel therapeutic target to prevent survival and relapse of Glioblastoma” **poster presentation** during 106th Annual Meeting of American Association for Cancer Research (AACR-2015, April 18-22) in Philadelphia, PA, USA.
- **Ekjot Kaur**, Jyothi Nair, Ankit Kushwaha, Akshat Shetty, Anurag Srivastava, Aliasgar Moiyadi, Shilpee Dutt “A novel mechanism of homotypic cell fusion promote formation of Glioma resistance cells facilitated by NHEJ driven repair” **Selected amongst top 12 abstracts for oral presentaion** at 75<sup>th</sup> Tata Memorial Centre Platinum Jubilee Conference, 26-28th Feb 2016, Mumbai, India.

Signature of Student: 

Date: 5/04/2016

**Doctoral Committee:**

S. No.	Name	Designation	Signature	Date
1.	Dr. Neelam Shirsat	Chairperson		5/4/16
2.	Dr. Shilpee Dutt	Guide & Convener		05/04/16
3.	Dr. Sanjay Gupta	Member		05/04/16
4.	Dr. Prasanna Venkatraman	Member		5/4/16
5.	Dr. Anjali Shiras	Invitee		13.04.16.
6.	Dr. Amit Dutt	Technology expert		5/4/16

  
 Dr. S.V. Chiplunkar  
 Director, Chairperson  
 Academics Training Program,  
 ACTREC-TMC  
**Dr. S. V. Chiplunkar**  
 Director  
 Advanced Centre for Treatment, Research &  
 Education in Cancer (ACTREC)  
 Tata Memorial Centre  
 Kharghar, Navi Mumbai 410210.

  
 Prof. K. Sharma  
 Director, Academics  
 Tata Memorial Centre  
**PROF. K. S. SHARMA**  
 DIRECTOR (ACADEMICS)  
 TATA MEMORIAL CENTRE,  
 PAREL, MUMBAI

## List of figures

<b>Figure 1.1: Anatomy of the brain and location of glioblastoma.</b> .....	3
<b>Figure 1. 2: MRI image of GBM</b> .....	5
<b>Figure 1. 3: Extent of alterations in DNA damage response (DDR) proteins in different cancers</b> .....	10
<b>Figure 1.4: Double strand break repair pathway in humans.</b> .....	12
<b>Figure 1.5: NHEJ and HR pathway in humans.</b> .....	14
<b>Figure 2.6: Radiation resistant cells are enriched with radiation induced multinucleated and giant cells which are not pre-existing.</b> .....	40
<b>Figure 2.7: MNGCs exhibit non-apoptotic and senescent phenotype.</b> .....	45
<b>Figure 2.8: Survival analysis of individual molecular parameters.</b> .....	46
<b>Figure 2.9: Survival analysis of p53 and tumour volume.</b> .....	48
<b>Figure 2.10: Correlation and survival analysis of resistance associated molecular parameters with the radio-pathological features.</b> .....	49
<b>Figure 2.11: Endo-reduplication and entosis do not significantly contribute in MNGCs formation.</b> .....	51
<b>Figure 2.12: Cell-cell fusion leads to formation of MNGCs in the radiation resistant cells.</b> .....	52
<b>Figure 2.13: MNGCs give rise to relapse cells with similar ploidy number.</b> .....	53
<b>Figure 2.14: MNGCs over- express anti-apoptotic genes and activate AKT to evade apoptosis</b> .....	55
<b>Figure 2.15: Radiation resistant cells are arrested predominantly at G2-M phase of the cell cycle.</b> .....	56
<b>Figure 2.16: Premature mitosis kills radiation resistant cells.</b> .....	58
<b>Figure 2.17: Blocking cytokinesis induced apoptosis of resistant cells preventing recurrent cell formation.</b> .....	59
<b>Figure 2.18: Schema showing the multi-step in-vitro radiation model recapitulating the progression of GBM and demonstrating the non-proliferative phase.</b> .....	60
<b>Figure 2.19: Recurrent cells generated from cellular model shows similar morphology and growth rate as that of parent cells.</b> .....	70
<b>Figure 2.20: Recurrent cells reveal differences as compared to parent cells at the molecular level.</b> .....	71

<b>Figure 2.21: PCA plot of global transcripts showing differences between parent and recurrent cells.</b> .....	73
<b>Figure 2.22: Mean and difference spectra from parent and recurrent population reveals spectral features unique to recurrent population. ....</b>	75
<b>Figure 2.23: Mean and difference spectra from parent and recurrent population reveals higher lipid peaks in recurrent population. ....</b>	76
<b>Figure 2.24: PCA analysis classifies the recurrent cells from parent cells. ....</b>	78
<b>Figure 2.25: PCA-LDA analysis classifies the recurrent cells from parent cells. ....</b>	80
<b>Figure 2.26: Raman spectroscopic analysis distinctly classifies the non-responders from responders group of patients.....</b>	83

## List of tables

<b>Table 1.1: Incidence rates of adult glioma sex as reported in CBTRUS 2005 – 2006 <sup>[2]</sup>...</b>	<b>3</b>
<b>Table 2.1.1: Lethal dose of radiation for all 20 primary cultures .....</b>	<b>34</b>
<b>Table 2.1.3: Percentage of multinucleated and giant cells in different patient samples.</b>	<b>42</b>
<b>Table 2.1.4: Surgical, radiological and pathological details in the patient cohort (N=20).</b> .....	<b>47</b>

# ABBREVIATIONS

AKT- Protein kinase B  
ATM - Ataxia Telangiectasia Mutated  
ATR - Ataxia Telangiectasia and Rad3 related  
Bcl-xL- B-cell lymphoma-extra large  
BIRC3- Baculoviral IAP repeat-containing protein3  
BIRC4- Baculoviral IAP repeat-containing protein 4  
BRCA2 - Breast cancer type 2 susceptibility protein  
BSA- Bovine Serum Albumin  
CBTRUS- Central Brain Tumour Registry of the United States  
CCD- Charge-coupled device  
CCDC26- CCDC26 Long Non-Coding RNA  
Cdk1- Cyclin-dependent kinase 1  
CDK4 - Cyclin-dependent kinase 4  
CDK6 - Cyclin-dependent kinase 6  
CDKN2A - Cyclin-Dependent Kinase Inhibitor 2A  
CDKN2B-AS1- Cyclin Dependent Kinase Inhibitor 2B antisense RNA 1  
cDNA- complementary Deoxyribonucleic acid  
CNS- Central Nervous System  
CpG- 5'—C—phosphate—G—3'  
CT- Computed Tomography  
DAPI- 4',6-diamidino-2-phenylindole  
dATP - deoxyadenosine triphosphate  
dCTP - deoxycytidine triphosphate  
DEPC - Diethylpyrocarbonate  
dGTP - deoxyguanosine triphosphate  
DMEM - Dulbecco's minimum essential (or modified Eagle) medium  
DMSO - Dimethyl sulfoxide  
DNA- Deoxyribonucleic acid  
DNase - Deoxyribonuclease  
dNTP - deoxynucleoside triphosphate  
Dot1L- DOT1 Like Histone H3K79 Methyltransferase  
DTT - Dithiothreitol  
EANO- European Association of Neuro-Oncology  
EDTA- Ethylenediaminetetraacetic acid  
EGFR - Epidermal Growth Factor Receptor  
ERK1/2- Extracellular Signal-Regulated Kinases  
EtBr- Ethidium bromide  
EZH2- Enhancer Of Zeste 2 Polycomb Repressive Complex 2 Subunit  
FACS- Fluorescence-activated cell sorting  
FBS- Fetal bovine serum  
FPKM- Fragments Per Kilobase of transcript per Million mapped reads  
GAPDH- Glyceradehyde 3- phosphate dehdrogenase  
GATA4- GATA Binding Protein 4  
GATA5- GATA Binding Protein 5  
GBM- Glioblastoma  
Gy- Gray  
IDH1/2- Isocitrate Dehydrogenase 1/2  
IR- ionizing radiation  
KAP1- [Kruppel-Associated Box Domain]-Associated Protein 1

LDA- Linear Discriminant Analysis  
MDM2 - E3 ubiquitin-protein ligase Mdm2  
MET - Hepatocyte growth factor receptor precursor  
MLH1- MutL homolog 1  
MRI-Magnetic Resonance Imaging  
mRNA- messenger ribonucleic acid  
NF1- Neurofibromin 1  
NSD1- Nuclear Receptor Binding SET Domain Protein 1  
PBS- Phosphate Buffer Saline  
PCR- Polymerase chain reaction  
PDGFRA - Platelet-derived growth factor receptor alpha  
PHLDB1 -Pleckstrin Homology-Like Domain, Family B, Member 1  
PTEN- Phosphatase and tensin homolog  
Rb- Retinoblastoma protein  
RNA - Ribonucleic acid  
RNase - Ribonuclease  
RPA2 - Replication Protein A 32kDa subunit  
RQ - Relative quantity  
RT- Radiotherapy/ room temperature  
RTEL- Regulator of Telomere Elongation Helicase 1  
RUNX3- Runt Related Transcription Factor 3  
SCC- Squamous Cell Carcinoma  
SDS- Sodium dodecyl sulphate  
SETMAR- SET Domain And Mariner Transposase Fusion Gene  
shRNA- s short hairpin RNA  
Suv39H2- Suppressor Of Variegation 3-9 Homolog 2  
T1W- T1 weighted  
T2FLAIR- T2-Weighted-Fluid-Attenuated Inversion Recovery  
T2W- T2 weighted  
TERT - Telomerase reverse transcriptase  
TP53- Tumor Protein P53  
Tris- Tris (hydroxymethyl) aminomethane  
qPCR- Quantitative PCR  
UV –Ultraviolet  
WHO-World Health Organization  
XPC - Xeroderma Pigmentosum, Complementation Group C  
XRCC4 - X-Ray Repair Complementing Defective Repair in Chinese Hamster Cells 4  
XRCC5- X-Ray Repair Complementing Defective Repair in Chinese Hamster Cells 5  
µg micro gram  
µl micro litre  
µM micro molar

**Chapter 1**

***Introduction and Review of literature***

This chapter introduces brain tumours followed by discussion on important aspects of glioblastoma including diagnostic techniques, prognosis and treatment modalities. The latter part of the chapter covers the current problems associated with glioblastoma management and mechanisms associated with the therapy resistance seen in these tumours.

## **1.1 Glioblastoma**

Brain tumours account for 3.5% of the total tumour burden worldwide [1]. Out of these, gliomas constitute 80% of the total primary malignant brain tumours [2]. Gliomas comprise of tumours arising from star-shaped glial cells or non-neuronal cells that are required to support the neurons and maintain homeostasis. Depending on the type of cell, increasing degrees of undifferentiation, anaplasia and aggressiveness, gliomas are classified as astrocytic tumours (World Health Organization classification astrocytoma grades I, II (astrocytoma), anaplastic astrocytoma (Grade III) and glioblastoma or GBM (Grade IV) [3]. WHO grade II tumours (diffuse astrocytomas, oligodendrogliomas, and oligoastrocytomas) are more differentiated neoplasms that perpetually lead to development of higher-grade tumour.

Glioblastoma is the most common and highly aggressive primary glial tumour predominantly seen in adults of 50-60 years arising in cerebrum (Figure 1.1). This tumour accounts for 50% of all the gliomas and approximately 12-15% of all brain tumours [4].

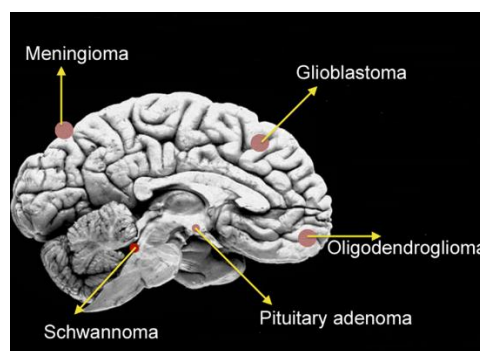


**Figure 1.1: Anatomy of the brain and location of glioblastoma.** Pictorial representation of different anatomical locations of brain tumours. Image taken from [www.slideshare.net](http://www.slideshare.net).

Each year approximately 51,000 primary brain tumours are diagnosed in the United States of which 36% are gliomas, mostly are of WHO grade IV GBM with approximately 3 in 100,000 new cases with GBM [5]. Across the developed countries, an estimated 3.5 cases per 100,000 people are reported each year with GBM as shown in table 1.1 [6].

In India, the incidence rates of glioma varies from 5.8% in Mumbai, 6.7% in Bangalore, 3.5% in Chennai, 5.6% in Dibrugarh, and 28.2% in Trivandrum among males and 6.3% in Mumbai, 5.6% in Bangalore, 7.5% in Chennai, 0% in Dibrugarh, and 21.8% in Trivandrum among females as per the by Indian Council for Medical Research 2009 report [7]. The demographic data from Tata Memorial Hospital based on 1 year prospective study conducted on 656 patients also revealed increased proportion of high-grade gliomas 151 cases (59.5%) amongst the total CNS tumours registered [8].

Adult glioma by major histologic subtype	Number of cases	Median age at diagnosis (years)	Total rate <sup>a</sup>	Male rate <sup>a</sup>	Female rate <sup>a</sup>
Glioblastoma	12,943	64	3.05	3.86	2.39
Anaplastic astrocytoma	2,029	51	0.47	0.56	0.38
Astrocytoma, NOS	1,994	45	0.46	0.54	0.38
Anaplastic oligodendroglioma	781	48	0.18	0.20	0.16
Oligodendroglioma	1,559	41	0.35	0.38	0.33
Malignant glioma, NOS	1,668	43	0.38	0.42	0.35

<sup>a</sup>Rates are per 100,000 population, age-adjusted to the 2000 US (19 age-groups) standard, and based on data from the following registries: Arizona, Colorado, Connecticut, Delaware, Idaho, Maine, Massachusetts, Minnesota, Montana, New Mexico, New York, North Carolina, Rhode Island, Texas, Utah and Virginia. Abbreviation: NOS, not otherwise specified.

**Table 1.1: Incidence rates of adult glioma as reported in CBTRUS 2005 – 2006 [2].**

### 1.1.1 Pathology, symptoms and risk factors

This type of tumour is characterized histologically by hypercellularity and increased mitotic activity along with presence of microvascular proliferation and necrotic tissue with or without cellular pseudo-palisading. Due to the presence of pleomorphic tumour cells, glioblastomas were initially called as ‘glioblastoma multiforme’, a term that is no longer

used. Confined to the central nervous system (CNS), glioblastomas are highly invasive, infiltrating surrounding normal brain parenchyma, but do not show metastases.

The most common symptoms in glioblastoma patients includes a slow progression of neurologic deficit usually motor weakness, increased intracranial pressure including headaches, nausea, seizures, vomiting, and cognitive impairment caused due to infiltration of the tumour cells in different parts of the brain [9].

Accumulation of genetic alterations arising from both intrinsic and environmental factors contributes to the development of glioblastomas. Several of the hereditary syndromes including Cowden, Turcot, Li-Fraumeni, Neurofibromatosis type 1 and type 2, Tuberous Sclerosis, and familial Schwannomatosis have been associated with an increased risk of glioma [10]. Association with few genetic susceptibility loci such as 20q13.33 (*RTEL*), 5p15.33 (*TERT*), 9p21.3 (*CDKN2BAS*), 7p11.2 (*EGFR*), 8q24.21 (*CCDC26*), and 11q23.3 (*PHLDB1*), have also been identified however, variability is observed across different molecular subsets [11].

## **1.1.2 Diagnosis, prognosis and treatment of Glioblastoma**

### *1.1.2.1 Diagnosis*

Based on the EANO guidelines, diagnosis of GBM is attained through MRI or CT imaging techniques, with glioblastoma tumours appearing as a space-occupying, heterogeneously contrast enhancing lesion surrounded by irregular boundaries associated with peritumoral edema as shown in figure 1.2 [12]. Advanced techniques like diffusion weighted imaging (DWI), perfusion-weighted imaging (perfusion MR) and MR spectroscopy have enabled better understanding of the pathophysiology of GB tumours and its differentiation from other brain tumour-mimics like infarction.

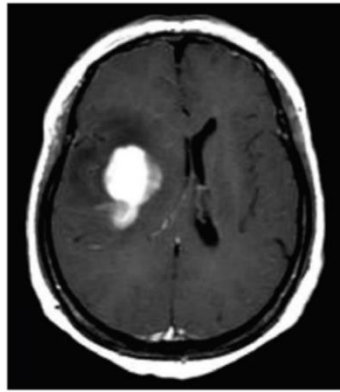


**Figure 1.2: MRI image of GBM:** T1-weighted gadolinium enhanced MRI scan showing contrast enhancing GBM tumour <sup>[13]</sup>.

#### 1.1.2.2 Prognosis

Prognosis in GBM relies on the routinely used clinical markers of tumour size, its anatomical location, Karnofsky Performance Score (KPS), recursive partition analysis (RPA), histo-pathological and radiological features namely MIB-1 labelling index, contrast enhancing tumours, amount of tumour necrosis on preoperative MRI, peritumoral edema and perfusion parameters [14-16]. The prediction of therapy response and stratification of GBM patients for chemotherapy is currently based on the evaluating Isocitrate Dehydrogenase 1 and 2 (IDH1/2) mutation and the promoter methylation status of O-6-methylguanine-DNA-methyltransferase (MGMT) in the tumour samples. Independently, MGMT hypermethylation has been shown to improve prognosis and overall survival of patients from 24% to 49% at 2 years and 5% to 14% at 5 years when treated with RT+TMZ compared patients treated with RT alone [17, 18]. However, patients harbouring unmethylated MGMT also demonstrate long term survival, thus suggesting involvement of other contributing factors in the therapy response.

Identification of four molecularly distinct subgroups of GBM: classical, mesenchymal, proneural and neural by Verhaak *et al* based on 840 gene signatures have

provided newer insights into the pathogenesis of this tumour [19]. These subtypes display variable genomic and transcript alterations along with the clinical outcomes. While the classical subgroup shows amplification of mutant EGFR variant III and loss of PTEN; the mesenchymal subtype exhibits NF1 mutations, loss of TP53 and CDKN2A and is associated with poor prognosis. Constituting of younger group of patients, the proneural subgroup distinctly shows enrichment of IDH1/2, TP53 mutations in along with amplifications of PDGFRA, CDK6, CDK4, and MET and show higher survival rate. Lastly, the neural subtype displays molecular signatures similar to that of neurons but does not show unique distinguishing alterations compared to other subtypes. Furthermore, Noushmehr *et al* using The Cancer Genome Atlas (TCGA) dataset identified a distinct subtype of GBM tumors referred to as a glioma CpG island methylator phenotype (G-CIMP), displaying hypermethylation at multiple loci [20]. These G-CIMP samples had distinct molecular and clinical features, harboring IDH1 mutation at high frequency. The molecular profiling of GBM tumors has thus, further strengthened the understanding of its underlying biology. However, the existing knowledge of the tumour has not successfully been able to improve the clinical outcome of the patients and hence, there is an urgent need to identify newer molecular markers for better prognosis and treatment of this disease.

#### *1.1.2.3 Standard of care*

The treatment regime includes radical surgical resection followed by adjuvant radiotherapy combined with chemotherapy. A total of 60Gy divided in 30 fractions is typically given for GBM treatment. The DNA alkylating agent temozolomide is administered orally, concomitantly with radiotherapy for 6 cycles, followed by an adjuvant course based on randomized phase 3 study conducted by Stupp *et al* that reported the increase in median survival to 15 months vs 12 months with radiotherapy and temozolomide vs radiotherapy

alone, respectively (hazard ratio, 0.63;  $P < .001$ )[17]. An increase in 2-year survival rate was also observed in the same set of patients as compared to radiotherapy alone. Subsequent analysis revealed that tumours harbouring promoter methylation of the DNA repair enzyme O6-methylguanine-DNA methyltransferase (MGMT) were to display better response from the addition of temozolomide to radiotherapy as compared to patients with unmethylated tumours[18]. However, a subpopulation of glioblastoma patients having low MGMT expression without promoter methylation are also reported [25], indicating that multiple regulators control the MGMT expression.

Bevacizumab or avastin, a humanized vascular endothelial growth factor (VEGF) monoclonal antibody targeting blood vessel formation (VEGF-A target) has been investigated for GBM. However, preliminary results of large randomized trials have demonstrated improvement in the progression-free survival (PFS) but did not result in increased overall survival [21, 22].

Apart from the conventional therapy, several additional therapies have been examined for GBM patients. Interstitial brachytherapy using iodine-125 (I-125) has been employed as an adjuvant treatment for smaller brain tumors and has indicated an improvement in median survival for few highly selected patients [23].

However, despite multimodal therapy, the clinical outcome of GB patients remains dismissible with low survival of 12-15 months and high rate of recurrence. Only about 10% of the patients survive till 5 years post therapy contributed by the highly resistance nature of these tumour cells.

## **1.2 Factors responsible for tumour resistance and recurrence**

Despite the advancement in the knowledge about glioma pathogenesis, this disease continues to be a major therapeutic challenge due to the existence of both inherent and

acquired resistant tumour cells. Several factors attributed to the treatment resistance have been reported. Incomplete debulking of the tumour due to the presence of highly infiltrative neoplastic cells in the inaccessible regions of the brain and an aberrant vasculature comprised hyper-proliferative, leaky and unorganized blood vessels are frequently the sources for disease recurrence. Furthermore, the dissemination of these highly invasive cells resistant to apoptosis in the normal brain parenchyma further reduces the efficacy of therapeutic drugs impermeable to blood-brain barrier. Importantly, these cells display cross resistance to other drugs that act by inducing apoptosis, thereby tolerating the chemotherapy.

Over-expression of proteins like Epidermal growth factor receptor/variant VIII (EGFR/EGFRVIII), Platelet Derived Growth Factor Receptor (PDGFR), Phosphatidylinositide 3-kinase (PI3K), and Signal Transducer and Activator of Transcription (STAT3), Survivin, BIRC3 and altered metabolic proteins has been reported in these resistant GBM cells [24-27]. Moreover, tumour suppressor genes such as p53, p21, p16, and PTEN are commonly mutated in GBMs while cell cycle regulators CDK4 and MDM2 are amplified in approximately 13% of the tumours, pointing to the instability in these cells [28, 29]. The genomic and transcriptomic sequencing of multiple regions of the same tumour as well as of single tumour cell has identified the presence of genetically different clones with innate capacity to resist the treatment, illustrating intra-tumoral heterogeneity [30, 31].

Lastly, GBM consists of highly tumorigenic cancer-initiating or glioma stem cells (GSC) capable of repopulating the entire tumour after therapy and exclusively expressing the neural stem cell surface marker CD133 [32]. The highly resistance nature of CD133-positive GSC more resistant to radiation therapy than CD133-negative tumour cells [33] has necessitated a change in the drug designing strategies.

### *1.2.1 DNA repair and cancer*

Eukaryotic cells are equipped with mechanisms to protect them against internal agents such as free radicals generated by cellular metabolism and exogenous agents like ionising radiation, UV light, chemical carcinogens and chemotherapeutic drugs that perturb the structure of DNA[34]. Cells have developed highly conserved DNA-damage responses that activate different repair pathways to maintain the genome integrity and survive the genotoxic stress. These responses are tailored to the type of insult inflicted on the DNA and includes: (a) direct repair of alkyl adducts by O6-alkylguanine DNA alkyltransferase (AGT); (b) base excision repair (BER) to repair single strand breaks and mutated bases; (c) double strand breaks repair by homologous recombination (HR), non-homologous end joining (NHEJ) and single strand annealing (SSA); (d) nucleotide excision repair (NER) for the removal of DNA adducts; (e) repair of cross-links by DNA inter-strand cross-link repair and (f) DNA mismatch repair (MMR) for the repair of mismatches and insertion/deletion in the DNA[34]. Since chemotherapy and radiation are the two main treatment modalities currently used to improve poor clinical outcomes of cancer patients, the cytotoxicity of these agents is directly dependent on the cell's ability to illicit an efficient DNA damage repair (DDR) response.

Several studies have demonstrated that the activation of DDR proteins during early stages of tumorigenesis [35, 36], induced due to the oncogene-mediated DNA damage, limits the proliferation and growth of tumour cells [37, 38]. Therefore, not surprisingly, a plethora of reports have indicated modulation of DNA repair proteins by the tumour cells during the progression of the disease and later also affecting their response to chemotherapeutic drugs. The summary of the aberrations in DNA repair genes across different cancers has been depicted in figure 1.3. Apart from these, aberrations including MGMT methylation has been associated with lymph node metastasis in gastric carcinoma [39], related to poor prognosis in human lung adenocarcinomas [40] and better clinical response in diffuse large B-cell lymphoma patients [41] and glioblastoma (hypermethylated MGMT) upon treatment with

temozolomide [42]. Furthermore, loss of mismatch repair proteins hMLH1 and hMSH2 have been predicted to confer resistance to therapy in lymph node positive breast cancer patients [43] and was predominantly observed in invasive muscle and high grade transitional cell carcinoma (TCC) of the bladder than the low grade tumours [44]. Mao *et al* have shown that the refractory or relapsed AML patients

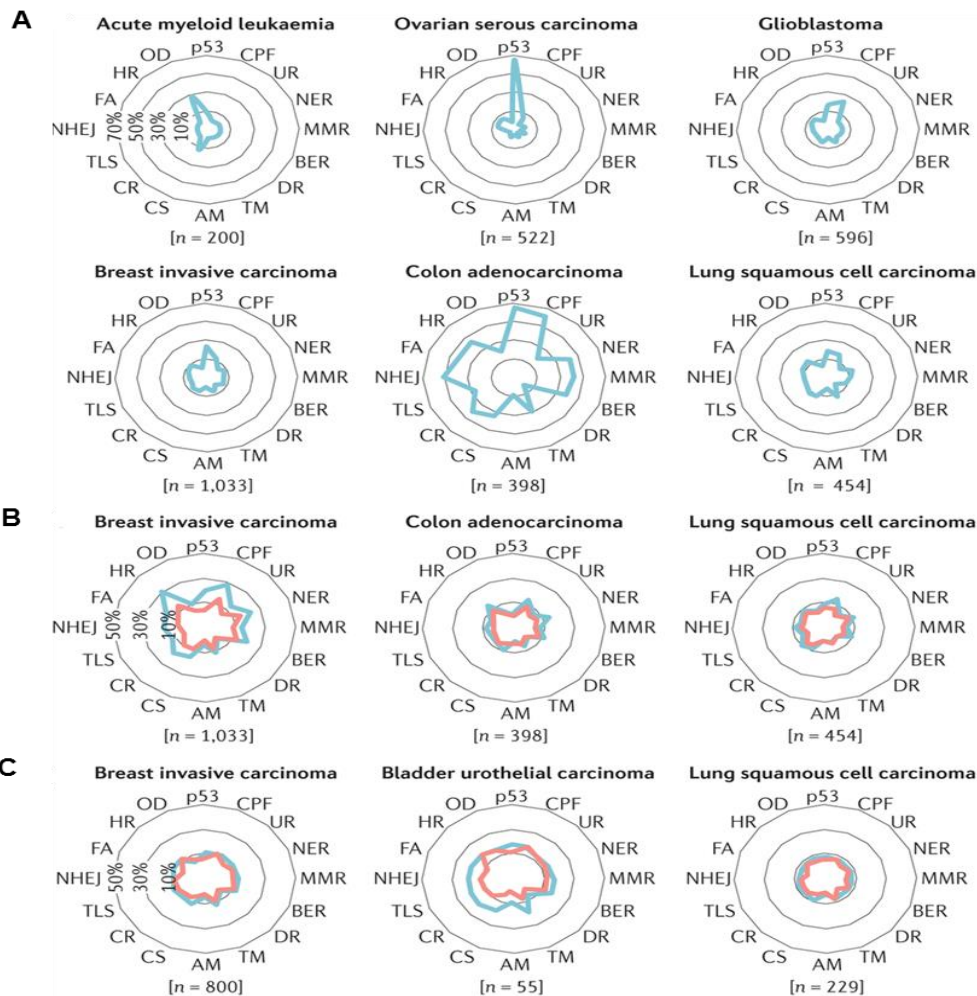


**Figure 1. 3: Extent of alterations in DNA damage response (DDR) proteins in different cancers.** Concentric circles depict the percentages of patients harbouring mutations. A) Radial plots showing the proportion of patients with protein-coding mutations in DNA repair and its related pathways as determine by the radius length. B) Copy number variation in the different DDR pathways (red indicates loss of genes; blue indicates gain of genes). C) Expression level variation in DDR pathways (red indicates down-regulation; blue indicates

up-regulation). AM, alternative mechanism for telomere maintenance; BER, base excision repair; CPF, checkpoint factor; CR, chromatin remodelling; CS, chromosome segregation; DR, direct repair; FA, Fanconi anaemia pathway; HR, homologous recombination; MMR, mismatch repair; NER, nucleotide excision repair; NHEJ, non-homologous end joining; OD, other double-strand break repair; TLS, translesion synthesis; TM, telomere maintenance; UR, ubiquitylation response<sup>[45]</sup>.

significantly harbour more frequent MMR defects compared to the newly diagnosed patients and may aid in disease progression [46]. Recent reports have also shown that the repeated exposure of glioblastoma patients to temozolomide leads to induction of mutations in mismatch repair genes making the tumour cells resistant to the drug [47].

Of all the insults to DNA, double-strand breaks are the most deleterious and if left unrepaired can cause apoptosis or senescence while erroneous repair can result in genomic instability [48]. The radiation as well as several chemotherapeutic treatments used as a first line of therapy in most of the cancers induces highly lethal form of DNA damage: double strand breaks (DSBs). Additionally, DNA damage induced by alkylating drugs are then further converted by mismatch repair into secondary lesions like stalled replication forks that eventually lead to the formation of DNA double-strand breaks[49]. Cellular responses to this cytotoxic lesion includes activation and induction of DNA repair proteins along with several cell cycle checkpoint proteins operative in G1,S and G2-M phases of the cell thus, providing time for the efficient repair of the DSBs [50]. An important aspect of the DNA-damage response is the reorganization of chromatin structure at the site of DNA damage triggered by the phosphorylation of H2AX in the mammalian cells, making damaged DNA accessible to repair proteins[51].

The DNA repair signalling cascade in mammalian cells involves a serine/threonine protein kinase ATM, a crucial repair component that senses the damage, undergoes auto-phosphorylation at serine 1981 and further activates the downstream substrates including H2AX, p53, Chk2 (checkpoint kinase 2), BRCA1 (breast cancer 1) and NBS1 (nijmegen breakage syndrome 1 protein) [52] as shown in figure 1.4.

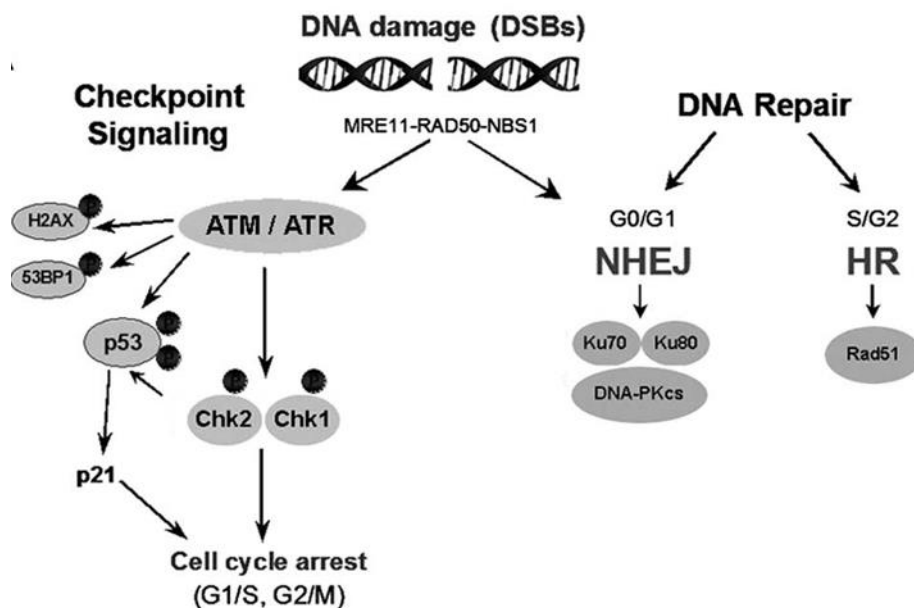


**Figure 1.4: Double strand break repair pathway in humans.** Shows the proteins involved in sensing (ATM/ATR) and downstream activation of DSB repair pathway [53].

Deficiency of ATM leads to development of an autosomal recessive hereditary disorder ataxia-telangiectasia (A-T) displaying sensitivity to ionising radiation and increased the risk of cancers. In line with its tumour suppressor function, ATM is frequently reported to be mutated in many human cancers including lung [54], colorectal [55], breast [56], mantle cell lymphomas [57] and haematopoietic cancers [58]. Furthermore, loss of ATM has been shown to enhance the growth and progression of glioblastoma [59]. However, in contrast to the bulk tumour, glioblastoma stem cells (GSC) show up-regulation of ATM activity, Chk1

(checkpoint kinase 1) and Chk2 which upon ATM inhibition abrogates the survival of GSC's [33, 60].

Apart from ATM, ATR (Ataxia Telangiectasia and Rad3 related) activation is brought about by different damages including DSBs, replication stress, base adducts and is required in the repair of persistent single-stranded DNA. Loss of ATR leads to early embryonic lethality in the mouse [61, 62] while causes reduction in cellular viability in chicken DT40 B-lymphocytes, suggesting its uncompensated role in repair during early development. However, in case of cancer cells, recent reports have suggested that selective inhibition of ATR in cancer cells could induce cytotoxicity in them, ameliorated by depletion of p53. Functional inhibition of ATR in a p53-deficient tumours was shown to enhance the oncogene induced replication stress, increasing the levels of DNA damage and eventually inhibiting the growth of tumour cells [63-65]. Importantly, Schoppa *et al* demonstrated that hypomorphic ATR mutation induced apoptosis of RAS-driven tumours while having minimal toxicity on normal bone marrow and intestine [65], suggesting that the partial inhibition of ATR may be sufficient for selective killing of cancer cells. Overall, these studies have encouraged development and use of specific, potent ATR inhibitors for targeting cancers.

DSBs are mainly repaired by homologous recombination (HR) and non-homologous end-joining (NHEJ)[66] as depicted in figure 1.5. While HR occurs during S and G2 phases of the cell cycle, requiring extensive homology or sister chromatid as a template for the repair of DNA DSBs, NHEJ requires limited or no homology for end joining, operates throughout the cell cycle and hence is more error prone[66-68].

NHEJ pathway is triggered by the binding of heterodimeric DNA binding regulatory Ku complex, Ku70 and Ku80 onto the free DNA ends. This complex further recruit DNA-dependent protein kinase (DNA-PKc), which then undergoes activation by the DNA-bound Ku complex. The ligation of the broken ends is then further conducted by Artemis, the

XRCC4/ligase IV recruited to the complex. These NHEJ repair proteins have long been implicated in carcinogenesis, owing to its role in the maintenance of genomic instability [69]. In vivo experiments have shown that the mice lacking Ku70 protein displayed higher incidence of thymic lymphomas [70], although spontaneous mutations in Ku70 or Ku80 have not been reported in humans suggesting their requirement for viability. Similarly, studies on human samples with altered DNA-PKcs activity have shown an indirect correlation to its activity, genomic instability and cancer incidence in breast and cervical cancer [71].

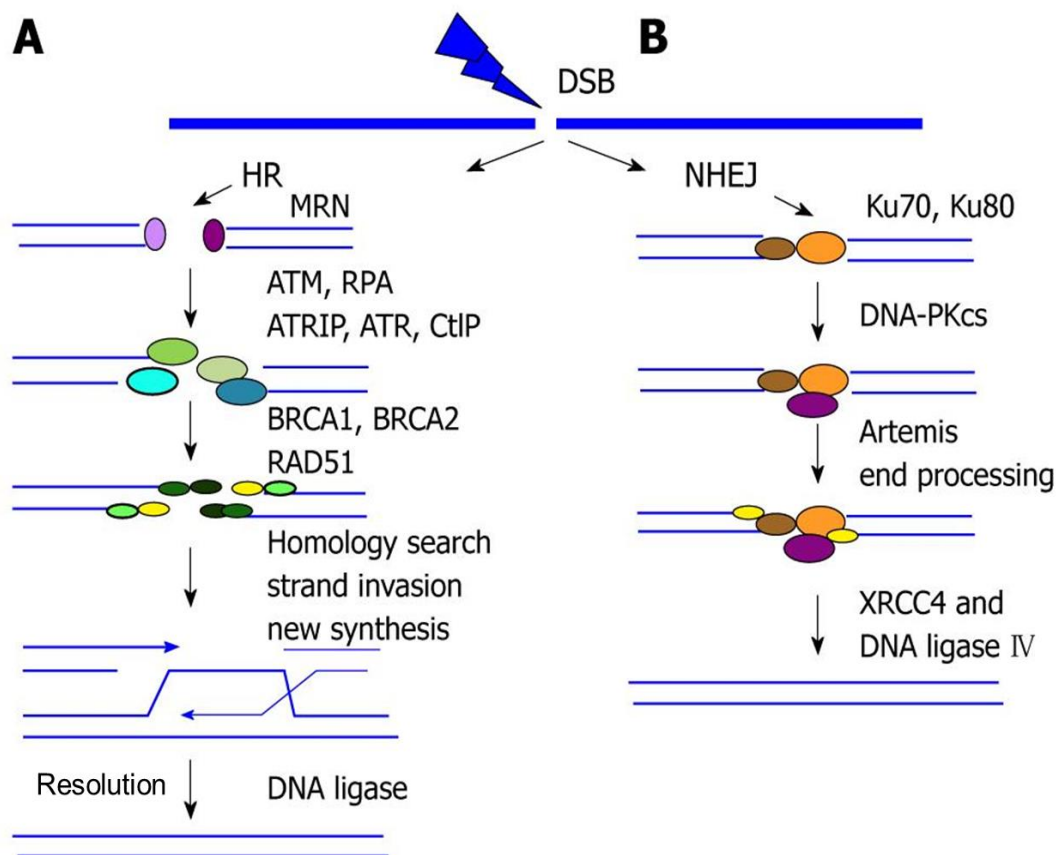


**Figure 1.5: NHEJ and HR pathway in humans.** A and B) Shows the molecular players involved at different stages of the HR and NHEJ repair pathways, respectively. Modified from <sup>[72]</sup>.

Mice lacking DNA-PKcs show higher sensitivity to IR and other DNA cross-linking agents [73]. Furthermore, XRCC4 and DNA ligase IV deficiency in p53 null mice develop pro-B lymphomas while in a functionally active p53 background led to neuronal apoptosis during early embryogenesis [74-77]. Overall, several studies have demonstrated a significant role of NHEJ pathway in maintaining genomic stability and suppressing carcinogenesis. Thus, there have been extensive studies focused on developing drugs that target NHEJ repair components. Based on these studies, NU7026, a specific DNA-PKcs inhibitor was developed and was reported to enhance the cytotoxicity of topoisomerase inhibitors in leukemia cells [78]. Similarly several compounds specific to DNA-PK have been developed and tested in different cancer models, demonstrating their potential as chemo- or radio-sensitizers [79, 80].

Compared to NHEJ repair, homologous recombination repair (HR) is a high-fidelity, template-dependent repair process that recognizes variety of DNA damages including DNA gaps, DNA double-stranded breaks (DSBs) and DNA interstrand crosslinks (ICLs)[81]. The conventional model for HR pathway: double strand break repair pathway (DSBR) begins with recognition and processing of DSBs by the MRN (Mre11-Rad50-NBS1) complex, creating short 3' single-stranded overhangs. Further, the single stranded overhangs are bound by RPA32 which along with Rad51 protein forms a filament of nucleoprotein coating the single stranded DNA [81]. This nucleoprotein filament after finding sequences similar to that of the overhang, begins to move onto the similar or identical recipient DNA duplex and forming a Holliday junction with the homologous chromosome. Chromosomal cross-over eventually leads to the sealing of the double strand breaks[81]. Mutation in many of these HR machinery components including RAD genes show embryonic lethality in mice [82, 83], caused due to excessive accumulation of unrepaired damage [84]. Additionally, these HR-defective cells display hypersensitivity to cisplatin or thymidine agents that work by causing stalling of the replication forks [85, 86]. Furthermore, germline mutations in the BRCA2

protein which is known to interact with RAD51 protein [87], accounts for 5-10% breast cancer and 10-20% ovarian cancer [88]. In glioblastoma particularly, glial initiating cells have been reported to undergo homologous recombination repair more efficiently as compared to the non-tumorigenic neural progenitor cells to repair the damage induced by radiation and thus, could be targeted using small molecule inhibitor against ATM [89, 90].

Thus, several reports have successfully demonstrated the potential of using DNA repair inhibitors either alone or in combination with the current therapeutic agents to prevent tumour formation. However, understanding of the regulation of DNA repair pathway will be required for development of highly specific and efficient drugs targeting specifically the cancer cells and not being toxic to the normal cells.

### *1.2.2 Epigenetics, DNA repair and cancer*

Epigenetics defines the study of changes that alters the expression of genes, independent of the genetic changes. These non-heritable changes are brought by epigenetic modifications like DNA methylation, histone post-translational modifications and alteration of the positioning of the nucleosomes. Initially known to regulate the normal embryonic development, epigenetics now has been shown to co-operate with the genetic alterations in promoting cancer development and progression. Epigenome of the cancer can be characterized by global changes in the DNA methylation as well as histone modification patterns along with the altered expression of chromatin-modifiers which eventually can confer a growth advantage to tumor cells promoting tumorigenesis.

Global DNA hypo-methylation at various genomic sequences including retrotransposons as well as specific genes like MGMT has been implicated in variety of cancers, increasing the genomic instability and conferring resistance to chemotherapeutic drugs[18]. Apart from hypo-methylation, hyper-methylation of CpG island of the tumor suppressor genes like *Rb* ,

*p16*, *BRCA1* as well as silencing of transcription factors such as *RUNX3* in esophageal cancer[91] and *GATA-4* and *GATA-5* in colorectal and gastric cancers [92], and DNA repair genes like *XPC*, *MLH1*, *BRCA1*, *XRCC5* etc. may further promote tumor progression [93-95].

Histones are highly basic proteins found in eukaryotic cell nuclei that package and order the DNA into structural units called nucleosomes. These nucleosomes consists of 4 core histones H3, H4, H2A, and H2B forming a histone octamer wrapped around 146bp of DNA [96]. These histones undergo variety of posttranslational modifications (PTMs) including methylation, acetylation, phosphorylation, ubiquitylation and SUMOylation commonly occurring on the flexible N-terminal tail regions [97]. These modifications alter the chromatin structure directly or indirectly through the recruitment of histone modifiers and/or nucleosome remodelling complexes[98]. Recent advances in the high-throughput sequencing have led to the mapping of cancer-associated chromatin changes that regulate the chromatin state, dynamics and gene expression. Several of the identified histone modifications include hypo-acetylation of H4-lysine 16 (H4K16ac) and provide a few more examples of acetylation of Histones in cancer [99]. These acetylation marks are removed by the histone deacetylases or HDACs reported to be highly over-expressed in various cancers and notably targeting of these HDACs have shown promise for epigenetic therapy of cancer [100, 101]. In addition to histone acetylation, methylation patterns have also been implicated in altering the gene expression in the cancer cells [95]. While methylation of H3K9 and H3K27 is associated with gene silencing, methylation of H3K4, H3K36 and H3K79 induces transcriptional activation in many cancers [102-104]. These histone modifications recruit other nucleosome remodelling complexes, for example interaction between H3K9 and H3K27 bound by HP1 (Heterochromatin Protein 1) and Polycomb repressor complex 2 (PRC2), respectively to bring about the chromatin architectural changes [105].

Importantly, apart from its role in transcription regulation, recent studies have also demonstrated a role of histone methylation in cell cycle checkpoints and several of histone methylations have now been identified as key regulators of double strand break repair response. H3K9me<sub>3</sub> is known to be required for mediating cellular response to DNA damage in the early and late phases of the response. In the early phase of repair response, immediate loading of HP-1, KAP1 complexes onto the damaged DNA cause up-regulation of H3K9 methylation which in turn induce a large repressive heterochromatin state. This further leads to chromodomain mediated binding of Tip60 to H3K9me<sub>3</sub> which subsequently acetylate, activate ATM [106-109]. A recent study have shown that H3K9di-methylation mediate interaction with HP-1 and is required to retain BARD1 and BRCA1 at the DNA damage sites, thus promoting HR repair [110]. Similarly, Botuyan *et al* showed that a direct interaction between 53BP1 and histone methylation H4K20me<sub>2</sub> via tudor domains in 53BP1 leads to its relocation onto the DNA DSBs sites [111].

Histone methylation are catalysed by histone methyltransferases (HMT) belonging to two groups: 1) containing the SET or Su(var)3-9, Enhancer of Zeste [E(Z)], and Trithorax (trx) domain and 2) lacking SET domain. These modifications are reversed by flavin adenine dinucleotide (FAD)-dependent histone demethylases and Jmjc domain-containing histone demethylases [112]. Many of these histone methyltransferases/demethylases are also reported to be involved in carcinogenesis [112]. For example, EZH2 methyltransferase responsible for H3K27 methylation is reported to be overexpressed and associated with metastatic breast cancer, specific down-regulating RAD51-like proteins thereby, impairing the HR repair[113, 114].

Overall, these studies have demonstrated the important role of histone methylation, HMT in cancer as well as in regulating DNA damage repair response.

## **Rationale**

Cancer therapy including radiation used in GBM works by causing double strand breaks (DSBs) in DNA and inducing apoptosis in cancer cells. The efficacy of DNA damage-based therapy in GBM can be modulated by DNA repair pathways. Since the physiological substrate of DNA damage repair machinery is packed into chromatin, the efficiency of DNA damage repair in a cell depends on the accessibility of these repair proteins to the damaged DNA. In this regard, histone methylations play a key role in regulating DNA repair response by directly interacting with the repair proteins. This led us to hypothesize that residual resistant GBM cells differ from the bulk tumour cells such that they alter the of DNA damage repair response by exhibiting differential chromatin modifications, either acquired during the administration of radio-therapy or innately present. These changes in chromatin structure that regulate DDR pathway efficiency and choices in turn influence the survival of residual cells post therapy. Therefore, understanding of the chromatin mediated DDR response in the resistant cells may enable development of therapeutic strategies for specific targeting of these cells. Therefore, this thesis work explores the role of the chromatin mediated DDR response in the resistant cells and may thus form the basis of identification of newer targets specific to the resistant GBM cells.

As a prerequisite for these studies, generation of an *in vitro* radiation resistant model derived from patient derived primary cultures and cell lines has been developed that enabled us to study the molecular changes occurring in the tumour post radiotherapy and elucidate mechanisms contributing to the survival of resistant cells

**Key Question:**

To understand the role of chromatin and DNA damage repair pathway that contribute to the survival and relapse of glioblastoma cells post radiation.

**Specific Aims:**

- 1. Establishment and characterization of the in vitro radiation resistant model from glioblastoma cell lines and patient samples.*
- 2. Identification of differential double strand break repair pathway activation and chromatin changes in radiation resistant cells.*

## **Chapter 2**

***Establishment and characterization of the in vitro radiation resistant model from glioblastoma cell lines and patient samples***

This chapter is divided into two parts: 1) discuss the establishment of *in-vitro* radiation model whereby we observed a small percentage of innately resistant cells (RR) surviving the lethal dose of radiation which further went on to form recurrent population. The characterization of the RR cells is also included in the first part of the chapter; 2) discuss the characteristics of the recurrent cells and the potential of global techniques like RNA sequencing and Raman spectroscopy in the classification of these recurrent cells.

## **2.1. Establishment of the *in-vitro* radiation resistant model**

### **2.1.1 Introduction**

Current treatment modality for GBM includes maximum surgical resection followed by standard radical radiation and chemotherapy. Despite radiotherapy, the propensity for the local recurrence increases and therefore, the median survival time of GBM patients remains in the range of 21 months [17, 115]. Current GBM therapies, while killing the majority of tumour cells, fails to eliminate these residual resistant cells which survive to regenerate new tumours [116]. In this context, innate resistant characteristics of these cells influence the therapy response and outcome of the disease. The inability to identify the changes in the resistant cells during the course of the treatment hinders our understanding of the mechanism of radio-resistance in GBM or any clinical significance associated with them. As a result, GBM remains incurable and treatment of GBM poses a major challenge.

The current field relies on studying the course of GBM using *in vivo* mouse xenografts and orthotopic models [117, 118]. However, the number of observations post radiation therapy still remains limited. Determination of new methodologies for generation of patient derived cultures has enabled identification of novel molecular prognostic predictors. The use of patient derived cultures from different tumour tissues have led to the discovery of molecular signatures and phenotypes unique to the cancer cells, significantly correlating with

the clinical outcome [119-121]. Furthermore, studies using patient derived cultures have helped in predicting therapy response in each individual [122]. Hence, to explore the survival and relapse mechanisms in glioblastoma, we established an *in vitro* radiation resistant model from patient samples and cell lines that recapitulate the course of GBM from the treatment to its recurrence as occurring *in vivo*.

Multinucleated and giant cells (MNGCs) are frequently seen in human cancer tissues and cell lines, mostly associated with late stages of tumour [123-130]. The primary mechanism contributing to the formation of MNGCs has shown to be the failure of cytokinesis and endo-replication that eventually generate polyploid cells [131, 132]. Recent reports have also suggested a role of entosis or cell-in-cell structure formation in inducing multinucleated-giant cells [133]. Another mechanism, cell fusion is known to generate multinucleated cells during development [134] but in the context of cancer such events are rare and have been implicated only in virally induced transformation of the normal cells, tumours of tendon sheath and bone, enhancing the propensity to cause chromosomal instability and eventually resulting in aneuploidy [135-137]. Some of the studies also report the multinucleated cells formation as result of radiation, though these cells so reported eventually underwent cell death by mitotic catastrophe [138-140]. The pre-existing MNGCs in tumours are thought to be responsible for increased resistance to therapies [141-143] however, the precise functional role of these cells in cancer is still not known.

In this chapter, we show that in a heterogeneous population of glioblastoma, there exist a small population of mono-nucleated cells (radiation resistant cells) with innate capacity to survive the lethal dose of radiation. These radiation resistant cells survive the initial onslaught of radiation by activation of pCdk1 (Y15) leading to their cell cycle arrest during which they repair their damaged DNA. Although non- proliferative, these cells are highly motile and undergo cell - cell fusion at high frequency to form multinucleated giant

cells (MNGCs), fusion events also induce senescence. MNGCs release senescence associated proteins and activate pAKT and pro-survival genes.

On further examination of the clinical relevance of molecular features associated with radiation resistant cells from twenty glioblastoma patient samples, we observed that percentage of giant cells in RR population ( $p=0.046$ ) alone or in combination with tumour volume ( $p=0.008$ ) predicted clinical outcome demonstrating the potential of giant cell formation as a prognosticator.

Thus, our findings suggest that radiation resistant glioma cells can sustain survival under stressful conditions via MNGC formation during the transient non-proliferative phase. Accordingly, we show that relapse in glioblastoma can be prevented by disrupting the non - proliferative phase of the radiation resistant cells with inhibitor of Wee1 kinase, a negative regulator of cell cycle and specifically targeting MNGCs by using Wiskostatin, an inhibitors of cytokinesis.

## **2.1.2 Materials and methods**

### *2.1.2.1 Cell culture and drug treatment*

Glioblastoma Grade IV cell lines U87MG and SF268 were obtained from ATCC in 2011. These cell lines were last authenticated in the laboratory by Short Tandem Repeat (STR) profiling based on eight markers in May 2014. The cell lines were maintained in DMEM containing 10% (v/v) FBS, penicillin (200 U/ml), streptomycin (100  $\mu$ g/ml) and incubated at 37°C in a humidified incubator with an atmosphere of 50 mL/L CO<sub>2</sub>. Wee1 kinase inhibitor (MK1775) and Wiskostatin were obtained from Calbiochem.

### *2.1.2.2 Patient samples*

The project was approved by the institutional review board and informed consent in the language understood by the patients was also taken prior to tumour collection. Tissue was collected after surgery from 20 patients with confirmed glioblastoma. The survival status of these patients was determined based on the medical records and telephonic interviews.

Patients underwent either maximal safe resection or subtotal resection depending on the depth and location of the tumour. The extent of resection was further determined based on post-operative MRI which was done within 48 hours post-surgery.

All the patients received focal conformal radiotherapy by 3D-CRT technique with concurrent temozolomide. A total of 60Gy in 30 fractions over 6 weeks was given to 12/20 (60%) while 6 cycles of adjuvant temozolomide was given to 12/20 (60%) patients. Only one patient received weekly once radiation of 35Gy in 5 fractions over 5 weeks. This patient did not receive any concurrent temozolomide but went on to receive six cycles of maintenance temozolomide after radiation therapy.

All the patients underwent diagnostic Magnetic Resonance Imaging (MRI) scan on a 3Tesla machine prior to surgery and within 48 hours of surgery. MR sequences included T1W images with contrast, T2W, T2FLAIR, MR perfusion and MR spectroscopy. On T1W contrast images, degree of contrast enhancement and volume of the enhancing tumor was calculated on volumetric contrast enhanced MR sequences using the post-processing software on Advantage Workstation (AW version 4.4) GE Medical Systems®. The lesions were further characterized on T2W images and the amount of perifocal edema was noted on T2FLAIR images. Relative cerebral blood flow (rCBF) and relative cerebral blood volume (rCBV) were assessed by commercially available post processing software on Advantage Workstation (AW version 4.4) GE Medical Systems®. The perfusion parameters were

calculated based on the rate of flow of the contrast within the tumour normalized to the normal brain parenchyma on a first-passage contrast-enhanced T2-weighted single-shot gradient-echo echo-planar sequence. The area under the perfusion curve (AUC) (Figure 2.1, lower panel) represents the rCBV value which is simply the volume of blood within a given mass of the region of interest (ROI) and the rCBF is represented by the net flow of blood within the same ROI (Figure 2.1, lower panel). Information regarding perfusion (rCBV & rCBF) was available in 12 patients. Additionally, MRS features like choline: NAA, choline: creatine and presence of lipid/lactate peaks were also investigated in the study.

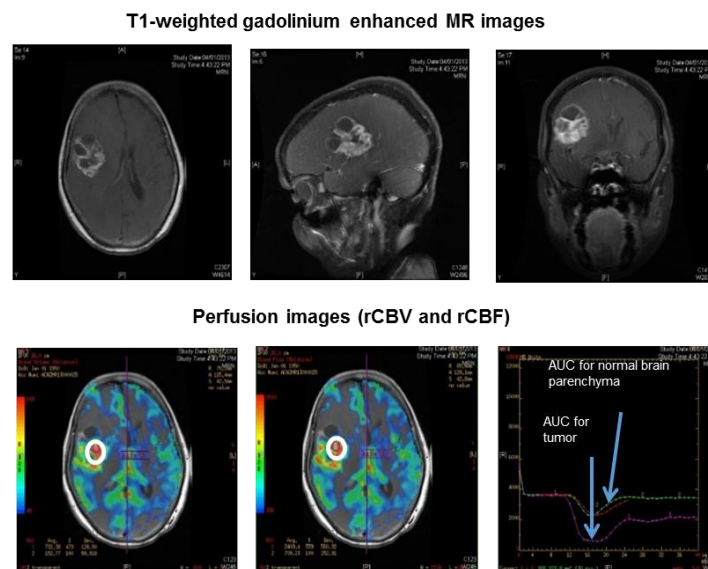


**Figure 2.1: T1-weighted and perfusion MR images depicting GBM.** T1W gadolinium contrast MR images from patient representing axial, sagittal and coronal planes showing solid cystic contrast enhancing space occupying lesion in temporal-parietal region of the brain (upper panel). Perfusion images for rCBV and rCBF measurements along with the graph depicting perfusion values from the region of interest compared to the contra-lateral normal brain parenchyma (lower panel).

Tumor sections were evaluated for necrosis classified as Confluent Necrosis (CN) or Palisading Necrosis (PN), calcification, MIB-1 labelling index (1:50, Dako, Glostrup, Denmark), P53 expression (clone D07, 1:50, Dako, Glostrup, Denmark), IDH1R132H (clone H09, 1:200, Dianova, Hamburg, Germany) by immunohistochemistry. P53 immunoreactivity was labelled as ‘positive’ in case of diffuse and strong staining in more than 50% of tumour cells, ‘focally positive’ wherever the staining was observed in 10-50% of cells and ‘negative’ if there were very few cells (<10%) with weak or moderate intensity or no staining. IDH1 mutation was labelled as either positive or negative.

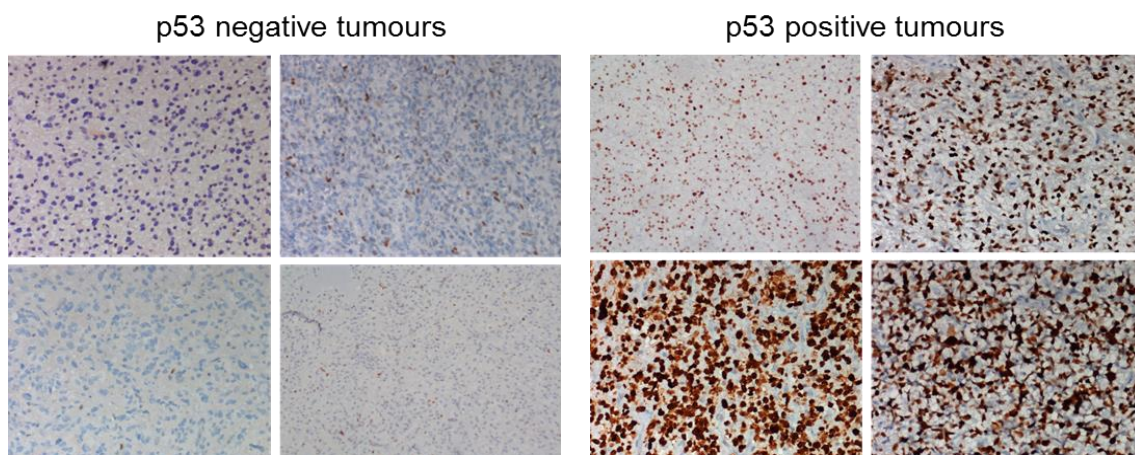


**Figure 2.1: Spectrum of p53 negative and positive tumours in our cohort.** The GBM tumour sections used in this stained for p53 are represented. The p53 expression varied in different samples where dark brown staining shows over-expressing or p53 positive tumours while absence of dark brown stain shows p53 negative tumours. Magnification X200. Scale bar- 50µm.

Fresh tissue samples were collected in DMEM containing 400U/ml of penicillin, 200 µg/ml of streptomycin. Single cell suspension was made using Brain Tumor Dissociation Kit (P) (catalogue number 130-095-942) as per the kit instructions. The tissues were first washed with PBS to remove blood vessels and necrotic tissue from the tumour samples and then transferred the tissue into C-tube containing pre-heated 3890µl of buffer X, 50µl of enzyme

N and 20µl of enzyme A. The tissues were then subjected for mechanical disruption using gentle MACS dissociator program h\_tumor\_02, followed by 15 minutes incubation at 37 °C under slow, continuous rotation. Further, the C tubes containing the samples were run on the gentleMACS Program h\_tumor\_03 and incubated for 10 minutes at 37 °C under slow, continuous rotation. In the final step, samples were run on gentleMACS Program m\_brain\_01 and the pellet was collected after centrifuging briefly and was seeded in DMEM: F12 media containing 15% (v/v) FBS, 1% of antibiotic cocktail containing fungizone and incubated at 37°C in a humidified incubator with an atmosphere of 5% CO<sub>2</sub>.

#### *2.1.2.3 Cell synchronization*

Cells from all the cultures were grown to 70% confluency in medium containing 10% serum. Cells were then washed with 1X PBS and incubated in medium containing 0.05 % serum for 72 hours. After 72 hours, cells were released in media containing 10% serum and irradiation using <sup>60</sup>Co γ-rays was carried out.

#### *2.1.2.4 Trypan blue assay*

Two million synchronized cells from all cultures were seeded in 10 cm<sup>2</sup> dishes and irradiated with their respective lethal dose of radiation. Viable cells from these plates were counted every alternative day till 22 days to monitor the cell survival post radiation on a hemocytometer using trypan blue dye.

#### *2.1.2.5 Clonogenic survival assay*

To determine the survival fraction at 2Gy (SF2) as well as lethal dose of radiation for all the primary cultures and cell lines, clonogenic assay was carried out in a 60mm dish using 1000-3000 cells as per the plating efficiency of the glioma cultures. The colonies (>35 cells) were fixed with pre-chilled methanol: acetic acid (3:1), stained with 0.5% crystal violet and

counted after 10-15 days of radiation. SF2 values and lethal dose was calculated from the radiation-survival curve using SPSS software version 21®.

#### *2.1.2.6 Propidium Iodide Staining*

Cells were harvested, washed once with 1X PBS and fixed with 70 % cold ethanol overnight at 4 °C. Fixed cells were then washed with PBS and incubated with RNase A (40µg/ml) and Propidium Iodide (40 µg/ml) for 1 hour at 37 °C. These cells were acquired on FACS Caliber, BD Biosciences. Cell cycle analysis was done using ModFitLT 2.0 program.

#### *2.1.2.7 BrdU staining*

Briefly, cells coated onto the coverslips were incubated with 10µM of BrdU for 24 hours for each of the cell type. These were then fixed with 4% paraformaldehyde for 20 minutes at room temperature. After three washes with 1X PBS, the cells were treated with 2N HCl for 1 hour at room temperature. The cells were then washed with 1X PBS followed by three washes with 20mM glycine. The cells were then incubated with 2.5% normal donkey serum for 1 hour at room temperature to block non-specific sites followed by overnight incubation with anti-BrdU antibody (rat; 1:250; Abcam) at 4 °C. After washing thrice for 5 min with PBS, coverslips were incubated with FITC conjugated goat anti- rat antibody (1:450; Cell Signalling) for 45 min at RT. Nuclei were counterstained with DAPI (0.5 µg/mL) for 1 minute, washed thrice with 1X PBS and mounted using VECTASHIELD mounting media (Vector Labs). The cells were visualized under Zeiss LSM 510 Meta Confocal Microscope.

#### *2.1.2.8 CD133 staining*

The staining was varied out as per the product's instructions. Briefly, cells were harvested, washed with PBS and re-suspended in 10ul of staining buffer containing 0.5% of BSA in PBS. The cells were then incubated with 1ul of CD133/1 (AC133) antibody (MACS Miltenyi

Biotec) for 15 min in dark at 4 °C. The cells were then washed twice with staining buffer, re-suspended in 200ul of the buffer were acquired on FACS Caliber, BD Biosciences.

#### *2.1.2.9 RNA extraction, cDNA synthesis and qPCR*

Total RNA was extracted by TRIZOL Reagent (Invitrogen) according to the manufacturer's protocol. cDNA was synthesized using the SuperScript III First-Strand kit (Invitrogen) as per the manual instructions. qPCR was carried out using Roche Light Cycler Master Mix using Light Cycler 480 real time PCR system. GAPDH was used as an internal control. Relative changes of mRNA amounts were calculated using the  $\Delta\Delta C_t$  method. A list of all primers used for real time PCR are provided in Annexure I.

#### *2.1.2.10 $\beta$ -galactosidase activity staining*

Parent cells and radiation resistant cells were washed with 1X PBS, fixed with 0.5 ml of fixative solution provided in the Abcam Senescence detection kit (Ab65351) for 10 - 15 min at room temperature. Cells were then washed twice with 1X PBS and incubated overnight with 0.5 ml staining solution containing 20mg/ml of X-gal. They were microscopically analysed using Olympus IX- 71 for positive staining.

#### *2.1.2.11 Immunofluorescence*

Cells seeded on cover slips were fixed with methanol: acetic acid (2:1) at -20 °C for 10 minutes then washed with 1X PBS and permeabilized with 0.5% Triton X-100 for 15 minutes on ice. After subsequent washing, the cells were incubated for one hour at 37 °C in 5% BSA solution. The cells were then incubated with primary antibody: Nestin (rabbit; 1:500; Abcam),  $\beta$ -actin (mouse; 1:500; Sigma Aldrich), N-cadherin (rabbit; 1:500; Abcam) overnight at 4 °C. After washing thrice for 5 min with PBS, coverslips were incubated with FITC conjugated goat anti- rabbit antibody (1:100; Cell Signalling) for 45 min at RT. Nuclei were counterstained with DAPI (0.5 $\mu$ g/mL) for 1 minute, washed thrice with 1X PBS and

mounted using VECTASHIELD mounting media (Vector Labs). The cells were visualized under Zeiss LSM 510 Meta Confocal Microscope.

#### *2.1.2.12 Cell sorting based on scatter*

Trypsinized cells were washed with 1X PBS and suspended in DMEM containing 10 % FBS to make single cell suspension. For primary cultures, single cell suspension was made in DMEM: F12 media containing 15% FBS. Flow cytometric analysis was carried out based on their side and forward scatter. Sorting was performed using 100 $\mu$ m nozzle with BD Biosciences FACS Aria III cell sorter. 10,000 events were reported. Small and giant cells were sorted at a flow rate of 1000 cells/s to maintain the cell viability and were then finally seeded for subsequent experiments.

#### *2.1.2.13 Generation of stable cell lines over-expressing green and red florescence to monitoring cell-cell fusion*

The cells were transfected with 3 $\mu$ g of pEGFP-N<sub>2</sub> and pCDNA3.1-TdRed (to establish green and red florescence expressing cells) plasmids, mixed with 9 $\mu$ l of Lipofectamine 2000 (Invitrogen) and incubated overnight. Next day, DMEM containing 20% FBS was added to stop the transfection. These transfected cells were then put under selection with 500 $\mu$ g/ml of G418 for two to three weeks.

#### *2.1.2.14 Time Lapse studies*

pEGFP and TdRed expressing cells were co-cultured in equal number and radiated with lethal dose of radiation. After 6 days post radiation, time lapse images were taken with 30 minutes of interval time for 24 hours on Zeiss A.1 inverted microscope at 10X magnification.

#### *2.1.2.15 Annexin V/PI staining*

The protocol as defined by the Abcam kit manual (ab14085) was followed. The cells were trypsinized and washed with DMEM media. In each of the tube, 500 µl of the 1X binding buffer, 5 µl of Annexin V-FITC and 5 µl of propidium iodide was added and incubated for 10 minutes. The data were then acquired on FACS Caliber, BD Biosciences and analysed by Cell Quest.

#### *2.1.2.16 Western Blot analysis*

Cells were lysed using EBC lysis buffer (120 mM NaCl, 50 mM Tris-Cl (pH 8.0), 0.5% (v/v) Nonidet P-40, 50 µg/ml PMSF and protease, phosphatase inhibitor cocktail for 45 minutes on ice. The supernatant was collected and 30ug of protein was used for immuno-blotting using anti-pAKT (rabbit; 1:1000; Cell Signaling), anti-AKT (rabbit; 1:1000; Cell Signalling), and anti-pY15Cdk1 (mouse; 1:1000; Abeam). Actin (Sigma; 1:5000 dilutions) was used as a loading control. Immune-reactive proteins were visualized using an enhanced chemiluminescence (ECL) reagent (Pierce).

#### *2.1.2.17 Statistics*

Overall survival time (OS) was calculated from the date of surgery till the date of death due to any cause. The continuous parameters were grouped according to their levels with respect to the median values. These parameters were used for analysing the overall survival by Kaplan Meier curves and the level of significance (p-value) was tested by Log Rank test. Normality of the data was tested using Shapiro-Wilk Test. Bivariate correlation analysis (Spearman's correlation test) was computed to identify association between variables. All statistical analyses were carried out using SPSS software, version 21<sup>®</sup>.

The statistical significance of functional studies was evaluated using a two-tailed t-test.

### 2.1.3 Results

#### 2.1.3.1 Recapitulating radiation resistance in an in vitro cellular model developed from patient samples and cell lines. Subpopulation of Glioma cells survive lethal dose of radiation and become transiently non proliferative

The inability to monitor the radiation resistant residual cells of Glioblastoma after subjecting patients to treatment hinders the investigation of molecular steps that leads to the relapse of these cells into full grown tumours. Therefore, we developed a cellular model for resistance in the laboratory to investigate steps leading to relapse. We used 20 short term primary cultures, patient samples (PS) derived from fresh Glioblastoma grade IV patient samples and two GBM grade IV cell lines U87MG and SF268. First, we determined the lethal dose of gamma radiation for the primary cultures and cell lines by clonogenic assay. For this G1 synchronized cells were subjected to different doses of  $\gamma$  radiation and percentage survival was calculated from the colonies counted after 11-15 days post radiation (Figure 2.3). Lethal dose for patient samples ranged from 6-6.5 Gy (Figure 2.3 and Table 2.1.1) whereas for U87MG and SF268 it was calculated to be 8Gy and 6.5Gy, respectively showing their variation to the radiation sensitivity.

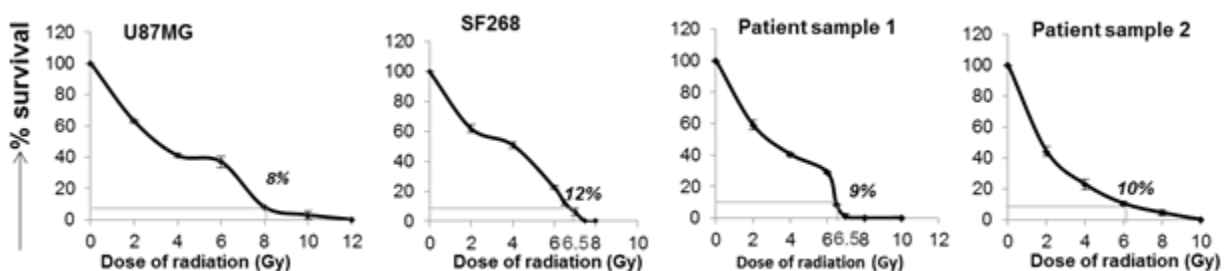


**Figure 2.3: Clonogenic assay of glioma cells showing percentage of surviving cells at different doses of gamma radiation.**

**Table 2.1.1: Lethal dose of radiation for all 20 primary cultures**

<b>Patient Sample Number</b>	<b>Lethal dose of radiation (Gy)</b>
<b>1</b>	6.50
<b>2</b>	6.00
<b>3</b>	5.00
<b>4</b>	5.50
<b>5</b>	7.00
<b>6</b>	4.50
<b>7</b>	6.00
<b>8</b>	6.00
<b>9</b>	6.00
<b>10</b>	4.00
<b>11</b>	8.00
<b>12</b>	7.00
<b>13</b>	5.00
<b>14</b>	5.50
<b>15</b>	7.00
<b>16</b>	7.00
<b>17</b>	6.00
<b>18</b>	4.50
<b>19</b>	4.00
<b>20</b>	4.00

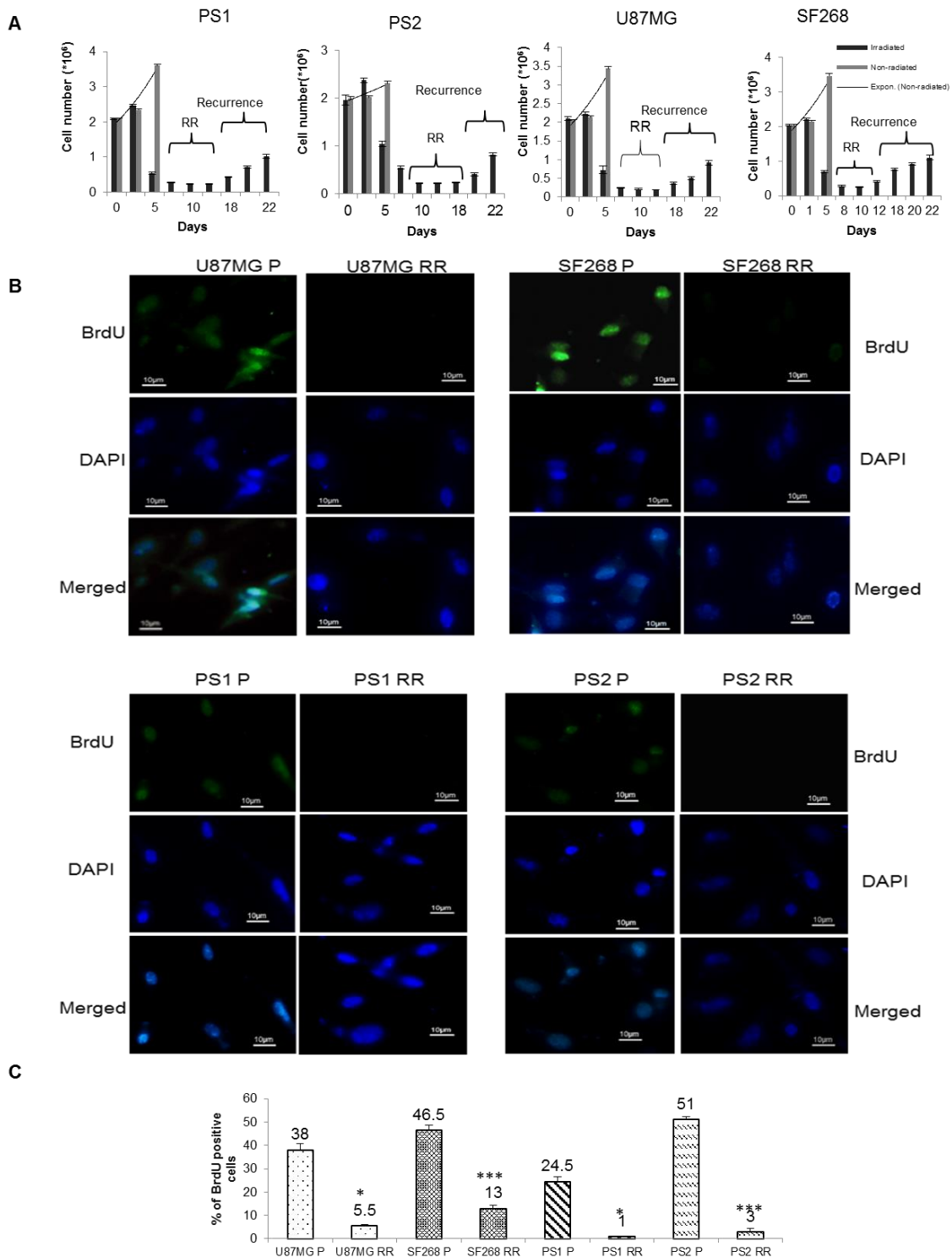


**Figure 2.4: Sub-population of Glioma cells escape lethal dose of radiation and survive.**

A) Bar graph showing the growth pattern of exponentially growing non-irradiated cells (grey bars) and irradiated cells (black bars). Cell numbers are plotted at different days after treating

the cells with lethal dose of radiation. Graph shows initial burst of proliferation and survival of radiation resistant residual tumours cells which relapse. B) BrdU staining in the parent and RR cells. Scale bar- 10 $\mu$ m. C) Quantitation of the cells showing positive staining of BrdU. \* denotes  $p \leq .05$ , and \*\* denotes  $p \leq .01$ .

Once the lethal dose of radiation was determined, glioma cultures were subjected to their respective lethal dose of radiation. Initially for 48hrs there was rapid proliferation of cells which was followed by massive cell death. However, approximately~7-10% cells in all the cultures escaped cell death and survived. These cells, subsequently called as radiation resistant (RR) cells from all the four cell cultures (U87MG, SF268, patient sample 1 and patient sample 2) exhibit a transient non-proliferative phenotype as shown by trypan blue assay and BrdU staining which last for approximately 7-10 days for all the cultures except for SF268 cells that show a shorter non- proliferative phase of about 3-4 days (Figure 2.4, B and C and table 2.1.2). However, after about 10 days of non-proliferation the RR cells regain their proliferative capacity, undergo cell division and resume normal growth to form relapse population.

#### *2.1.3.2 Radio-resistant tumour cells are enriched with radiation induced Multinucleated Giant Cells (MNGCs) and stem cell markers*

Further examination of radiation resistant cells showed that these cells obtained from patient sample and cell lines showed a significant enrichment of CD133 a known GBM stem cell marker, however a majority of the population was CD133 negative (Figure 2.5A).

Interestingly, there were also high number of multinucleated and giant cells (MNGC) confirmed by staining with  $\beta$ -actin or nestin and nuclear stain DAPI (Figure 2.5B).

Several reports exist from breast and ovarian cancers that have demonstrated the occurrence of pre-existing giant cells in the heterogeneous tumour [144]. These have been shown to impart

**Table 2.1.2: Characteristics of radiation resistant cells from 20 primary cultures.**

<b>Patient Sample Number</b>	<b>Day of resistant cell formation</b>	<b>Length of non-proliferative phase (NP)</b>	<b>Day of recurrent cell formation</b>
<b>1</b>	8	14	22
<b>2</b>	9	16	25
<b>3</b>	10	10	20
<b>4</b>	7	15	22
<b>5</b>	12	12	24
<b>6</b>	8	12	20
<b>7</b>	10	9	19
<b>8</b>	9	6	15
<b>9</b>	8	14	22
<b>10</b>	7	17	24
<b>11</b>	6	10	16
<b>12</b>	12	12	24
<b>13</b>	8	10	18
<b>14</b>	7	12	19
<b>15</b>	12	10	22
<b>16</b>	9	12	21
<b>17</b>	11	10	21

<b>18</b>	10	13	23
<b>19</b>	12	9	21
<b>20</b>	8	14	22

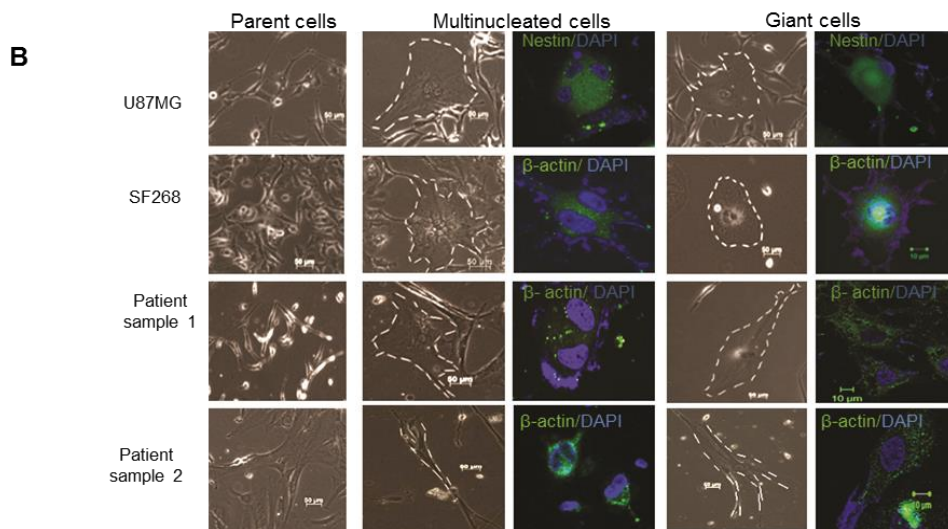
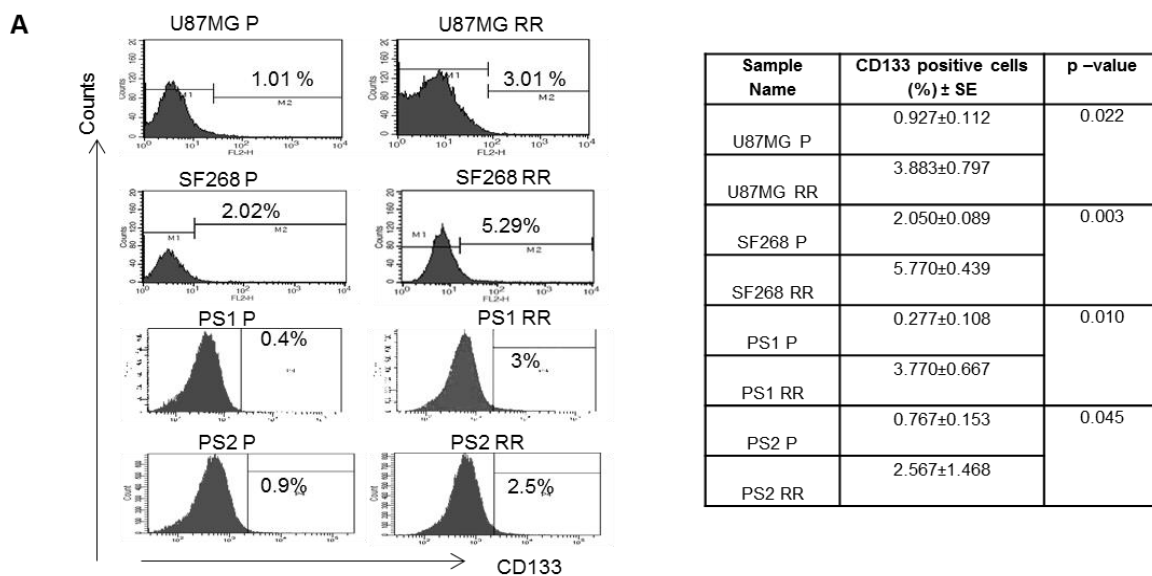


**Figure 2.5: Radiation resistant cells are enriched with radiation induced multinucleated and giant cells.** A) Histogram showing the percentage of CD133 positive cells in parent and radiation resistant cells. Table shows the % CD133 cells determined from three independent experiments. B) Phase contrast and immunofluorescence images of multinucleated and giant

cells from U87MG, SF268, patient sample 1 and patient sample 2. Images represent day 12, 5, 12 and 14 of non-proliferative phase for U87MG, SF268, patient sample 1 and 2, respectively. White dotted line in the phase contrast images shows the cell boundary. Multinucleated and giant cells are stained with Nestin and  $\beta$ -actin and counterstained with DAPI. Scale bar-10 $\mu$ m.

resistance phenotype to the cancer cells. We also observed small percentage (8-14% in cell lines and 1-2% in patient samples) of giant cells in our GBM samples therefore, we checked if the giant cells observed in resistant population were pre-existing giant cells from parent population or radiation induced. For this, we flow sorted the giant cells (consisting of mono and multinucleated) and small cells (mono-nucleated) from the parent cultures. Clonogenic assay was performed in the individual populations with increasing doses of  $\gamma$  radiation (Figure

2.6A). In contrast to previous reports, we found that pre-existing giant cells in glioma showed higher sensitivity to radiation than the small cells. Moreover, when given single lethal dose of radiation and monitored for survival and recurrence, the giant cells from parent population did not show any survival advantage beyond 7 days (Figure 2.6B).

To further confirm that giant cells formed in radiation resistant population are radiation induced, we quantitated our observation of different cell morphology namely mono-nucleated, giant and multinucleated giant cells post radiation at different time points during the non-proliferative phase. We observe significant decrease (50%) in mono-nucleated cells and concomitant increase in multinucleated and giant cells (60%) in all the cultures over time. In SF268 and in PS2 and 4 there was significant increase in the giant cell population while in U87MG and PS1, 3 & 5 there was significant increase in multinucleated cells (Figure 2.7C). Additionally, on analysing RR cells from the remaining patient samples, similar increase in MNGCs was observed, however the distribution varied in different

samples (Table 2.1.3). These data confirm that the MNGCs seen in non-proliferative phase are not pre-existing giant cells from parent population but their formation is induced by radiation.

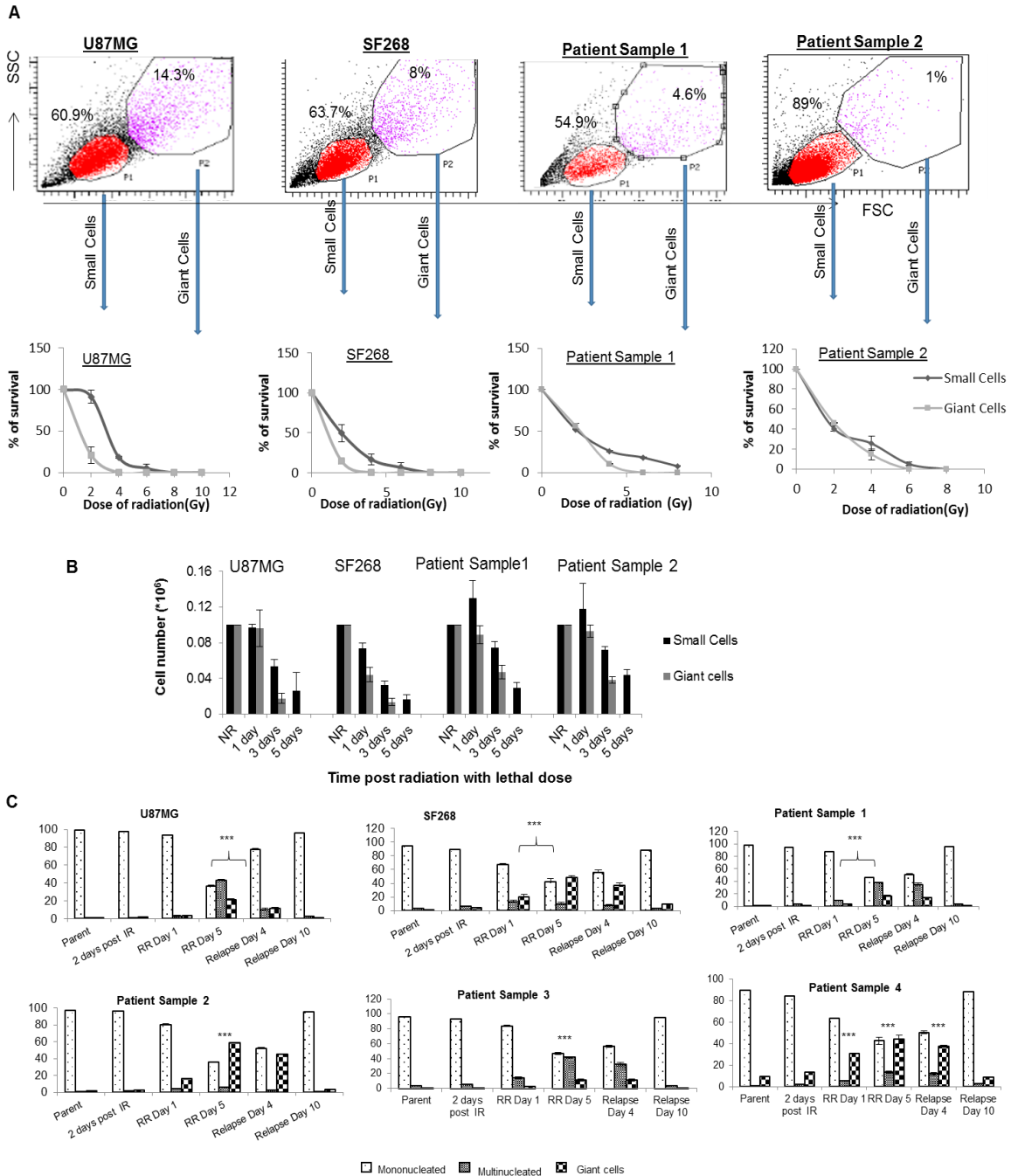


**Figure 2.6: Radiation resistant cells are enriched with radiation induced multinucleated and giant cells which are not pre-existing. A) Clonogenic survival assay curve at different**

doses of gamma radiation for the flow- sorted pre-existing giant cells and small cells from the parent population. B) Graph shows quantification of mono-nucleated, multinucleated and giant cells at different days during non-proliferative phase and in relapse population. At least 5000 cells were counted for each experiment. \*\*\* denotes  $p \leq .001$ .

#### *2.1.3.3 Non-apoptotic MNGCs show transient senescence and eventually resume growth to form viable mono-nucleated recurrent cells*

Interestingly, we observed that the resistant cells so formed are non-apoptotic and show transient loss of proliferation (Figure 2.7A). Hence, we checked these cells for senescent marker  $\beta$ -galactosidase. Interestingly, the  $\beta$ -galactosidase staining showed positivity only in MNGCs but not in mono-nucleated cells (Figure 2.7B). Senescent phenotype has been characterized by the changes in the expression of various genes collectively called as senescence associated secretory proteins (SASPs) [145]. SASPs can provide survival signals to the cells in an autocrine and paracrine manner [146]. In an independent study, we performed transcriptome analysis of RR population and found up-regulation of SASPs in the radiation resistant cells. We confirmed significant increase in the transcripts of GM-CSF, SCF IL-6 and IL-8 in resistant cells as compared to the parent population by quantitative real time PCR (Figure 2.7C). Cellular senescence is known to limit proliferation of potentially detrimental cells and the current literature reports that radiation induced MNGCs do not survive but die of mitotic catastrophe [147]. Therefore, we asked whether mono nucleated cells (30-40 % cells of the RR cells) and not the senescent MNGCs (60-70% of the RR cells) are the prime contributor to the mono-nucleated recurrent population. For this, we first checked if MNGCs were mitotic division competent by staining these cells for  $\alpha$ -tubulin towards the end of the non-proliferative phase. We observed MNGCs with multiple mitotic spindle poles ranging from 3-9 and small mono-nucleated cells with bipolar spindle poles, suggesting that both the cell types are capable of entering mitosis (Figure 2.7D).

**Table 2.1.3: Percentage of multinucleated and giant cells in different patient samples.**

<b>Patient Sample Number</b>	<b>Percentage of Multinucleated Cells</b>	<b>Percentage of Giant Cells</b>
<b>1</b>	38.32	16.14
<b>2</b>	6.03	58.57
<b>3</b>	41.62	11.45
<b>4</b>	13.50	43.90
<b>5</b>	32.05	19.03
<b>6</b>	9.52	49.37
<b>7</b>	12.48	47.89
<b>8</b>	39.57	17.39
<b>9</b>	35.66	14.51
<b>10</b>	52.97	12.45
<b>11</b>	69.47	11.31
<b>12</b>	33.54	29.63
<b>13</b>	40.26	15.22
<b>14</b>	32.56	21.60
<b>15</b>	32.69	34.28
<b>16</b>	40.25	14.98
<b>17</b>	39.61	22.54

<b>18</b>	22.55	32.68
<b>19</b>	41.80	11.68
<b>20</b>	40.30	10.34

To further confirm that MNGCs could actually undergo mitosis to give rise to mono-nucleated cells and not die of mitotic catastrophe during the process of division, we sorted MNGCs and mono-nucleated cells from the radiation resistant population, based on side and forward scatter using FACS and single cell dilution was carried out. The single cells were then monitored for 10 days for cell division events. Out of 48 single MNGCs scored from U87MG, SF268, primary culture 1 and primary culture 2; 28, 36, 24 and 31 cells underwent cell division to generate viable mono-nucleated cells. Similarly, the mono-nucleated cells also underwent cell division at a rate similar to that of the MNGCs (Figure 2.7E). These data confirm that the MNGCs overcome the cell cycle arrest and divide. Since there are higher number of MNGCs present in the non-proliferative phase, this result also suggest that the MNGCs are predominant contributor of the relapse cell population. The expression of SASPs: cytokines and pro-inflammatory interleukins have been known to provide survival and proliferation signals to the cells, promoting tumour formation [148] and thus, contribute to the survival of MNGCs.

Overall, we found that irrespective of genetic heterogeneity and background, RR cells, NP phase and MNGC formation was invariably seen in all 20 primary cultures, prompting us to ask if these molecular aberrations of RR cells could be clinically relevant to predict therapeutic outcome of GBM patient as the current prognosis of GBM rely highly on subjective and variable radiological and pathological measurements. We thus explored molecular features of RR cells generated after radiation exposure to parent cells: 1) survival fraction at 2Gy (SF<sub>2</sub>), 2) days required for emergence of RR cells (D<sub>rr</sub>), 3) percentage of

multinucleated cells, 4) percentage of giant cells, 5) length of non-proliferative phase and 6) total days taken to form recurrent population ( $D_r$ ).

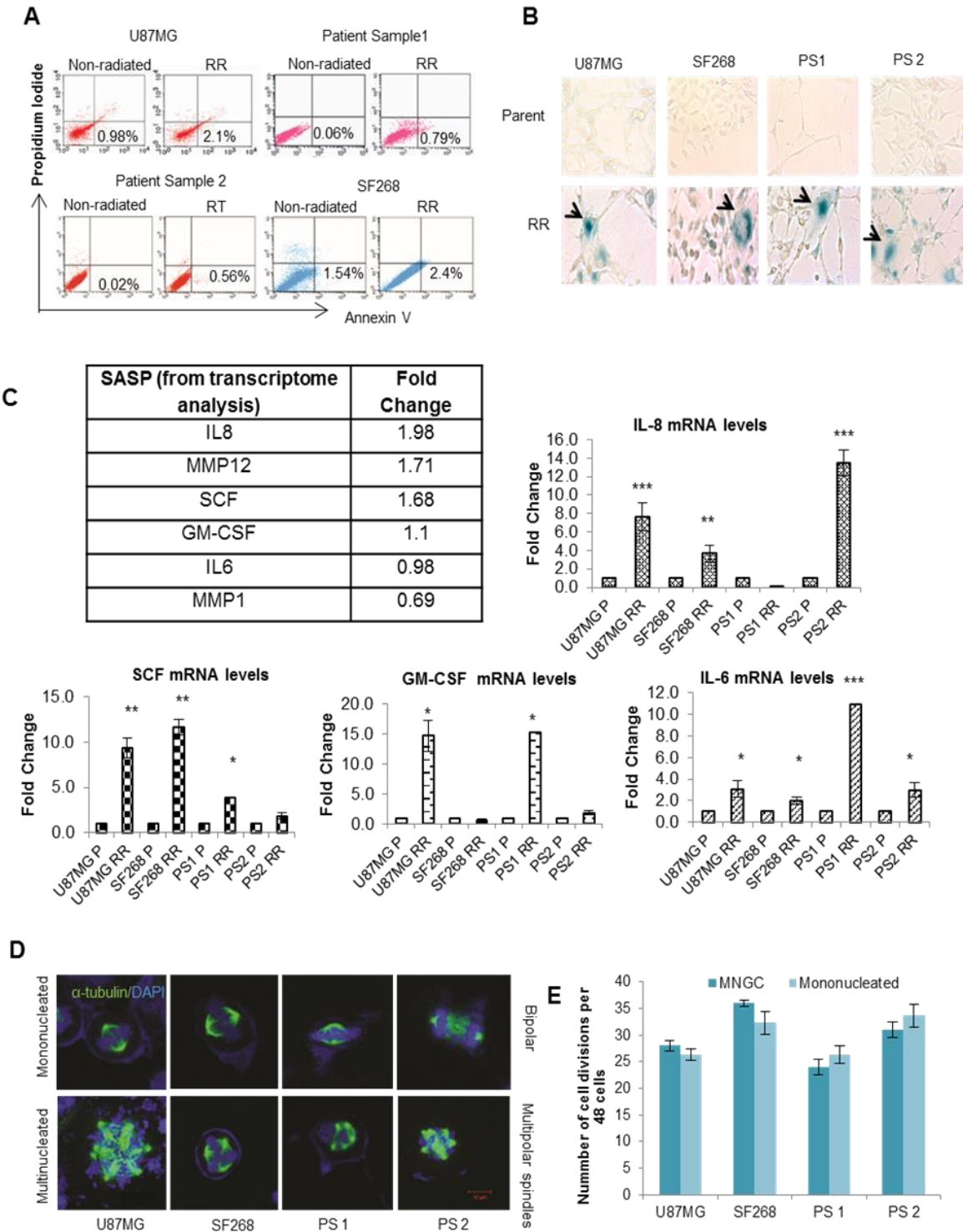


**Figure 2.7: MNGCs exhibit non-apoptotic and senescent phenotype.** A) Annexin V/PI staining in the resistant cells of U87MG, SF268, PS1 and PS2 is shown. B) Senescence associated  $\beta$ -galactosidase staining of the radiation resistant cells U87MG SF268, PS1 and PS2 was done on day 10 post radiation (original magnification X 10). C) Expression levels of SASP genes IL-6, 8, GM-CSF and SCF was determined using qPCR. D) Immunofluorescence images of MNGCs stained for  $\alpha$ -tubulin at day 9 post radiation shows bipolar spindles in mono-nucleated cells while multipolar spindles in MNGCs. Scale bar- 10 $\mu$ m. E) Graph depicts the number of cells undergone division out of 48 cells counted. PS1- patient sample 1 and PS2- patient sample 2. \* denotes  $p \leq .05$ , \*\* denotes  $p \leq .01$  and  $p \leq .001$ .

#### *2.1.3.4 Association of molecular, radiological and pathological parameters with patient survival in GBM*

First, we examined the clinical correlation of each of the molecular features mentioned above individually with the clinical outcome of the GBM patients. We found that higher survival fraction at 2Gy (SF2) did have a negative impact on the survival of the patients as also shown previously [149] with marginal significance ( $p=0.052$ ) as shown in figure 2.8A. Other parameters including days required for emergence of RR cells ( $D_{rr}$ ), length of non-proliferative (NP) phase, total days taken to form recurrent population ( $D_r$ ) and percentage of multinucleated cells did not show any significant correlation with overall survival of GBM patients (Figure 2.8B-E). However, percentage of giant cells ( $p=0.046$ ) significantly predicted the clinical outcome of the GBM patients (Figure 2.8F).

Routinely used pathological (p53 expression) and radiological (tumour volume, rCBV and rCBF values) markers (Table 2.1.4) were first assessed for their prognostic value in our cohort. For this, Kaplan Meier curve was plotted and it was observed that the patients with

p53 over-expression showed better survival as compared to the p53 negative tumours, although it was marginally significant ( $p=0.082$ ) (Figure 2.9A). Amongst the radiological measurements, as expected and reported [150], volume of the tumour had a stronger impact on the overall survival (Figure 2.9B) with patients having tumour more than  $60.93\text{mm}^3$  had mean overall survival of 5.67 months (95% CI: 2.41-8.922) as compared to patients with less than or equal

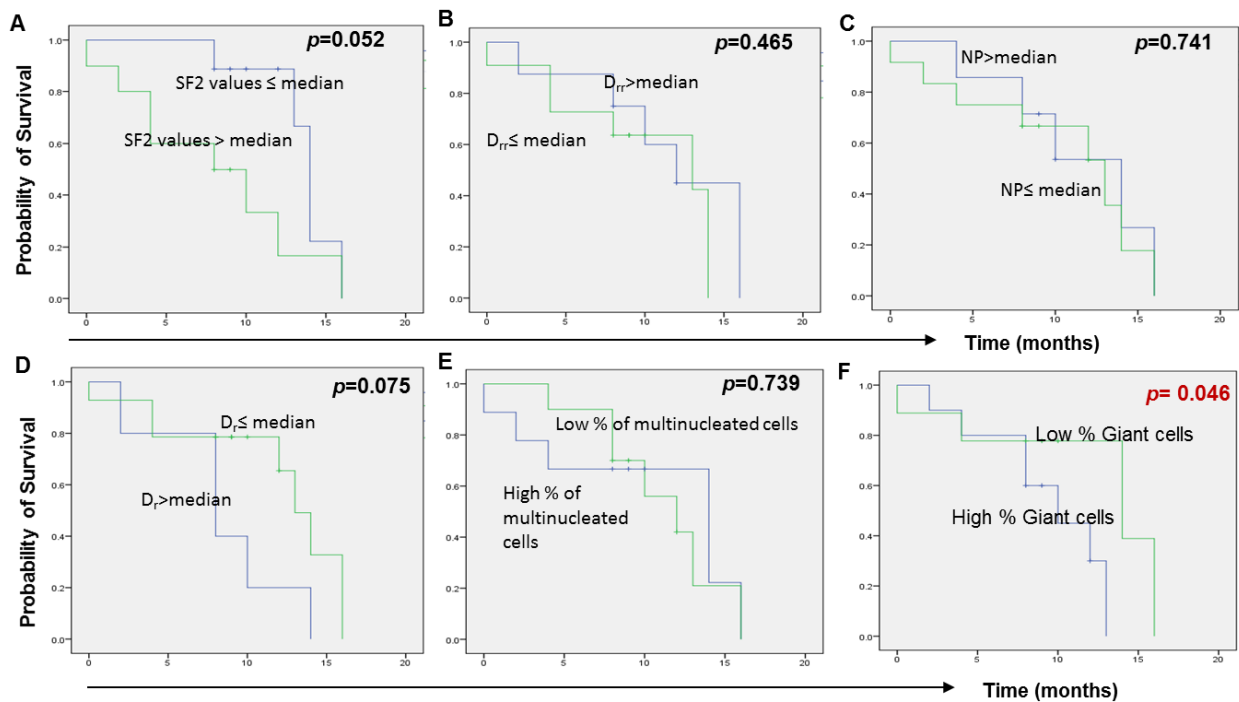


**Figure 2.8: Survival analysis of individual molecular parameters.** (A-F) Kaplan Meier Curves of the patient samples for all the 7 molecular features associated with resistant cells are shown.

to  $60.93\text{mm}^3$  tumour volume (14.74 months; 95% CI: 13.28-16.22). No significant correlation could be seen with pre-treatment MR perfusion parameters rCBV, rCBF, NAA, choline: creatine and presence of lipid/lactate peaks and the overall survival. Other pathological parameters including IDH1, MGMT, MIB-1 index, necrosis and calcification did not predict clinical behaviour.

**Table 2.1.4: Surgical, radiological and pathological details in the patient cohort (N=20).**

Variables	Median (IQR)	Number (%)	
Age	54 years (48.25-63.75)	≤ 54	10/20 (50%)
		>54	10/20 (50%)
Extent of Resection	-	Complete resection	8/20 (40%)
		Subtotal resection	10/20 (50%)
		No information	2/20 (10%)
MIB 1 labelling index	22.5 (16.5-32.5)	≤22.5	11/20 (55%)
		>22.5	6/20 (30%)
		No information	3/20 (15%)
RT Dose	59.4 Gy (59.2-60)	RT Alone	1/20 (3%)
		RT+TMZ	12/20 (60%)
		No information	7/20 (35%)
Adjuvant TMZ	-	≤ 6 cycles	12/20 (60%)
		> 6 cycles	1/20 (3%)
		No information	7/20 (35%)
Calcification	-	Yes	20/20 (100%)
		No	0/20 (0)
Necrosis	-	CN+	13/20 (65%)
		PN+	1/20(5%)
		CN/PN+	2/20 (10%)
		No information	2/20 (10%)
p53 expression	-	Positive	7/20 (35%)
		Negative	10/20 (50%)
		Not reported	3/20 (15%)
Tumor volume	60.93 (30.38-91.2)	≤60.93	8/20 (40%)
		>60.93	7/20 (35%)
		No information	5/20 (25%)
Pre-operative rCBV	306 (202-424.5)	≤306	5/20 (25%)

		>306	4/20 (20%)
		No information	11/20 (55%)
<b>Pre-operative rCBF</b>	244 (180.5-363.0)	≤244	5/20 (25%)
		>244	4/20 (20%)
		No information	11/20 (55%)

CN: Confluent Necrosis, PN: Palisading necrosis, PPN: Pseudo-palisading necrosis

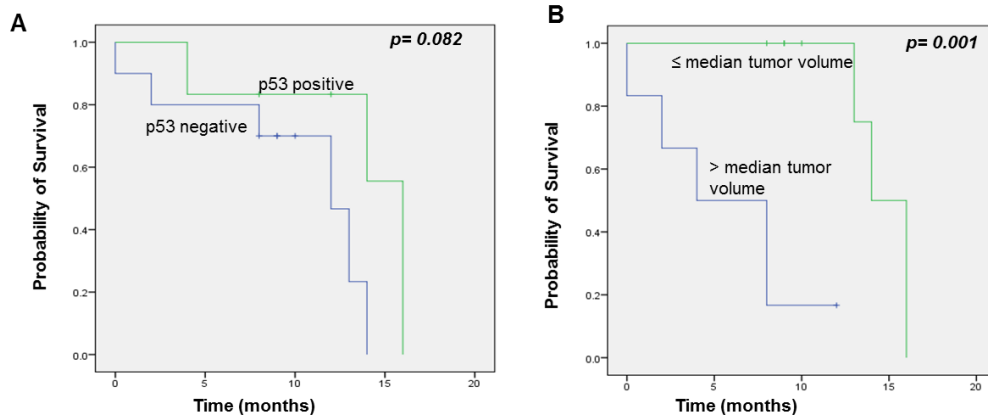


**Figure 2.9: Survival analysis of p53 and tumour volume.**

*2.1.3.5 Percentage of giant cells with tumour volume significantly predict patient survival*

Tumour volume showed a significant positive correlation with SF2 values ( $r=0.504$ ,  $p=0.056$ ), length of non-proliferation phase ( $r=0.758$ ,  $p=0.007$ ) and percentage of giant cells ( $r=0.682$ ,  $p=0.021$ ) suggesting that the larger tumours have higher number of resistant cells (Figure 2.10A-C).

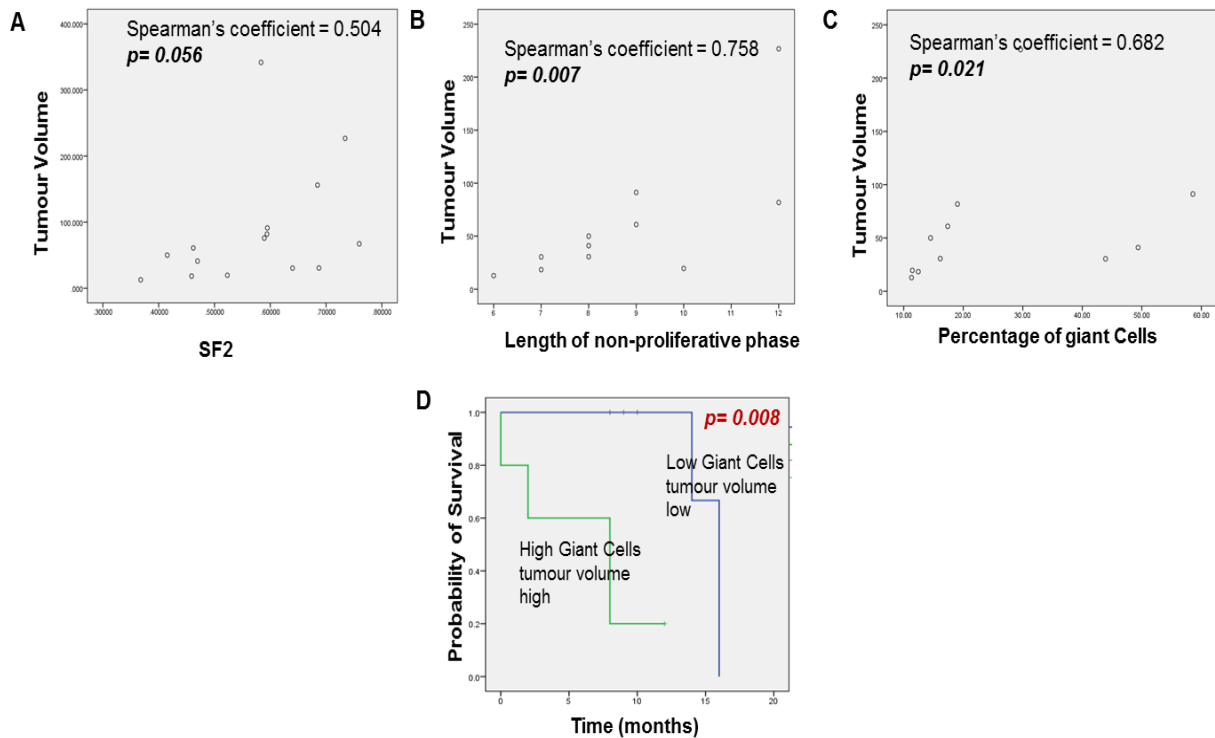


**Figure 2.10: Correlation and survival analysis of resistance associated molecular**

**parameters with the radio-pathological features.** (A-C) Dot plots indicating the correlation between resistance associated molecular alterations and radio-pathological features. (D) Kaplan Meier Curve for the combined tumour volume and percentage of giant cells.

Based on these results, we then analysed molecular and pathological parameters in combination for their influence on the patient's survival. Out of the all combinations analysed, patients with lower tumour volume and lower percentage of giant cells had better prognosis (15.33 months, 95% CI: 14.04-16.64) (Figure 2.10D) as compared to the patients with higher tumour volume and higher percentage of giant cells (6 months, 95% CI: 2.159-9.841).

*2.1.3.6 MNGCs are formed primarily by homotypic cell fusion of mono-nucleated radio-resistant cells*

Since we observed that MNGCs are the major contributors of the recurrent population and display potential prognostic value, we wanted to understand the mechanism of MNGC formation, we posit three possibilities that could explain their formation: 1) by acytokinesis (endo-reduplication), the most predominantly reported mechanism, 2) by entosis [133] and 3) by rare in cancer homotypic cell fusion events [151]. We investigated which of these mechanisms were operative in our cultures.

Endo-reduplication is an evolutionarily conserved process where the multiple rounds of replication of the genome continues without cell division giving rise to polyploidy [152]. To investigate for endo-reduplication, we examined ploidy levels of radiation resistant cells [139]. Except for the patient sample 2, RR population from all other three cell lines contained significant number of cells with more than 4N DNA content compared to the parent cells (Figure 2.11A). However, the increase was not very high as was expected, ruling out the possibility of endo-reduplication as the major event in MNGC generation.

Next to investigate if entosis, which is a newly discovered phenomenon of whole cell internalization [133] could lead to MNGC formation, we stained the MNGCs with N-Cadherin (a membrane protein on neural cells) the staining shows absence of cell-in-cell structures). H&E staining also confirmed the lack of entosis in MNGCs (Figure 2.11B).

Finally, to examine homotypic cell fusion, we made two stable parent cell lines one expressing pEGFP and the other expressing TdRed for all the samples. The green and the red fluorescent cells were co-cultured in equal numbers and subjected to lethal dose of radiation. At least 50 radiation resistant cells were counted in each culture and scored for yellow fluorescence (corresponding to the cell-cell fusion events). We found 67.3% (37/55 cells), 54.6% (30/55 cells), 62% (34/55 cells) and 61.8% (34/55 cells) of yellow fluorescent cells

out of the total MNGCs present in U87MG, SF268, PS1 and PS2 respectively (Figure 2.12A and B).

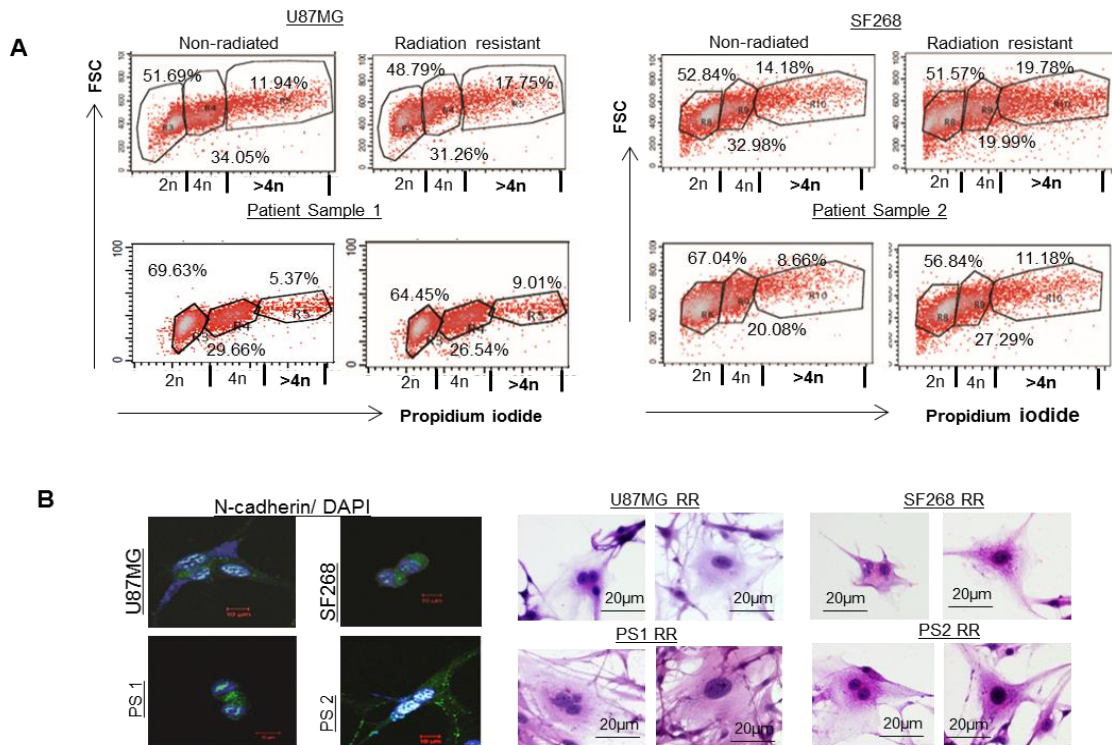


**Figure 2.11: Endo-reduplication and entosis do not significantly contribute in MNGCs formation.** A) Scatter plot shows percentage of radiation resistant cells with different DNA content at day 5 of non-proliferative phase. B) Representative images depicting the N-cadherin (green) counterstained with DAPI (blue) as well as H&E staining in RR cells from U87MG, SF268, patient sample 1(PS1) and patient sample 2(PS2). Scale bar for confocal images-10 μm and phase contrast images- 20 μm.

suggesting high frequency of cell-cell fusion events. Cell-cell fusion was also confirmed by directly visualizing fusion in time lapse studies where the cells in the non-proliferative phase were monitored for 24 hours to capture fusion events (Figure 2.12C).

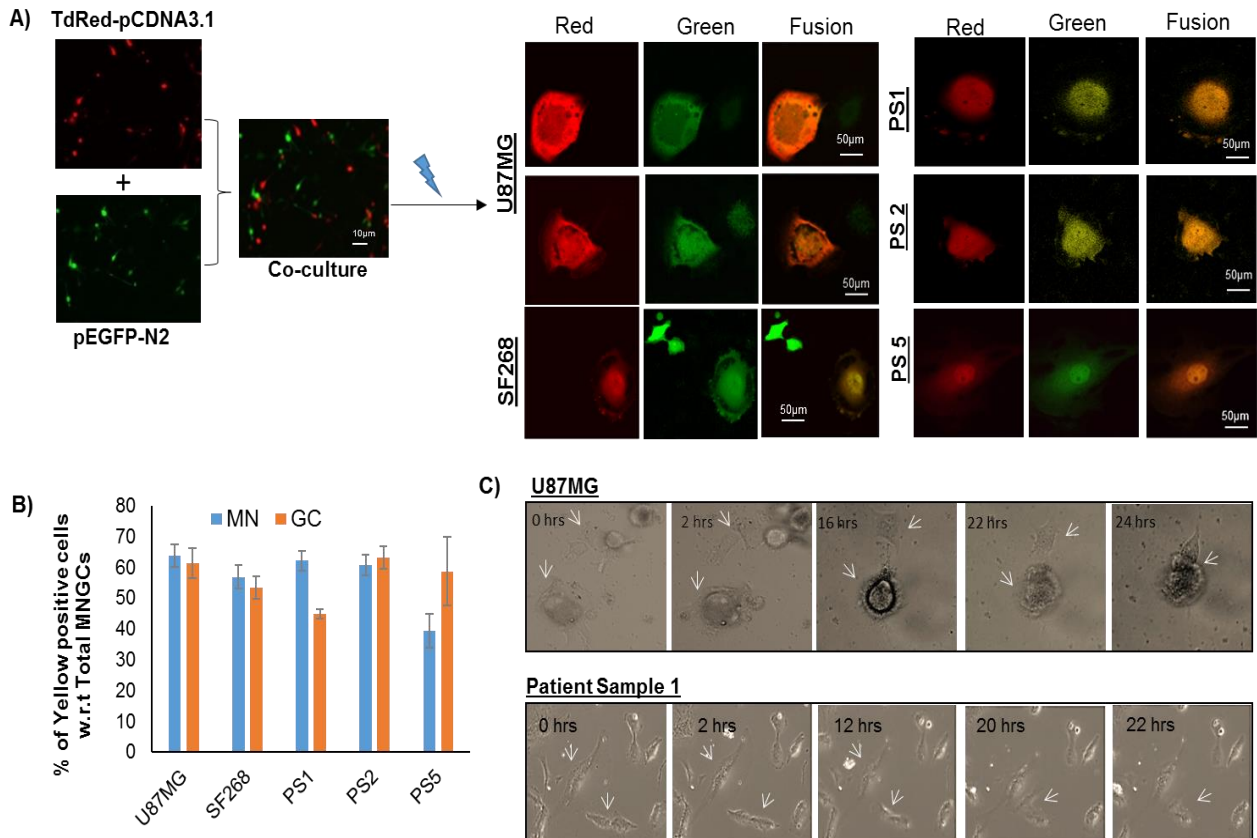


**Figure 2.12: Cell-cell fusion leads to formation of MNGCs in the radiation resistant cells.** A) Florescence images of RR cells expressing both pEGFP-N<sub>2</sub> and TdRed vectors (left panel images with 10X and right panel with 63X magnification images) of cell- cell fusion event. B) The graph represents the percentage of yellow fluorescent cells among the MNGCs. C) Snapshots from time lapse images demonstrating the cell-cell fusion in U87Mg and patient sample 1. Scale bar for immunofluorescence images- 50µm and for phase contrast images- 10µm. PS1-patient sample 1 and PS2- patient sample 2.

Recently cell-cell fusion has been identified as a trigger for induction of cellular senescence and promoting tumorigenesis [153]. Since MNGCs show positivity towards senescent marker  $\beta$ -galactosidase, cell-cell- fusion may have a possible role in inducing senescence in our cultures.

### 2.1.3.7 Cell fusion induced MNGCs give rise to relapse cells with similar ploidy

In some studies, MNGCs formed by endo-reduplication are shown to be responsible for the increased aneuploidy seen in cancer [151]. Because of the presence of aberrant spindle formation in MNGCs from our cultures we were intrigued to examine a possibility of aberrant division of MNGC leading to increased aneuploidy in recurrent population. We performed cytogenetics analysis of parent and recurrent cells, and found that the recurrent cells have similar modal chromosomes numbers as their parent population, suggesting that despite having multiple spindle poles, MNGC's underwent normal cytokinesis to give rise to recurrent cells (Figure 2.13).

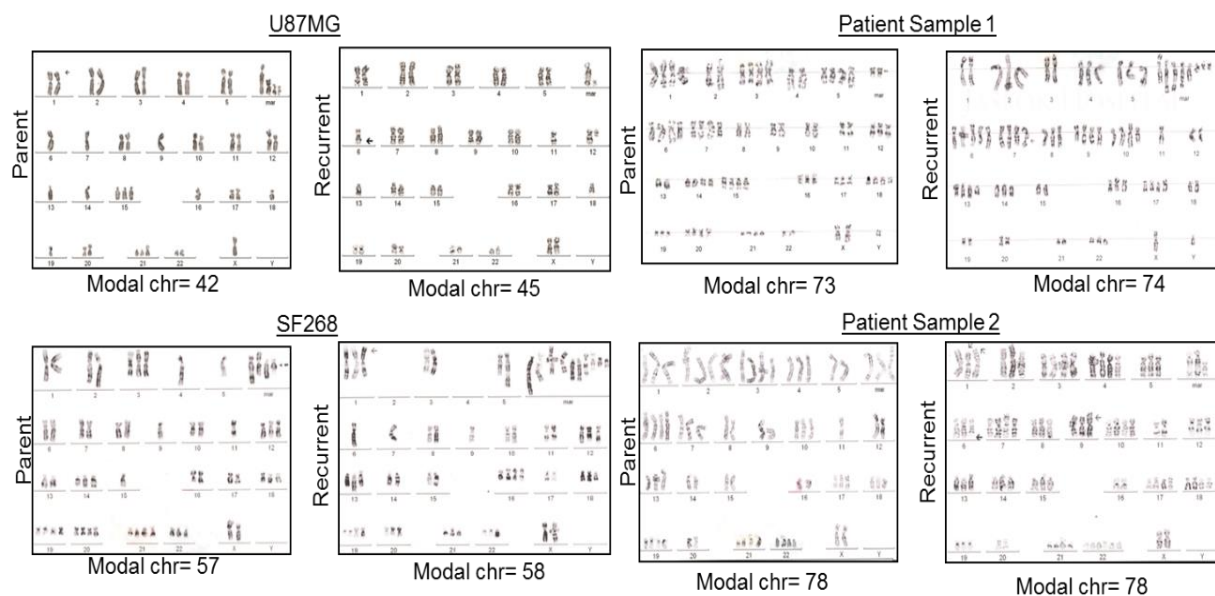


**Figure 2.13: MNGCs give rise to relapse cells with similar ploidy number.** Karyotype images of parent and relapse cells (at least 25 metaphase spreads analysed).

#### 2.1.3.8 MNGCs over-express senescent associated secretory proteins (SASPs), over express anti-apoptotic genes and activate AKT to evade apoptosis

Cell fusion between normal, non-transformed cells have recently been shown to induce genomic instability triggering both malignancy and evolution of the tumour [154]. However, a precise role of cancer cell fusion have not been demonstrated, although their role in

promoting tumour growth and therapy resistance have been hypothesized [155]. This led us to explore the possibility of MNGCs formation in providing a survival signal to the arrested cells. We then checked for the expression of survival and apoptotic genes in the RR cells. We found enhanced expression of anti-apoptotic genes BIRC3 and Bcl-xL (Figure 2.14A) whereas, Bax (pro-apoptotic protein) mRNA levels were unaltered (Figure 2.14B). However, down-regulation of Survivin and BIRC4 expression was seen. Consequently, Annexin V staining did not show any apoptotic cells in the RR population as shown in Figure 2.7A. In order to see if the MNGCs activate survival signals downstream to these survival proteins, we checked for the phosphorylation of AKT, which is a central convergence node of all the above mentioned signalling pathways and is known to be involved in the maintenance and survival of Glioblastoma tumours [156]. As shown in figure 2.14C, RR cells from cell lines and patient samples showed higher expression of pAKT. Both the AKT activation along with Bcl-xL are known to regulate apoptosis synergistically [157] and thus, might be aiding their survival.

#### *2.1.3.9 Relapse can be prevented by targeting pCdk1 (Y15) and cytokinesis*

The above mentioned data underscores the importance of cell cycle arrest of the radiation resistant cells, which gives them time to overcome stress via MNGC formation. Therefore, induction of premature mitosis in these cells should prevent cell-cell fusion. We first check the cell cycle distribution pattern of the residual resistant cells showed that these cells were enriched in G2-M phase as compared to the non-irradiated parent cells with concomitant decrease in G0/G1 phase (Figure 2.15A). Both the cell lines (U87MG and SF268) also showed significantly higher percentage of cells in S phase (Figure 2.15A).

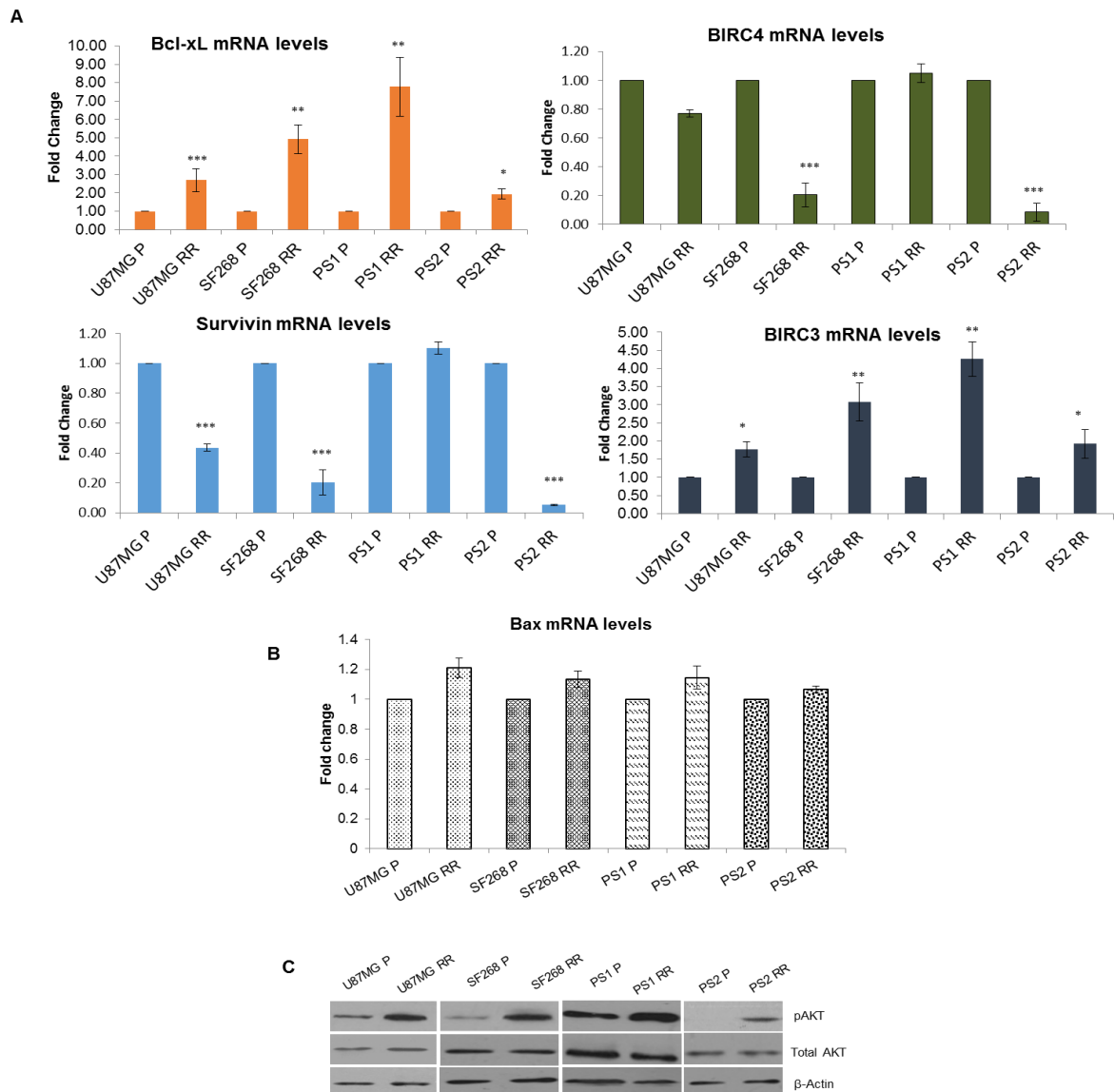


**Figure 2.14: MNGCs over-express anti-apoptotic genes and activate AKT to evade apoptosis.** A) Transcript levels of Bcl-xL, BIRC4, Survivin and BIRC3 in the resistant residual cells as determined by real time PCR. B) Western blot analysis probing with pAKT, AKT and beta-actin antibodies was carried out in the parent and resistant cells from cell lines and patient samples. \* denotes  $p \leq .05$ , \*\* denotes  $p \leq .01$  and \*\*\*  $p \leq .001$ .

Cell cycle regulators/ inhibitors belonging to Cip/Kip and Ink4 family are known to precisely control the cell cycle progression by inhibiting Cyclin-dependent kinases [158]. A member of Cip1 family, p21 has been implicated in growth arrest in S and G2 phase after

DNA damage by preventing activation of Cdk1 [159] and mediates cellular senescence of many tumour cells [160]. We observed significant increase of mRNA levels of p21 in the S, G2/M phase arrested resistant population (Figure 2.15B). We also observed higher levels of Cdk1 phosphorylated at the inhibitory site Tyr15 in the radiation resistant cells contributing to the arrest at G2 phase of the cell cycle (Figure 2.15C) except for SF268 which showed slightly decreased expression in the early time point of the non-proliferative phase.

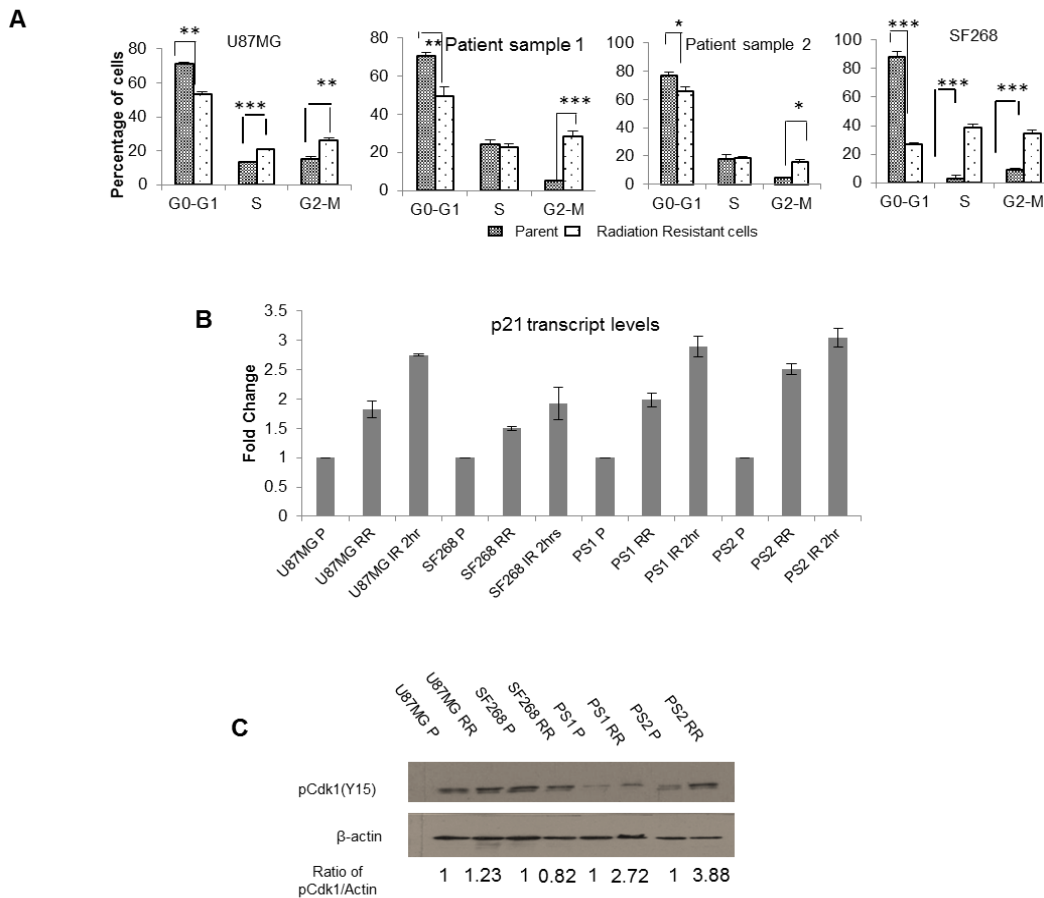


**Figure 2.15: Radiation resistant cells are arrested predominantly at G2-M phase of the cell cycle.** A) Bar graph showing the distribution of parent and resistant cells in different cell cycle phases as determined by propidium iodide staining. B) Transcript levels of p21 are shown. C) Western blot analysis was carried out to determine the expression of pCdk1 (Y15) in the radiation resistant population. Quantitation of blots was done using Image J software. \* denotes  $p \leq .05$ , \*\* denotes  $p \leq .01$  and \*\*\*  $p \leq .001$ .

Higher expression of Cdk1 has been shown to cause therapy induced senescence [161]. However, what we found was the higher levels of inhibitory Cdk1 phosphorylation (Y15) in the RR cells contributing to the arrest at G2/M phase of the cell cycle (Figure 2.15C). pCdk1 (Y15) gets activated by Wee 1 kinase, a negative regulator of mitosis, therefore we hypothesized that an inhibitor to this protein would induce RR to undergo premature mitosis [162]. We incubated the Glioma cells with 600nM of Wee1 kinase inhibitor (MK-1775) for 24 hours post 5 days of radiation treatment. Indeed, the RRs treated with the Wee 1 kinase inhibitor underwent apoptosis by day 5 of the treatment. PS 2 showed less amount of cell death (53%) initially (3 days) however, complete cell death was seen at day 5 (Figure 2.16A and B). The specificity of Wee 1 kinase inhibitor was confirmed by inhibition of Cdk1 phosphorylation at tyrosine 15 in the cells treated with the inhibitor (Figure 2.16C).

Secondly, after cell-cell fusion, blocking their cytokinesis should also lead MNGCs to cell death. Indeed, when we incubated MNGCs with 10 $\mu$ M of Wiskostatin, an inhibitor of cytokinesis, [163] for 24 hours, significant number of MNGCs underwent apoptosis by day 3. Addition of Wiskostatin had no effect on the non-irradiated parent cells, confirming that specificity of the inhibitor on MNGCs (Figure 2.17).

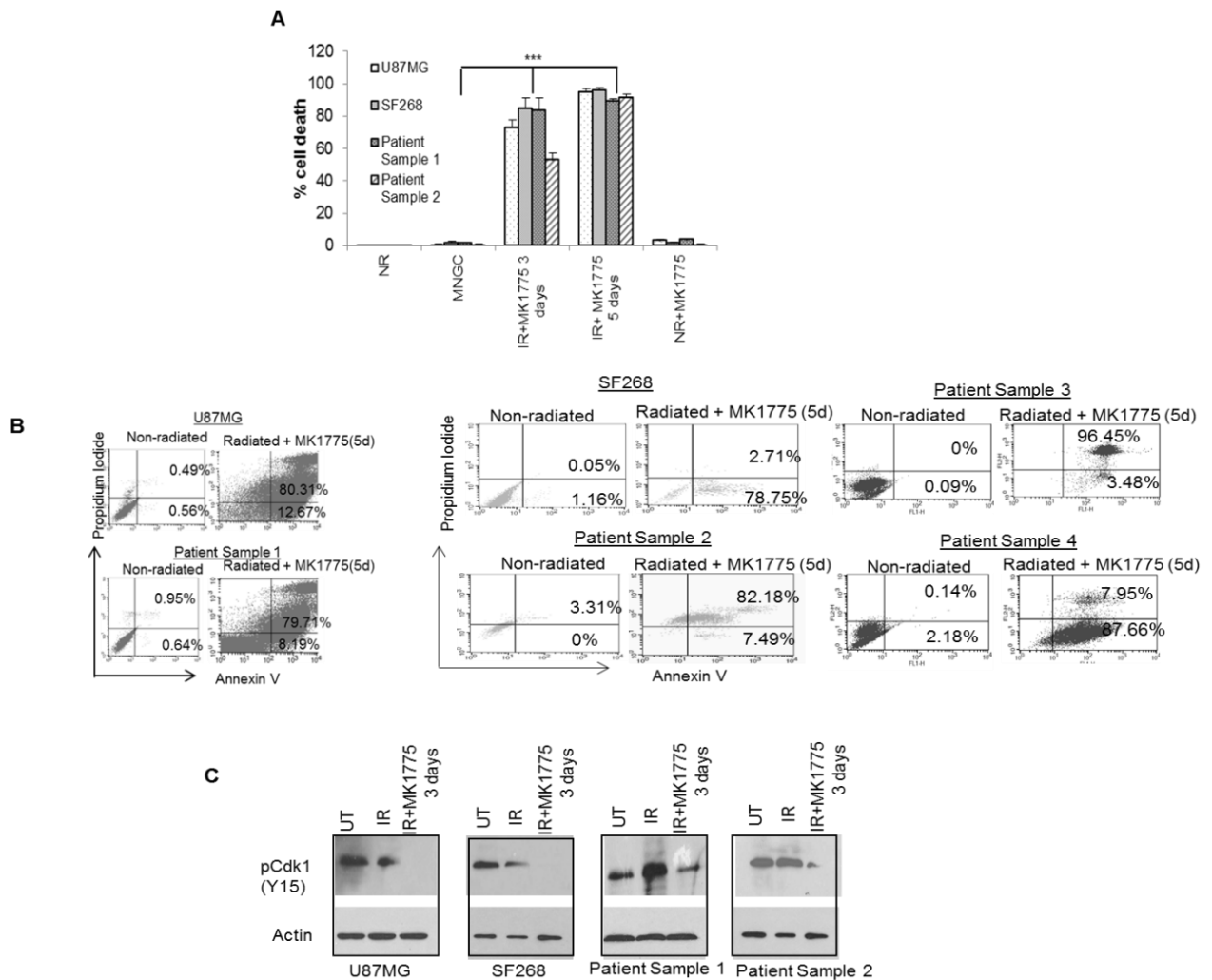


**Figure 2.16: Premature mitosis kills radiation resistant cells.** A) Bar graph shows percentage of cell death induced by Wee 1 kinase inhibitor (MK1775) given along with radiation as determined by trypan blue assay. B) Flow cytometry based Annexin V/ PI staining showing percentage of apoptotic cells at different conditions post incubation with 600nM of Wee1 kinase inhibitor (MK1775) for 24 hours. C) Western blot with phosphorylated Cdk1 (Y15) of Wee1 kinase inhibitor (MK1775) treated radiated and non-irradiated cells. Error bars denotes SEM and \*\*\* denotes  $p \leq 0.001$ . NR= Non-irradiated and IR= irradiated cell.

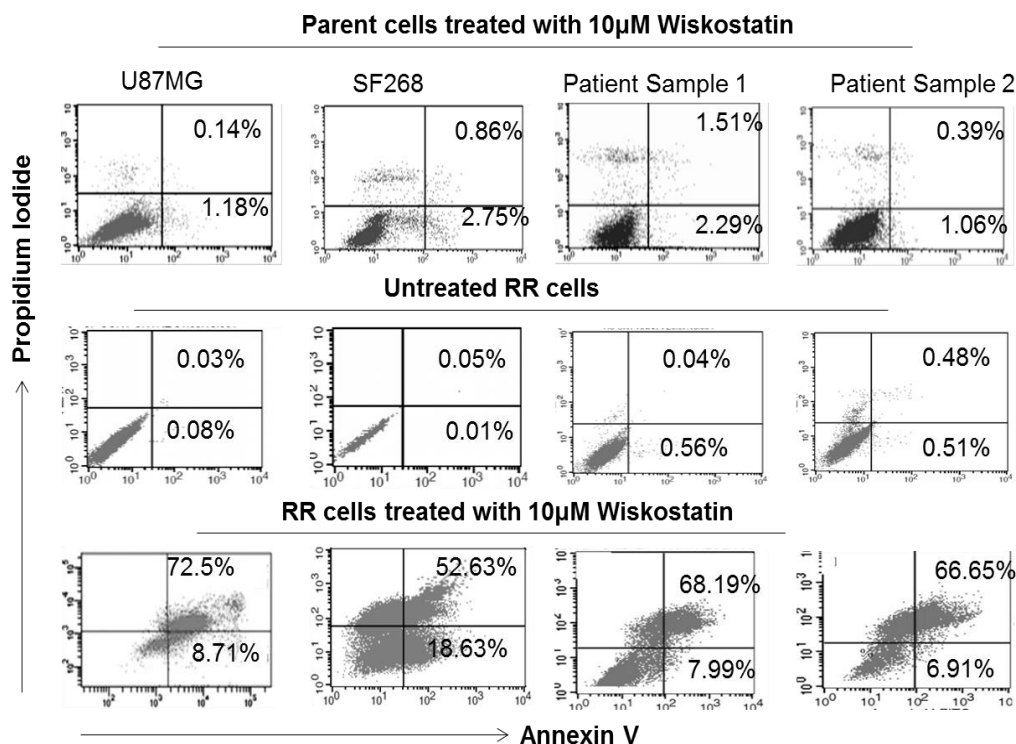


**Figure 2.17: Blocking cytokinesis induced apoptosis of resistant cells preventing recurrent cell formation.** Scatter plot showing apoptotic cells stained with Annexin V/PI after treatment of RR cells with Wiskostatin (10 $\mu$ M).

In aggregate, these findings demonstrate that homotypic cell fusion mediated MNGCs have the capacity to sustain survival under radiation induced stress via growth factors mediated survival signals. Therefore, we identify homotypic cell fusion as a potential new therapeutic target for the survival and relapse of glioblastoma. Our data also highlights the importance of the non-proliferative phase during which the radiation resistant cells undergo homotypic cell fusion and the cytokinesis of MNGCs in glioma relapse. Targeting these two mechanisms also lead to the apoptosis of RR cells providing potential therapeutic benefit for glioma treatment.

## 2.1.4 Discussion

Collectively, the data presented, summarized in Figure 2.18 suggest a paradigm of glioma survival, captured using the in-vitro radiation resistant model that we have established from fresh glioblastoma patient samples and cell lines. We show that in a heterogeneous mix of glioblastoma cells there exists a subpopulation of cells (radiation resistant cells) that is innately resistant to lethal dose of radiation. We observe that after the exposure to lethal dose of gamma radiation, the radiation resistant cells are arrested at G2/M phase of the cell cycle to become non-proliferative and undergo DNA damage repair. This observation is consistent with similar reports in other cancer types like hepatomas, epithelial cancer and fibrosarcoma [130,138, 164]. However, contradictory to these reports in which inevitably the non-proliferative cells undergo cell death, we do not see apoptosis of non-proliferative radiation resistant cells in our glioblastoma cultures. In fact, the non-proliferative state of these cells is transient and these cells resume growth.

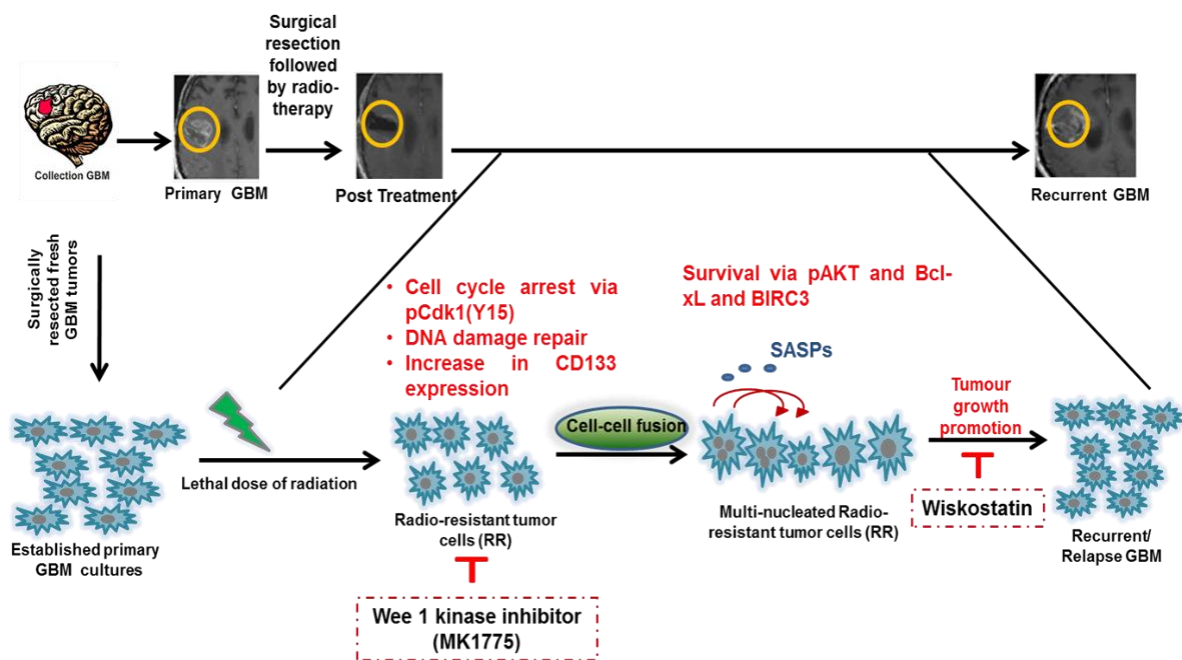


**Figure 2.18: Schema showing the multi-step in-vitro radiation model recapitulating the progression of GBM and demonstrating the non-proliferative phase.**

Interestingly, although non-proliferative, radiation resistant cells undergo cell-cell fusion events at high frequency forming non-proliferative multinucleated giant cells (MNGCs). It is noteworthy that the actual fusion events could be more than what is reported here as we could not quantitate the fusion events occurring between two green or two red fluorescent cells. Cell-cell fusion of cancer cells is a rare phenomenon. Recent reports based on the fusion between normal cells and between gastric epithelial cells and mesenchymal stem cells have demonstrated their role in initiation of tumour formation and epithelial-to-mesenchymal transition, respectively [154, 165]. However, no direct role has been attributed to be imparted by cancer cell fusion.

Literature reports have shown the dearth of therapy induced MNGCs in many cancers [140]. However, MNGCs formed in our glioma cultures are able to sustain viability through non-proliferative phase and resume growth suggesting that the MNGCs formed in glioblastoma are fundamentally different from other cancer types. Thus, formation of MNGCs is not the consequence of sudden shock of high dose of radiation but is an innate nature of Glioma cells to form MNGCs in order to overcome stress. The purposive formation of MNGCs in glioma cells provides an insight about the behaviour of cells and various mechanism used by the cells to overcome radiation stress. However, our understanding of molecular players involved in cell fusion is inadequate and requires additional studies. It is unclear at this stage how exactly non-viral cell-cell fusion amongst tumour cells helps the non-proliferative cells in overcoming radiation induced stress.

Senescence is a physiological state of cell established in response to several insults like DNA damage, telomere shortening and oncogenic stress. There is only one report linking the induction of cellular senescence by viral protein mediated cell-cell fusion [166]. Interestingly, cancer cell senescence is known to be beneficial as a tumour suppressor, though there are increasing evidences suggesting genotoxic stress and oncogene expression inducing

complex senescence and promoting EMT (epithelial-to-mesenchymal)-like changes in neighbouring cell populations via secretion of cytokines and pro-inflammatory factors called SASP (senescence-associated secretory proteins) [146, 167]. To best of our knowledge this is the first study showing that radiation induced homotypic cancer cells fusions can induce cellular senescence leading to higher expression of SASPs in MNGCs providing them with the growth signals to overcome stress. Consequently, induction of senescence and prevention of escape from senescence is recognized as a potential treatment of cancer. Results provided here also highlight the fact that the non-proliferative state of RR cells actually provides the time and mechanism that allows this subpopulation of cells to overcome the stress induced by radiation and enable their survival and recurrence.

We also identified percentage of giant cells in RR cells and tumour volume to be a potential prognostic marker for GBM, highlighting the use of primary cultures for such studies. Lack of significant number of cases did not allow for a more robust multi-variate analysis and hence, is the lacunae of this study. However, the data is promising and therefore warrants studies on a larger cohort of patient samples to confirm the significance of combination of radiation associated markers for stratifying these highly heterogeneous tumours into clinically relevant prognostic subgroups.

Importantly, our findings introduce two therapeutically relevant windows to improve clinical outcome of the patient with aggressive glioblastoma. Firstly, targeting non proliferative radiation resistant cells by inducing them to undergo mitosis before they could repair their radiation induced damage, hence causing their cell death by apoptosis. Indeed, radiation resistant cells treated with Wee1 kinase inhibitor (which abrogates S-phase and G2 arrest) show complete cell death, confirming the importance of non-proliferative phase in glioma resistance and relapse. Accordingly, combination of ionizing radiation and Wee 1 kinase could be a promising therapy for glioblastoma. As such, Phase I clinical trials

evaluating Wee 1 kinase inhibitor for refractory melanomas have already been carried out [168]. Secondly, targeting MNGCs during their division would also abrogate relapse. As expected, when we use inhibitor of cytokinesis to revoke division of MNGCs, significant cell death of MNGCs is seen in all the cultures. Further studies will certainly be required to establish the *in vivo* significance of the cell culture findings, as well as to determine more precisely the molecular mechanisms underlying reversible radiation tolerance and cell-cell fusion.

## **2.2 Characterization of recurrent cells using Raman spectroscopy**

In this study, recurrent cells obtained from RR cell were employed for biological and Raman spectroscopic analysis with the aim to identify attributes specific to the recurrent population.

### **2.2.1 Introduction**

Several factors have been attributed to increased recurrence rate seen in GBM. The presence of cancer cells in the heterogeneous GBM with innate capacity to survive the radio-chemotherapy has been associated with the increased resistance observed in GBM [32, 169-172]. Over-expression of proteins like EGFR, Survivin, MGMT and altered metabolic proteins has been reported in these resistant GBM cells [24-27]. Additionally, the cancer-initiating cells are thought to modulate DNA damage repair proteins including ATM, ATR and MSH6 to impart therapy resistance to GBM. Therefore, the presence of innately resistant cells in the parent tumour has implications in the survival and recurrence of the tumour. The identification of these resistant cells would help in better prognosis of the tumour and optimizing the treatment regimen of patients that may lead to better therapeutic outcomes. However, detection of such resistant sub-population of cells from bulk tumour population has not been possible using currently available diagnostic techniques.

Raman spectroscopy (RS) is a vibrational spectroscopic technique based on inelastic scattering of light where the energy of photons scattered by the sample is different from the incident photon due to transfer of energy to or from the vibrational modes of molecules in the sample. This technique can be applied on live cells and is sensitive enough to detect subtle biochemical changes in the cells. Because of these reasons, Raman spectroscopy is being extensively explored in the disease diagnosis [173-175]. RS has shown promising results in the diagnosis of several cancers including cervical, lung, oral and brain tumours [176-181]. Most of the studies on brain tumours have focused on *in vivo* and *ex vivo* diagnosis of tumours including gliomas, followed by recent studies on surgical demarcation to determine the precise tumour margins.[182-185]. Recent studies have also shown the utility of Raman spectroscopy and Stimulated Raman Scattering microscopy in detecting the brain regions infiltrated with tumour cells during the course of surgery and distinguishing them from the normal tissue[186, 187]. The spectroscopic technique has further been used for evaluating the tumour response upon radiation treatment identifying treatment associated changes in tumour [188-190]. Further, RS has been explored for detecting radio-response in cervical cancers, predicting radiation response in 2RT and 5RT tissues[191] and in oral cancers delving the feasibility of classifying a parental SCC cell line and its radio-resistant 50Gy and 70Gy clones[192]. An exploratory study in predicting recurrence of oral squamous cell carcinoma was also performed on a smaller cohort using serum Raman spectroscopy by our group[193]. Although such remarkable advances in Raman spectroscopy have enabled better tumour detection, Raman spectroscopy has not been explored for detection of the resistant tumour cells from parent population.

In this study, we used recurrent population derived from an *in vitro* radiation model established in our laboratory from primary Grade IV glioma patient samples and cell lines with the aim to explore if the recurrent population can be separated from the parent

population on the basis of bio-molecular differences. Here, we first show by biological assays that the recurrent cells are indeed different as they have resistance to radiation and enhanced survival capacity associated with the increased expression of pERK1/2 and Survivin. However, variations in these biological assays were seen in different recurrent populations. We further show that the whole transcriptome analysis invariably identified two different transcriptional landscapes of the parent and recurrent population of cells. Since detection of these resistant populations required a global means of detection, we demonstrate the efficiency of Raman spectroscopy, a non-invasive technique that can identify subtle biochemical variations, in differentiating naïve parent and recurrent populations. The data reveals that the Raman spectroscopy can classify the recurrent population into a cluster distinct from parent population. Spectral profiles demonstrate increase in lipid and an overall shift from protein to lipid as hallmarks of the recurrent population. The potential of Raman spectroscopy was then evaluated on an independent set of primary human GBM tissues wherein the efficacy of RS in classifying samples differing in their clinical outcome: responders and non-responders was investigated. Principal Component Analysis (PCA) and Principal Component-Linear Discriminant Analysis (PCA-LDA) revealed separate clusters corresponding to the responding and non-responding patient samples. The spectral profiles identified modulation of lipid along with an additional DNA-related features in the tissues from non-responders compared to the responders. Prospectively, studies on larger cohort of the GBM tissues will be required to validate findings of this preliminary study before implicating Raman spectroscopy in the prediction of GBM patient's outcome.

## **2.2.2 Materials and Methods**

### *2.2.2.1 Clinical tissues*

Six histopathologically confirmed GBM primary tumours were also collected after patient's consent and frozen at -80°C until the acquisition using Raman spectroscopy. All the patients underwent complete total resection followed by standard radio-chemotherapy. The clinical information was obtained from their medical records or by the telephonic correspondence. The survival patients with no recurrence or disease progression even after 3 years of follow up were included in the responders group. Patients with tumour-associated mortality within the study period were included in the non-responders group.

#### 2.2.2.2 Whole Transcriptome sequencing analysis

Total mRNA from recurrent and parent populations of two patient samples (PS1 and PS2) and two cell lines U87MG and SF268 were extracted (Dynabeads, mRNA Direct Micro Kit, Invitrogen), used for library preparation and sequenced them on Illumina's Hi-Seq 1000 platform. We generated 101 bases long paired-end reads for the parent (30 Million X 2 paired end reads), and recurrent samples (30 Million X 2 paired end reads) from each of the sample. Further, RNA-Seq analytical pipeline as detailed by Trapnell *et al* [194] was carried out, mapping these sequence reads to human hg19 genome, with reference gene based annotations from the UCSC's genome browser (UCSC knowngenes.gtf). FPKM values of all four samples of the same population (i.e SF268, U87MG, PS1 & PS2 parent cells and SF268, U87MG, PS1 & PS2 recurrent cells) were normalized amongst themselves. These normalized FPKM values were used for Principal Component Analysis (PCA) in R (v3.1.0) using *cummeRbund* Bio-conductor package.

#### 2.2.2.3 Raman Spectroscopy

##### 2.2.2.3.1 Sample preparation and spectral acquisition

Equal number of 6 independent generated batch cultures of parent and recurrent cells from U87MG & patient sample 2 and three independent cultures from SF268 and patient sample 1

were harvested and washed with PBS prior to spectra recording. The harvested cell pellet was placed on CaF<sub>2</sub> window and spectra were acquired using a Raman microprobe system as described earlier [175]. Briefly, this system consists of laser 785 nm (Process Instruments) as an excitation source and HE 785 spectrograph (Horiba-Jobin-Yvon, France) coupled with CCD (Synapse, Horiba-Jobin-Yvon) as dispersion and detection elements, respectively. Optical filtering of unwanted noise, including Rayleigh signals, is accomplished through ‘Superhead’, the other component of the system. Optical fibers were employed to carry the incident light from the excitation source to the sample and also to collect the Raman scattered light from the sample to the detection system. Spectra acquired at excitation wavelength ( $\lambda_{ex}$ ) = 785 nm, laser power = 30 mW, were integrated for 10 seconds and averaged over 6 accumulations. Estimated laser spot size at the cell pellet sample was 5–10  $\mu\text{m}$ . Approximately, 5-6 spectra were acquired from each cell pellet. Thus, a total of 30 spectra per group were acquired for each of the parent and recurrent population.

Spectral acquisition of GBM tissues was carried out by a fiberoptic Raman probe (In Photonics Inc, Downy St. USA) consisting of an excitation and a collection fiber of diameters 105 and 200  $\mu\text{m}$ , respectively. This commercial Raman probe was coupled to the Raman spectrometer described above. Spectral acquisition parameters were:  $\lambda_{ex}$  = 785 nm, laser power-80 mW, spectra were integrated for 15 seconds and averaged over 3 accumulations. About 7-8 spectra were recorded for each GBM tissue.

#### 2.2.2.3.2 Spectral pre-processing and data analysis

The acquired Raman spectra were corrected for CCD response and spectral contaminations from substrate and fiber signals. To remove interference of the slow moving background, first derivatives of spectra (Savitzky-Golay method and window size 3) were computed [175, 185, 195]. Spectra were interpolated in the two regions: fingerprint range (700-1800  $\text{cm}^{-1}$ ) and high wavenumber region (2800-3100  $\text{cm}^{-1}$ ) for the cell line study while 1200-1800  $\text{cm}^{-1}$  for

the GBM tissue study. Interpolated first derivative and vector normalized spectra were then subjected to multivariate unsupervised Principal component analysis (PCA) and supervised Principal component-linear discriminant analysis (PC-LDA). In brief, Principal Component analysis (PCA) is routinely used method for data compression and visualization. It describes data variance by identifying a new set of orthogonal features, called as principal components (PCs) or factors. In LDA, the classification criterion is identified using the scatter measure of within class and between class variance. LDA can be used in conjunction with PCA (PC-LDA) to increase the efficiency of classification. The advantage of doing this is to remove or minimize noise from the data and concentrate on variables important for classification. In our analysis, significant principal components ( $p < 0.05$ ) were selected as input for LDA. In order to avoid over-fitting of the data, as a thumb rule, total number of factors selected for analysis were less than half the number of the spectra in the smallest group [195]. PC-LDA models were validated by Leave-one-out cross-validation (LOOCV). Leave-one-out cross validation is a type of rotation estimation, a technique used for assessing performance of a predictive model with a hypothetical validation set when an explicit validation set is not available. Algorithms for these analyses were implemented in MATLAB (Mathworks Inc.) based in-house software [196].

For spectral analysis, average spectra were computed from the background-subtracted spectra prior to derivatization for each class and were baseline-corrected by fitting a fifth order polynomial function. These baseline corrected, smoothed (Savitzky–Golay, 3) and vector-normalized spectra were the used for spectral comparisons. Spectral assignments were performed as per existing literature. [197] [198].

### **2.2.3 Results**

### *2.2.3.1 Recurrent cells have similar morphology and proliferation rate as compared to the parent population*

In the first step, morphological characteristics of the parent cells were compared with its recurrent cell counterpart to explore the presence of any visually apparent differences. Cellular morphology of parent and recurrent cells from all cultures was visualized by fluorescence microscopy after staining for  $\beta$ -actin, a cytoskeletal protein. As shown in figure 2.19A, no substantial differences between the morphological features of the two populations were observed. Further, proliferation potential of these cells was analysed using trypan blue assay for 10 days. Variability was observed in case of the cell lines; recurrent cells from U87MG cell line showed lower proliferation rate whereas SF268 recurrent cells showed higher rate of proliferation as compared to the parent population. Whereas, recurrent cells formed from the primary cultures of patient samples did not show any enhancement in the growth potential as compared to their parent cells (Figure 2.19B). This suggests that recurrence of the glioma cells does not depend entirely on increased cellular proliferation. Indeed, Schröder *et al* showed that the proliferation index remained similar in both the recurrent and primary tumours[199].

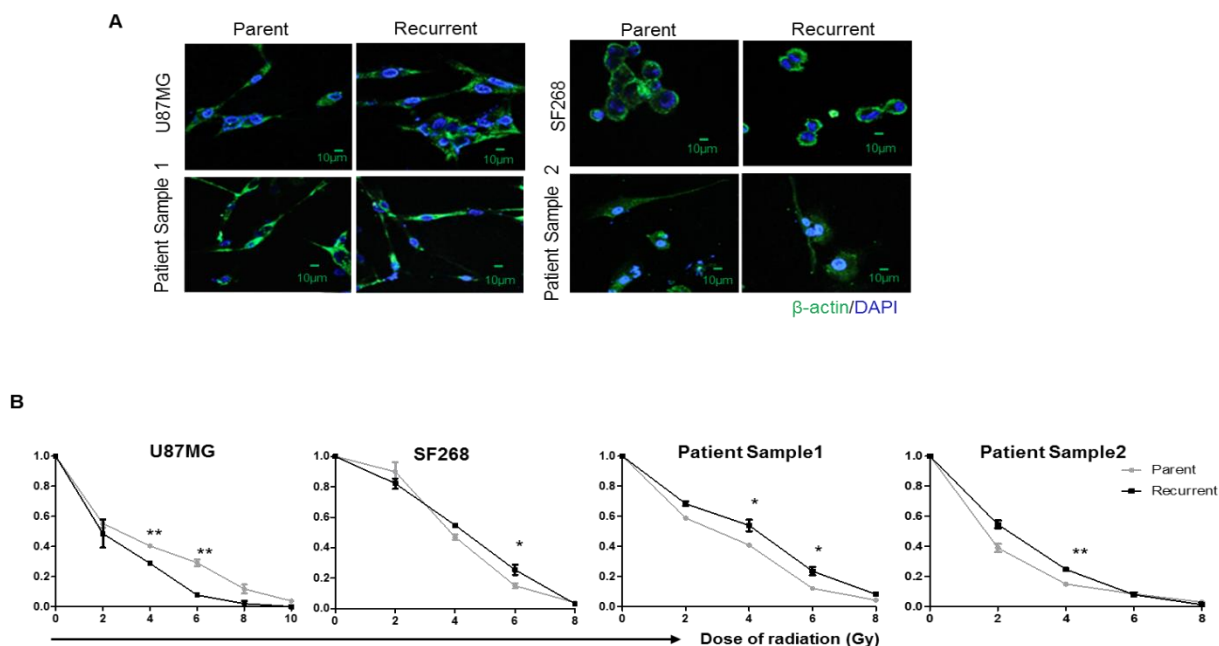


**Figure 2.19: Recurrent cells generated from cellular model shows similar morphology and growth rate as that of parent cells.** A) Immunofluorescence images of the parent and the recurrent cells from the two cell lines and patient samples as indicated. Cells are stained for  $\beta$ -actin (green) and counterstained with DAPI (blue) to visualize the nucleus. B) Line graphs show the growth curve for parent and recurrent cells. Cell growth was monitored by trypan blue assay. \* denotes  $p \leq 0.05$ , and \*\* denotes  $p \leq 0.01$ . Scale bar for immunofluorescence images-  $10\mu\text{m}$ .

### 2.2.3.2 Recurrent cells possess enhanced radiation resistance as compared to the parent population

Since the recurrent cells are formed from the innately radio-resistant cells, we examined the resistance potential of the recurrent and parent cells. As shown in figure 2.20A, clonogenic assay was performed to compare the survival of the parent and the recurrent cells at different doses of radiation. We observed that the recurrent cells from the patient samples as well as SF268 indeed had significantly higher cell survival at the low doses of radiation ranging from 2-6Gy (Figure 2.20A). The  $D_0$  (dose at which 37% of cells survive upon radiation treatment)

of the recurrent cells was found to be 4.1, 5.2, 4.7 and 4.2Gy whereas it was found to be 5.79, 4.79, 3.5 and 3.4Gy in the parent population of U87MG, SF268, patient sample 1 and patient sample 2, respectively. These data show the enhanced radio-resistant character of the recurrent cells from the patient samples and SF268. However, the U87MG recurrent cells showed higher radio-sensitivity as compared to the parent cells (Figure 2.20A).

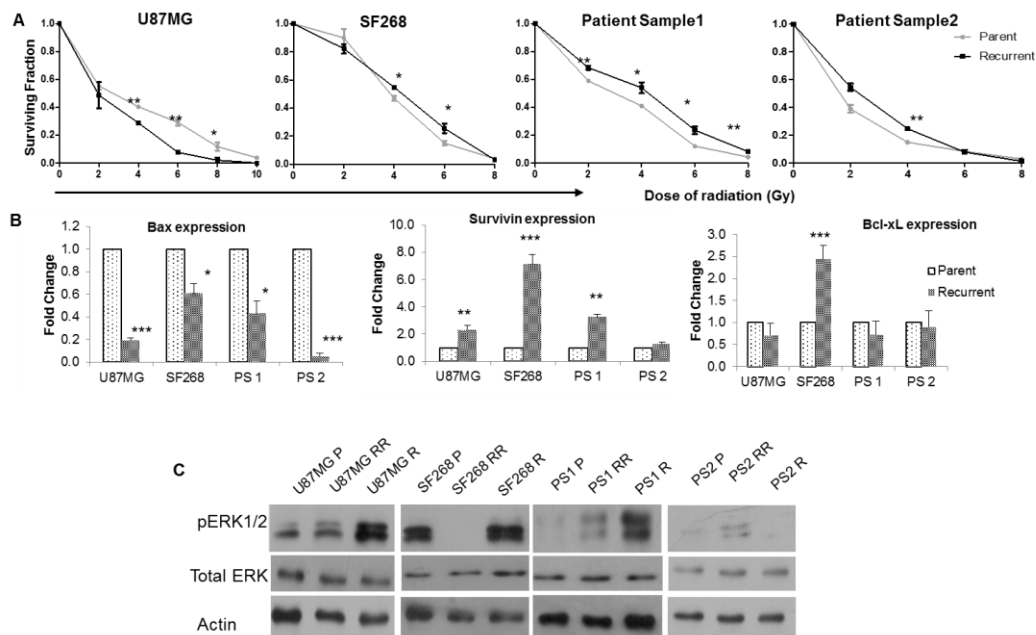


**Figure 2.20: Recurrent cells reveal differences as compared to parent cells at the molecular level.** A) Clonogenic survival assay curve showing the survival fraction at different doses of radiation for parent and recurrent cells of U87MG, SF268, patient samples 1 and patient sample 2. B) Bar graph shows the transcript levels of pro-survival genes Survivin and Bcl-xL and pro-apoptotic gene Bax in parent and recurrent population as determined by qPCR. C) Western blot analysis using anti-pERK1/2, total ERK and  $\beta$ -actin antibodies on parent cells (P), radiation resistant (RR) and recurrent (R) cells of the indicated samples. PS1 represents patient sample 1 and PS2 represents patient sample 2.

### 2.2.3.3 Recurrent cells show up-regulation of survival pathways

Enhanced survival capacity is a known property of treatment-resistant recurrent GBM cells. Therefore, the transcript levels of known pro-survival genes Survivin, Bcl-xL and pro-apoptotic gene Bax in the recurrent and parent cells were investigated by quantitative PCR (Figure 2.20B). The graph shows that recurrent cells had lower mRNA expression of pro-apoptotic gene Bax when compared to their parental counterpart whereas the transcript levels of Survivin was 2-7 fold higher in these cells compared to the parent cells. However, patient sample 2 (PS2) showed only a marginal increase in the Survivin expression. The increased expression of Survivin in the recurrent cells formed upon lethal exposure of radiation is noteworthy since Survivin has been shown to be overexpressed in Glioblastoma tumours associated with high anti-apoptotic activity [200, 201]. The expression of other pro-survival gene Bcl-xL in the recurrent cells remain unaltered except for SF268 cells (Figure 2.16B), may be due to the dependency of GBM recurrent cells on Survivin for its anti-apoptotic activity. MAPK pathway- another major survival pathway known to promote tumour growth was also investigated for the phosphorylation of ERK1/2 in the parent, immediately after IR in the RR cells and recurrent (R) cells. It was observed that as compared to parent cells, recurrent cells had higher expression of pERK1/2 indicative of heightened survival capacity in recurrent cells, except in the PS2 recurrent cells where the levels of pERK1/2 were comparable to parent cells (Figure 2.20C). The expression of pERK1/2 was less pronounced in the cells generated immediately after radiation as compared to the recurrent cells (R) probably due to late activation of survival signals.

#### *2.2.3.4 Whole transcriptome analysis confirms recurrent cells are different from parent cells*

As opposed to a particular biological behaviour where fewer molecular players impart that specific characteristic to a cell, whole transcriptome analysis provides a global picture of cellular transcriptional activity at any given time. Hence, we performed whole transcriptome

sequencing of the parent and recurrent cells. Principal Component Analysis (PCA) of the transcriptome data showed Principal Components 3 and 6 captured maximum variations from the data, distinguishing the recurrent cells from parent cells, while patient sample 1 parent clustered separately (Figure 2.21).

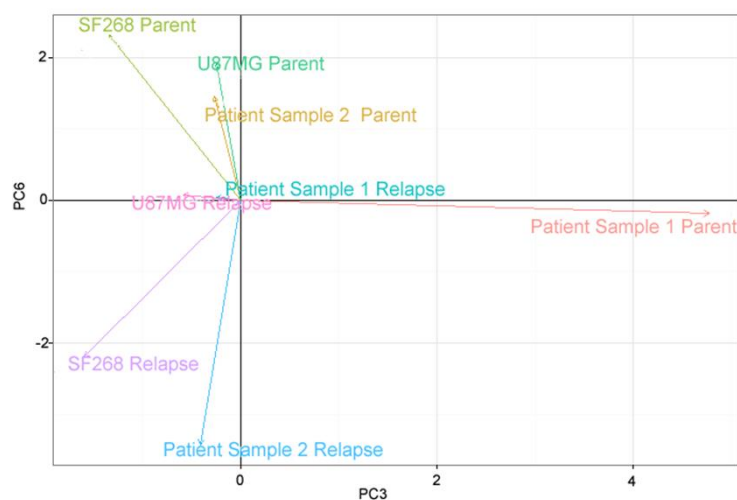


**Figure 2.21: PCA plot of global transcripts showing differences between parent and recurrent cells.**

Collectively, these data show that the parent and recurrent populations were morphologically similar but differing in certain biological properties like proliferation and radiation resistance. Because of the inconsistencies observed in these properties among different populations, neither of them can be used as a hallmark of either parent or recurrent population. However, global expression profile of these samples by RNA-sequencing revealed unique transcriptional landscape for these populations, separating them into distinct clusters. This result suggested that the use of methods that detect global molecular changes in parent and recurrent cells could uniquely identify parent and recurrent cell populations as separate entities. Thus, we explored Raman spectroscopy, a rapid, label-free, cost-effective, non-invasive approach which yields global or holistic information about the biochemical milieu of the sample and may provide recurrence - specific spectral markers.

### *2.2.3.5 Mean and difference spectra from Raman Spectroscopy of the parent and recurrent population reveals spectral features unique to recurrent population*

Raman spectroscopy of parent and recurrent cell populations of all the cultures was carried out as described in the materials and methods section. First, mean spectral comparisons were undertaken, followed by multivariate analysis of the data. The mean normalized spectra for parent and the recurrent cell lines from both the patient samples and cell lines were computed for both fingerprint (700-1800 $\text{cm}^{-1}$ ) as depicted in figure 2.22 and high wavenumber (2800-3100 $\text{cm}^{-1}$ ) regions as shown in figure 2.23. Average spectra from each parent population were overlaid with their respective recurrent population for better comparison and understanding. Additionally, difference spectra between parent and recurrent population were also generated as shown in figure 2.22A-D and figure 2.23A-D and annotated based on previous reports [197, 198, 202-204]. The analysis of the spectra showed that features corresponding to higher DNA content (1095  $\text{cm}^{-1}$ - DNA backbone, 1340  $\text{cm}^{-1}$ -total nucleic acid content and 1610  $\text{cm}^{-1}$ -cytosine base), protein related features like amide III (1260  $\text{cm}^{-1}$ ),  $\text{CH}_2$  bending at 1450  $\text{cm}^{-1}$ , phenylalanine (1008  $\text{cm}^{-1}$ ), tryptophan (1560  $\text{cm}^{-1}$ ) and sharp features around amide I (1660  $\text{cm}^{-1}$ ) characterized the parent populations. Thus, in parent population, higher DNA content and overall protein-related features were observed. On the other hand, prominent features of recurrent population included lipid-related features like 1272  $\text{cm}^{-1}$  and 1305  $\text{cm}^{-1}$ , sharp 1447 $\text{cm}^{-1}$ , 1725  $\text{cm}^{-1}$  and 1746  $\text{cm}^{-1}$ ; protein bands like amide III (1262  $\text{cm}^{-1}$ ), shifted  $\text{CH}_2$  bend (1447  $\text{cm}^{-1}$ ) and sharp amide I (1660  $\text{cm}^{-1}$ ). The band at 1660  $\text{cm}^{-1}$  could also be attributed to ceramide backbone as another minor shoulder band was observed at 1673  $\text{cm}^{-1}$  in some recurrent cells' spectra. Difference spectra were also computed by subtracting parent cells'

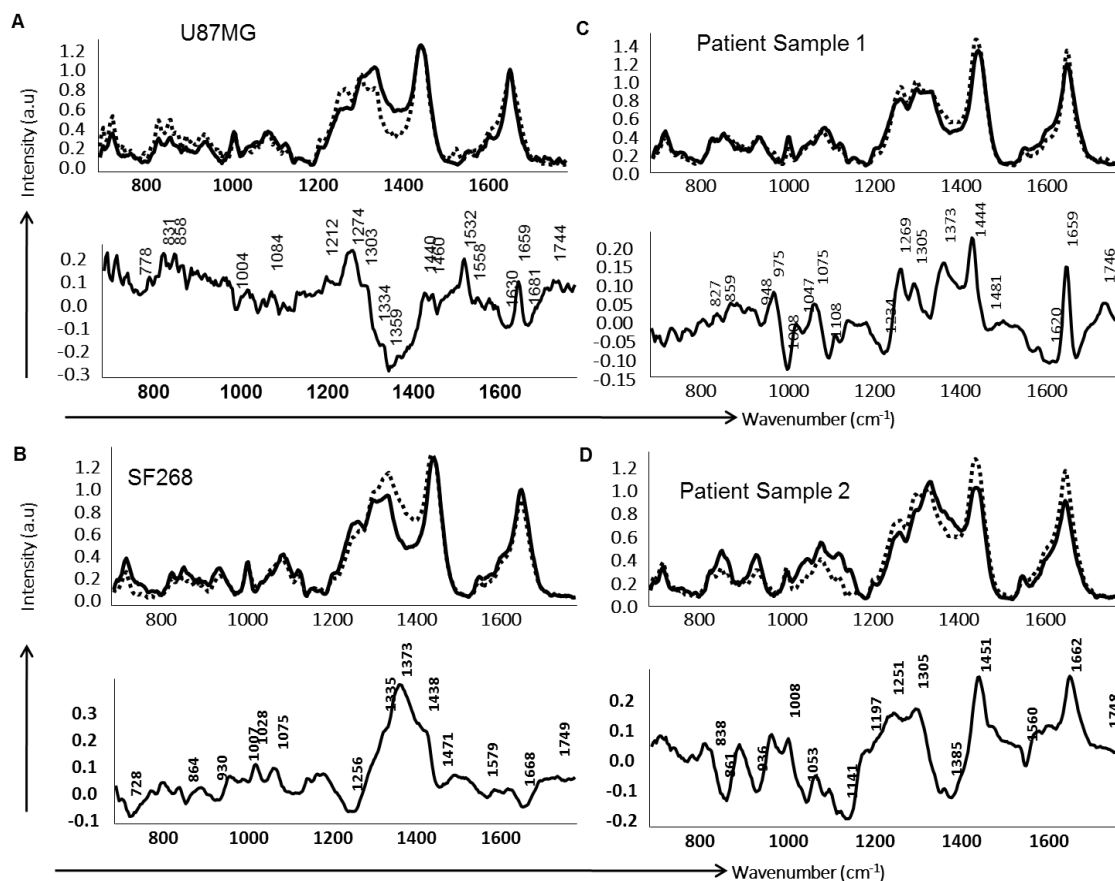


**Figure 2.22: Mean and difference spectra from parent and recurrent population reveals spectral features unique to recurrent population.** A-D) shows the mean spectra and difference spectra of parent and recurrent population obtained for U87MG, SF268, patient samples 1 and patient sample 2, respectively. Dotted lines represent recurrent cells and solid lines represent parent cells.

spectra from recurrent cells' spectra which showed positive peaks at  $1260\text{-}70\text{ cm}^{-1}$ ,  $1305\text{ cm}^{-1}$ ,  $1440\text{-}50\text{ cm}^{-1}$ ,  $1660\text{ cm}^{-1}$  and  $1744\text{ cm}^{-1}$  corresponding to lipid/phospholipid and protein content and negative bands at  $1075\text{-}1090\text{ cm}^{-1}$ ,  $1330\text{-}40\text{ cm}^{-1}$ ,  $1480\text{ cm}^{-1}$  corresponding to DNA (Figure 2.22A-D). However, SF268 recurrent population was characterized by lower protein and slightly higher DNA content compared to the parent cells. Mean spectral analysis in high

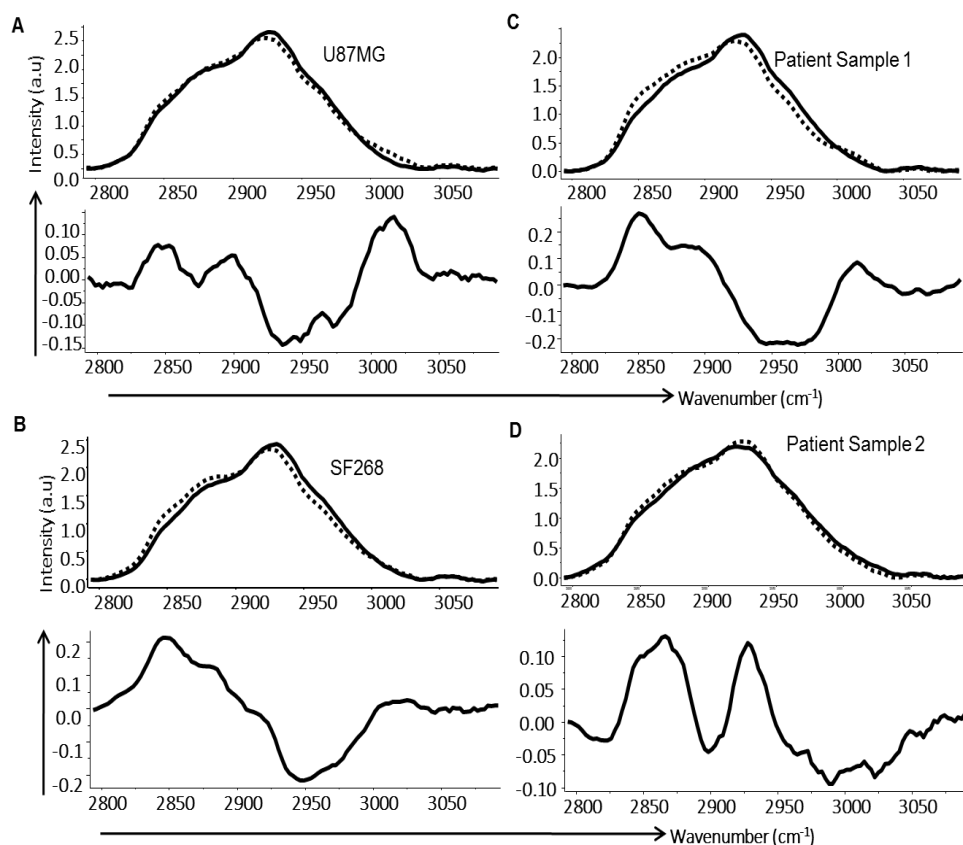


**Figure 2.23: Mean and difference spectra from parent and recurrent population reveals higher lipid peaks in recurrent population.** A-D) shows the mean spectra and difference spectra of parent and recurrent population obtained for U87MG, SF268, patient samples 1 and patient sample 2, respectively in high wavenumber region. Dotted lines represent recurrent cells and solid lines represent parent cells.

wavenumber region depicted in figure 2.23A-D indicated shoulder band in the  $2850\text{-}2900\text{cm}^{-1}$  region and band in the region of  $2900\text{-}2950\text{cm}^{-1}$ . In all the samples, a higher breadth and intensity in the  $2840\text{-}2880\text{cm}^{-1}$  region corresponding to lipid content was observed in the recurrent samples with respect to parent samples while positive peak around  $2900\text{cm}^{-1}$  indicative of protein was seen in parent cells. Thus, from parent to recurrent, in both the fingerprint and high wavenumber regions, a shift towards increased lipid content was observed. This shift from protein to lipid synthesis in the recurrent population is consistent

with several reports, demonstrating an increase in the lipid biogenesis contributing to resistance to chemotherapy and radiotherapy [205, 206] [207]. Also, a sharp peak observed at  $1660\text{ cm}^{-1}$  in the recurrent population attributed to ceramide has been implicated in driving cancer resistance to various chemotherapeutic drugs[208, 209] and may play a role in promoting radio-resistance. Thus, Raman spectroscopy analysis revealed characteristic features for both recurrent and parent cells in terms of peak position and intensity variations. Major features observed in recurrent cells included lower DNA content, higher lipids, phospholipids and proteins.

#### *2.2.3.6 Principal component analysis (PCA) identifies unique clustering of recurrent and parent cells*

As the parent and recurrent cells showed variations in their Raman spectra, the feasibility of classification of parent and recurrent population as distinct entities using RS was also explored. First, an unsupervised Principal component analysis (PCA) was performed to obtain a unique classification of the recurrent population (obtained from primary cultures and cell lines) as compared to their parent counterpart. PCA was carried out using 10 factors. Out of these, maximum variability could be captured between factor 2 and 4. Scatter plot between factor 2 and 4 indicated classification between each of the parent and recurrent population (Figure 2.24A). In fact, two almost distinct clusters corresponding to parent and recurrent population were observed. The loadings spectra corresponding to factors 2 and 4 are shown figure 2.24B. The loadings of factor 2 showed spectral features corresponding to DNA ( $1072\text{ cm}^{-1}$ ,  $1345\text{ cm}^{-1}$ ,  $1380\text{ cm}^{-1}$ ), and proteins ( $1255\text{ cm}^{-1}$ ,  $1448\text{ cm}^{-1}$ ,  $1665\text{ cm}^{-1}$ , tryptophan  $1559\text{ cm}^{-1}$ ) while factor loading 4 had features from lipids ( $1440\text{ cm}^{-1}$ ,  $1740\text{ cm}^{-1}$ ), DNA ( $1072\text{ cm}^{-1}$ ,  $1344\text{ cm}^{-1}$ ,

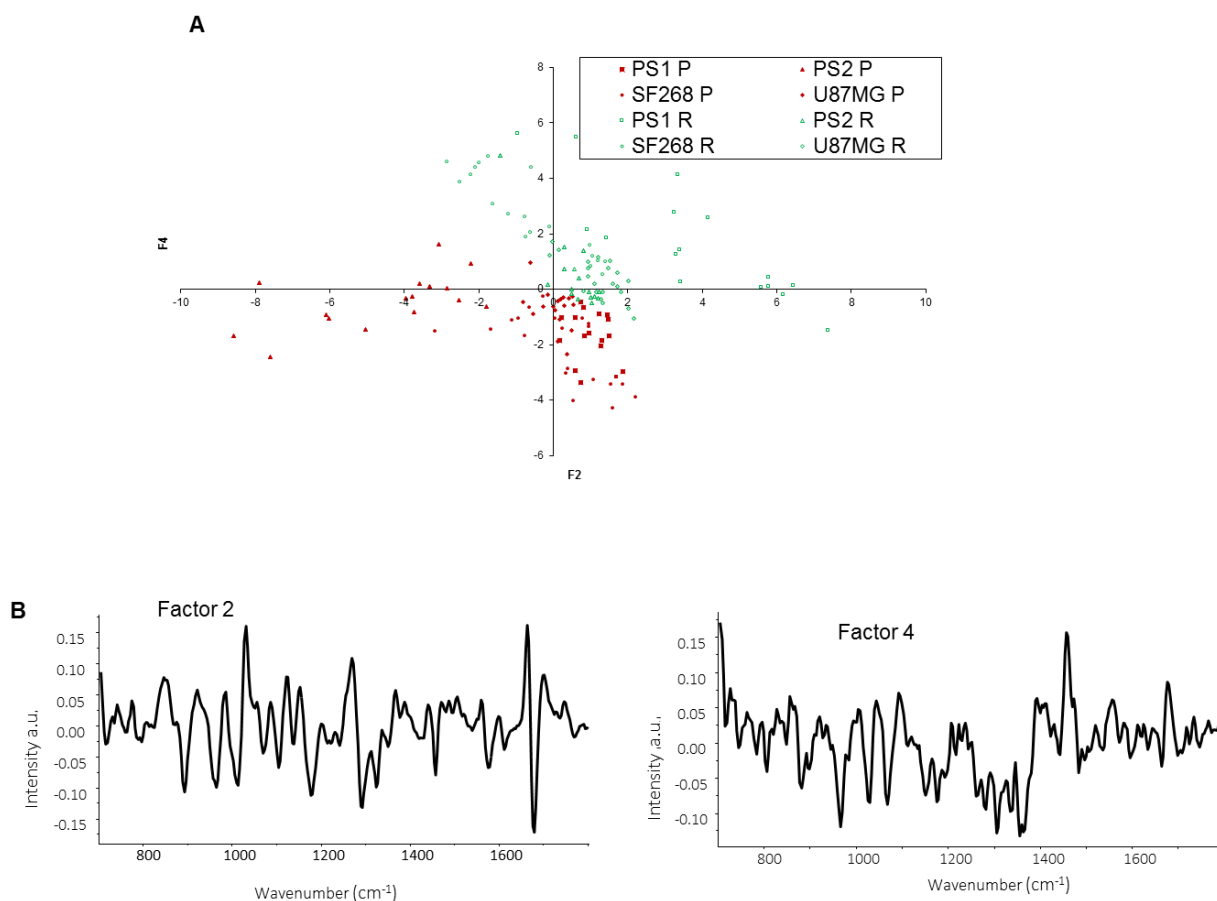


**Figure 2.24: PCA analysis classifies the recurrent cells from parent cells.** A) PCA scatter plot for parent and recurrent populations from the cell lines and two samples. B) Spectra show the loadings of factor 2 and 4.

1373  $\text{cm}^{-1}$ ) and proteins (1250  $\text{cm}^{-1}$ , 1650  $\text{cm}^{-1}$ , phenylalanine (1005  $\text{cm}^{-1}$ ). PCA for high wavenumber region (2800-3100  $\text{cm}^{-1}$ ) was also carried out and showed a tendency of classification between parent and recurrent spectra of all samples. Although PCA is a data visualization tool, this analysis indicated that the unique pattern clustering is due to overall differences in the biochemical profile of recurrent and parent cells. The data also revealed that exposure to radiation alters the biochemical profile of a cell.

*2.2.3.7 Principal component-linear discriminant analysis (PC-LDA) distinctly classifies the recurrent cells from parent cells*

Upon obtaining modest classification of all recurrent cells from parent population using PCA, a method used for exploratory data analysis unravelling trends and outliers in the data, PC-LDA, a supervised method of data analysis, was explored for better classification. In the first step, standard models using one set of experimental data from parent and recurrent populations of U87MG, SF268, patient sample 1 (PS1) and patient sample 2 (PS2) were built and validated by leave-one-out-cross-validation (LOOCV) In the subsequent step, the model was evaluated by independent data acquired from PS2 and U87MG cell line.

Five factors accounting for ~93% correct classification were used to build the standard model (Figure 2.25A). The scatter plot for PC-LDA is shown in figure 2.25B. Like PCA, two major clusters representing all parent and all recurrent populations were observed. As shown in table 2.2.1, almost 100% classification efficiency was achieved for all parent and recurrent populations, indicating important and distinct differences between these two populations. Moreover, even in LOOCV, >95% classification efficiency was observed for all groups with minor misclassifications between recurrent populations of U87MG, SF268 and PS1. Upon test prediction on this standard model, 16/16 spectra from PS2 parent group and 14/16 spectra from recurrent group were correctly classified. All 18 spectra from U87MG parent group were correctly classified and 16/22 recurrent population could be correctly classified. Of the 6 misclassifications in U87MG recurrent population, 5 were classified as PS2 recurrent group indicating overlapping features between these two samples. Thus, the efficacy of RS in correct identification of parent and recurrent populations was demonstrated.

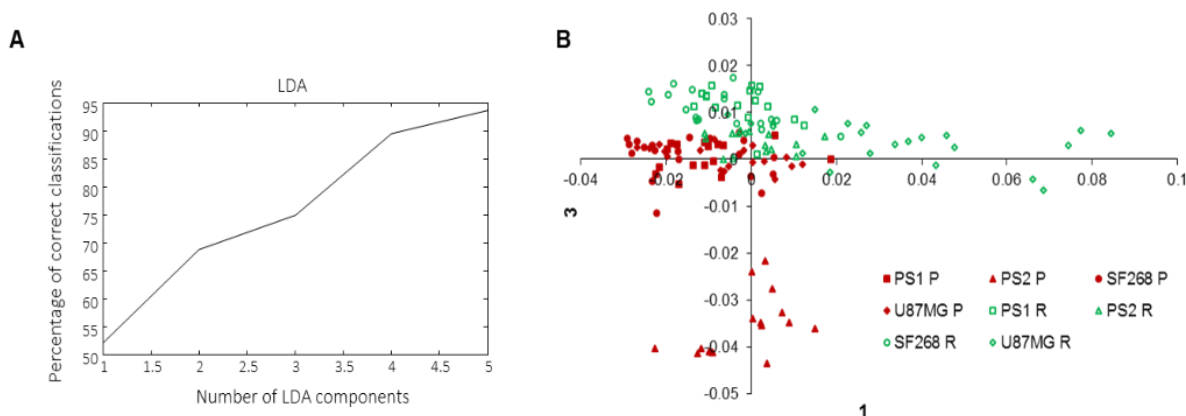


**Figure 2.25: PCA-LDA analysis classifies the recurrent cells from parent cells.** A) PCA factors used for the study is shown. B) PCA-LDA scatter plot for parent and recurrent populations from the cell lines and two samples.

### 2.2.3.8 Raman spectral analysis of GBM tissues classified a population of GBM tissues differing in clinical outcome

As shown above, we could demonstrate that Raman spectroscopy was able to distinguish between biologically variable recurrent cells from their parental counterpart. However, as patient derived primary cultures do not exactly recapitulate the clinical samples, we further went on to examine independently the feasibility of Raman spectroscopy in categorizing the highly heterogeneous primary tissue samples. As previously reported, presence of innately resistant cells within GBM tumours affect overall survival of the patients [32, 172]. Therefore, we hypothesized that patients responding to standard treatment (responders) may have lower or no percentage of innately resistant sub-population while the patients non-responsive to standard treatment (non-responders) may have higher percentage of these innately resistant cells. Based on this hypothesis, 6 GBM primary tissues with confirmed clinical outcome (responders=3 and non-responders=3) were analysed in this preliminary

study to investigate if tumours with differential treatment response can be distinguished using RS.

**Table 2.2.1: PC-LDA Standard model for recurrent and parent cells.**

Confusion Matrix								
	PS1 P	PS1 R	PS2 P	PS2 R	SF268 P	SF268 R	U87MG P	U87MG R
PS1 P	17	0	0	0	0	0	0	0
PS1 R	0	16	0	0	0	0	0	0
PS2 P	0	0	16	0	0	0	0	0
PS2 R	1	0	0	14	0	1	0	0
SF268 P	0	0	0	0	20	0	0	0
SF268 R	0	0	0	1	0	18	0	0
U87MG P	0	0	0	0	0	0	18	0
U87MG R	0	0	0	5	0	0	1	16
Leave-one Out cross (LOOCV) confusion matrix								
	PS1 P	PS1 R	PS2 P	PS2 R	SF268 P	SF268 R	U87MG P	U87MG R
PS1 P	17	0	0	0	0	0	0	0
PS1 R	0	16	0	0	0	0	0	0
PS2 P	0	0	16	0	0	0	0	0
PS2 R	1	0	0	14	0	1	0	0
SF268 P	0	0	0	0	20	0	0	0
SF268 R	0	0	0	1	0	18	0	0
U87MG P	0	0	0	0	0	0	18	0
U87MG R	0	0	0	5	0	1	1	15
Test prediction								
	PS1 P	PS1 R	PS2 P	PS2 R				
PS2 P	0	0	16	0				
PS2 R	1	0	0	14				
U87MG P	0	0	0	0				
U87MG R	0	0	0	5				

PCA and PCA-LDA of these tissues identified two almost distinct clusters belonging to responders and non-responders group with minor overlap (Figure 2.26A and B, Table 2.2.2). Average spectra analysis was also undertaken to understand the bio-molecular basis of classification. Spectral features for responders and non-responder tissues indicate prominent features of protein (amide III, CH<sub>2</sub> deformation, C=C, Tyr, Trp and amide I), DNA (1320, 1340, 1485 cm<sup>-1</sup>) and lipids (1313, 1750 cm<sup>-1</sup>) as shown in figure 2.26C. To understand the changes pertaining to non-responders group, difference spectra were computed. The non-responders difference spectra identified positive spectral features at 1313 cm<sup>-1</sup> (CH<sub>3</sub>/CH<sub>2</sub> twisting/bending/wagging of lipids; CH<sub>3</sub>CH<sub>2</sub> twisting mode of lipid/collagen), 1320-1321 cm<sup>-1</sup> (DNA bases, Amide III (alpha-helix), CH<sub>2</sub> deformation of lipids), 1340 cm<sup>-1</sup> (nucleic acid content), 1367 cm<sup>-1</sup> (phospholipids), 1485 cm<sup>-1</sup> (G and A bases of DNA), 1579 cm<sup>-1</sup> (DNA and heme) and 1750 cm<sup>-1</sup> (lipid) in the non-responding group (Figure 2.26D). Interestingly, some spectral similarities were observed in lipid related features between non-responding group and the recurrent samples from our cell cultures. However, biological meaning of this similarity requires further investigation. Additionally, spectral features of DNA also contributed to their individual classification. Overall these results indicate that Raman spectroscopic analysis of the highly heterogeneous primary tissues obtained before any chemo-radiation therapy may help in predicting prognosis of the patients.

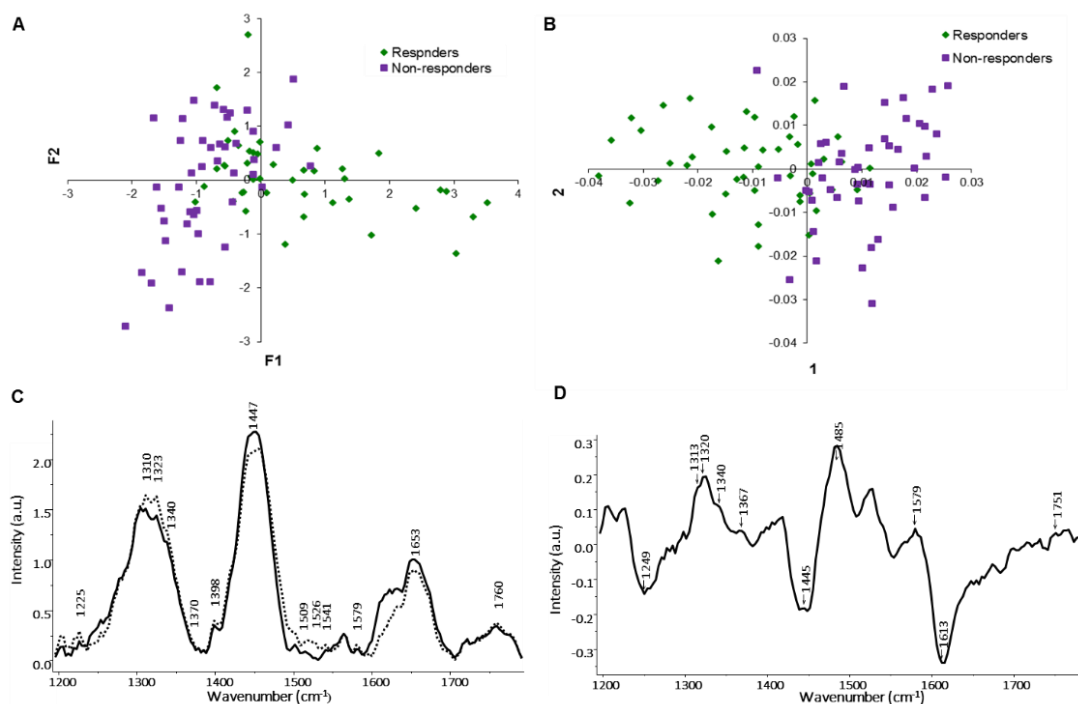


**Figure 2.26: Raman spectroscopic analysis distinctly classifies the non-responders from responders group of patients.** A) PCA scatter plot for non-responders and responders patient samples. B) PCA-LDA scatter plot for non-responders and responders patient samples. C) Mean spectra of the responding group from the non-responding group of samples. Dotted lines represent non-responding group while solid lines represent responding group of patients. D) Difference spectra computed after subtracting spectra of responding group from the non-responding group of samples.

## 2.2.4 Discussion

Even after extensive studies on GBM, the prognostic determinants have been limited to the methylation status of MGMT, mutations in IDH1, PTEN and Karnofsky performance score (KPS)[210]. RS is a non-invasive technique that provides insights into the chemical milieu of the samples. Apart from its application in the detection and classification of malignant cells from the normal cells, RS has also shown potential in predicting the radiation response from

**Table 2.2.2: PC-LDA standard model for responding and non-responding GBM tissues.**

<b>Confusion matrix</b>		
	Responders	Non-responders
Responders	34	11
Non-responders	3	42
<b>Leave-one Out cross (LOOCV) confusion matrix</b>		
	Responders	Non-responders
Responders	31	14
Non-responders	3	42

the tissues and recurrence from serum samples[179, 186, 188-190, 192, 193, 195]. A recent development of hand held Raman probe has enabled the detection of brain tumour cells with higher efficiency during the surgery [187].

These studies have so far investigated diagnosis and surgical demarcation in glioma. As radiation resistance is the primary cause of poor survival rates in glioma patients, early detection of these tumours can possibly help in optimizing the treatment regime and help in improving prognosis of these patients. To understand the mechanisms responsible for radiation resistance, a cellular radiation resistance model was developed as described in the first part of this chapter. Most of the recurrent populations generated in this model displayed higher survival capacity at low dose of radiation mediated by enhanced pERK1/2, higher mRNA expression of Survivin and down-regulation of Bax as compared to the naïve parent cells. Balance between the pro-apoptotic and pro-survival genes are known to determine the fate of the cells, with over-expression of pro-survival genes imparting resistance phenotype to the recurrent cells. Additionally, whole transcriptome analysis classified the recurrent samples separately from the parent cells, however; intra sample heterogeneity was also seen as it is the inherent property of GBM cells.

As an alternative, Raman spectroscopy- a sensitive technique based on vibrational spectroscopy known to provide holistic information about the biochemical changes inherent

to the sample, was evaluated for the detection of these recurrent cells. Using Raman Spectroscopy, we were able to distinguish the recurrent cells from the parent populations of primary patient cultures and cell lines. Raman spectral features in the recurrent cells revealed significantly different biological composition seen in lipid, DNA and protein content of these cells. Variations were also seen in the spectral features of individual recurrent and patient samples in the form of minor spectral shifts and intensity-related differences. These inter-sample differences apparent between parent (or recurrent) populations from different origins were however, less significant than spectral features characteristic to parent and recurrent cells. PCA and PCA-LDA highlighted these global features specific to both parent and recurrent cells and brought about classification between parent and recurrent populations from different samples. However, variation was seen in the recurrent cells from SF268 which revealed higher DNA content and lower protein content as compared to the parent cells. This cell line also demonstrated atypical behaviour in different biological assays; this unusual biological behaviour of SF268 cell line could be the basis for the observed findings. The variability observed with respect to SF268 cell line may be reflective of the multiformity existing in GBM and may lead to a reduced sensitivity of any analytical method aimed at detecting recurrent cells.

GBM tumours are known to be highly heterogeneous and the inherently recurrent cells may vary in different tissues. Previous reports with cell-based Raman spectroscopic studies have examined the feasibility of differentiating normal and abnormal (pre-malignant or malignant phenotype) cells in both oral and cervical cancers [211, 212] and also the feasibility of identifying a cancer cell in a mixed cell population having subtle variations has been demonstrated [213]. In case of oral and cervical cancers, heterogeneous cell populations were obtained on exfoliation. In most subjects, the atypical and malignant cells were obscured by presence of overwhelmingly large number of normal cells. However, using a

pellet-based approach, RS was able to identify the small number of abnormal cells among the heterogeneous group of samples with ~80% efficiency. Additionally, the classification and characterization of cancer cells exhibiting MDR phenotype has also been demonstrated in the sarcoma cell lines using RS[214]. RS analysis on primary GBM tissues was also conducted for this study to investigate the feasibility of RS to classify these primary tissues based on their clinical outcome (responders or non-responders to treatment). PCA and PCA-LDA classified these tissues into two groups with minor overlap observed amongst them, contributed by the common clonal cells. Spectral analysis revealed the presence of higher lipid and DNA related features in the non-responding group of patients compared to the responding group. Spectral similarity between the non-responders and the *in vitro* recurrent cells was observed but requires further examination for a meaningful interpretation of this observation. Additional features unique to either cells in culture or primary tumour samples were also seen, however a direct correlation between the two was not envisaged in this study. Further, several other spectral features characteristic to non-responders in the GBM tissue study could be attributed to increased spot size, tissue architectural and morphological contributions, including deeper areas attributed to a penetration depth of ~5mm using the fiber-probe based system.

These findings indicate potential of RS in identifying recurrent cells separately from the parent cells using cellular resistance model. Since cell line based model systems do not adequately represent the heterogeneous GBM disease, we examined Raman spectra of an independent cohort of tumour samples where we found that RS could classify these tissues based on their therapy response. Nevertheless, an extensive study on larger cohort of naïve primary GBM patients' needs to be undertaken to confirm the present findings. These studies can then set the stage for clinical translation of Raman spectroscopy for glioblastoma prognostics.

### Chapter 3

*Identification of differential double strand break repair pathway activation and chromatin changes in radiation resistant compared to the parent cells.*

This chapter investigates the role of DNA double strand break repair pathway and its regulation in mediating survival of glioblastoma radiation resistant cells. The first part of the chapter discusses the differential recruitment of sensory kinases ATM/ATR and preferential use of NHEJ repair in the radiation resistant cells which result in survival of resistant cells and impart differential survival capacity to recurrent cells (cells formed from radiation resistant cells). The second part of this chapter discuss the significance of chromatin predominantly histone methylation H3K36me2 and SETMAR methyltransferase in facilitating the NHEJ repair in the radiation resistant cells.

### **3.1 Introduction**

DNA is exposed to various types of damage resultant of endogenous metabolic and replication stress or exogenous exposure to UV, ionizing radiation and chemotherapeutics. One such damage: double strand breaks (DSBs) are the most toxic lesion generated by ionizing radiation [215-217]. Even if one such lesion remains unrepaired it could lead to genomic instability and/or cell death. Indeed, defective DSB repair is reported to be associated with various developmental, immunological, and neurological disorders and predispose to cancer [218, 219]. Therefore, cells have orchestrated elaborate mechanisms as discussed below to ensure proper repair of DSBs.

The repair of DSBs is brought about by two major repair pathways: homologous recombination (HR) and non-homologous end-joining (NHEJ). In NHEJ, the ends of the DSB are protected from 5' end resection by the double-stranded DNA (dsDNA) end-binding protein complex, the Ku70-Ku80 heterodimer (Ku) which holds the two ends together in close proximity to each other. Promoting direct ligation of the DSBs, NHEJ an error-prone repair occurs in all cell cycle phases, generating several insertions, deletions, translocations and substitutions at the break site during its process [68]. Compared to NHEJ, HR repairs

DNA in an error-free manner predominantly in S and G2 phase of the cell cycle, resecting the DSBs by nucleases and helicases including MRN, CtIP, EXO1, generating 3' single-stranded DNA (ssDNA) overhangs. RAD51 recombinase then further assembles onto the ssDNA creating a nucleoprotein filament which invades into homologous duplex DNA, acting as a template for the repair process [220].

Apart from the multiple protein regulators of DNA repair, chromatin plays an important role by controlling the accessibility of these repair factors to the lesions. Immediately after DNA damage, one of the early alteration that occurs at chromatin is the phosphorylation of the histone variant H2AX nearby the break site. The phosphorylated form of H2AX ( $\gamma$ H2AX) marks the nucleosomes by surrounding the DSBs, signalling the presence of damage and links the damage to repair machinery, initiating the recruitment of repair factors [221, 222]. This phosphorylation of H2AX at the DSB site is achieved by the PI3 kinases ATM, ATR or DNA-PK depending on the source of the damage, extending the signal beyond 2Mb of site of damage [223-225]. While ATM is rapidly activated by DSBs generated by DNA damaging agents like ionizing radiation [226, 227], ATR is activated by ssDNA generated at stalled replication forks and DSBs, coated with RPA2 protein [228]. The presence of phosphorylated H2AX is thought to stabilize the interaction between repair components at the break site, facilitating the accumulation of other DDR proteins [229-231]. Apart from H2AX, ATM phosphorylates and activates multiple downstream substrates including kinases like Chk2 while ATR conventionally is known to activate Chk1 [232, 233]. However, recent reports have also demonstrated a cross-talk between the ATM and ATR for the activation of these downstream target kinases [234]. DNA-PK, another serine/threonine kinase part of the PI3-kinase family of proteins [235], can be activated by the DNA damage induced by IR, UV or even V(D)J recombination. It is composed of a catalytic subunit and

possesses an inherent DSB binding activity that is stabilised by the Ku70–Ku80 heterodimer [236], hence is involved in NHEJ pathway of repair.

In addition to phosphorylation, histones undergo other modifications like phosphorylation, acetylation, methylation and ubiquitination during DNA repair as shown in figure 3.1. Of these modifications methylation of histones is especially known to directly bind

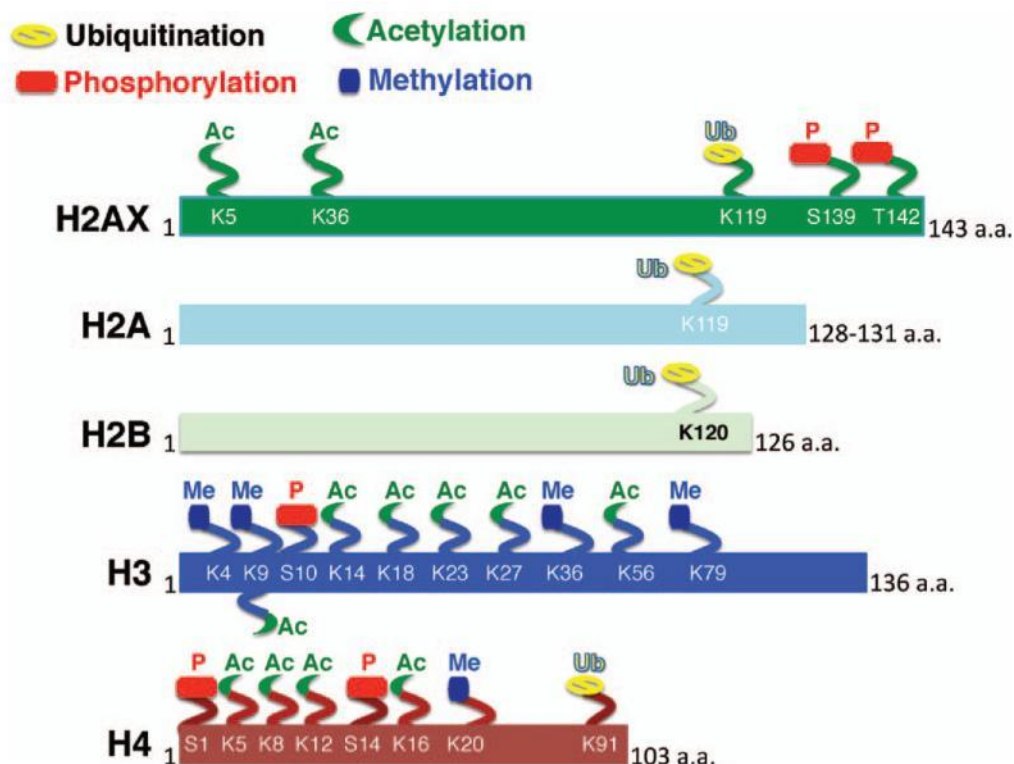


**Figure 3.1: Types of histone modifications involved in DNA repair** [237].

to the repair factors. Methylation of histone H3 at lysine 79 (H3K79me2) by Dot1 methyltransferase mediates recruitment of 53BP1 protein (via its tudor domain) after damage [238]. Direct binding of 53BP1 also occurs via MMSET and SET8 dependent H4K20me2 [111, 239]. Additionally, histone methylations including H3K4me2 and H3K36me2 have been associated with the transcription of active euchromatin, alternative splicing, dosage compensation and transcriptional repression, as well as DNA repair (via NHEJ pathway) and recombination [240, 241]. Furthermore, H3K79me2 and H3K27me2 are demonstrated to be

involved in regulating DNA damage response, cell cycle and transcriptional regulation [242, 243]. The enhancer of zest homolog-2 (EZH2), the catalytic component of Polycomb Repressor Complex (PRC2) induces the methylation of H3K27me1 and H3K27me2 in mammalian cells leading to transcriptional repression [243]. H3K9me2 is reported to prevent activation of gene expression by recruiting transcriptional repressors of the HP1 family and thus, inhibiting acetylation [105, 244]. Loss of this modification leads to increased spontaneous DNA damage in heterochromatin region and activation of DNA repair cell cycle checkpoints [245].

In addition to its function as a regulator of DNA repair process, histone methylations have been reported to be over-expressed in many cancers including prostate, lung, stomach and pancreatic cells [246].

Thus, in this study we aimed to investigate the role of DNA repair and histone dimethylations in mediating survival of glioblastoma cells. Glioblastoma Grade IV is the highly malignant form of brain tumour associated with poor overall survival contributed by the treatment refractory cells. In our previous report and chapter 1, we have shown using an *in vitro* radiation model that a sub-population of inherently resistant cells (RR) survives the radiation exposure, over-expressing multiple survival pathways. In this study, these resistant cells were examined to identify differences in DNA repair pathway contributing to their enhanced survival. We show that the radiation resistant cells undergo a global de-compaction of the chromatin mediated by over-expression of histone methylations H3K36me2 and H3K4me2 along with the increase in SETMAR methyltransferase that facilitate efficient NHEJ repair.

## **3.2 Materials and Methods**

### **3.2.1 Electron microscopy**

Three million parent and radiation resistant cells were harvested and washed with phosphate-buffer saline, following the cells were fixed with 3% glutaraldehyde for 2 hours at 4°C. The cells were then washed 3 times with 0.1M sodium cacodylate buffer for 5 minutes and centrifuged at 3000rpm. Post fixation, cells were treated with 0.1% osmium tetroxide for 1 hour at 4°C, followed by 3 washes with 0.1M sodium cacodylate buffer. Subsequently, the cells were dehydrated in increasing percentage of absolute alcohol: 30% absolute alcohol-15 minutes, 50% alcohol- 15 minutes, 70% alcohol- 30 minutes, 90% alcohol-15 minutes and finally in 100% absolute alcohol for 60 minutes. Dehydrated cells were then incubated with absolute alcohol and araldite A (1:1 ratio) for 30 minutes at 60°C, araldite A for 30 minutes at 60°C, araldite B for 30 minutes at 60°C and the finally in araldite B for 48-72 hours at 60°C for polymerization and embedding of the cells. Ultrathin sections of 70nm were then made using Leica Ultra microtome (UC7). The sections were then stained in 10% of alcoholic uranyl acetate for 10 minutes followed by 3 minutes incubation with lead acetate. The sections were then washed with CO<sub>2</sub> free distil water to remove any unbound stain. The imaging was then carried out on transmission electron microscope (Jeol 1400 plus).

### **3.2.2 Immunofluorescence**

The cells were seeded on coverslips at density of 0.5 million for at least 12 hours, following which the cells were washed with PBS and fixed with methanol: acetic acid (2:1) for 10 minutes on ice. The fixative was removed and cells were washed with PBS three times for 5 minutes each, permeabilized with 0.5% Triton X-100 (Sigma-Aldrich 93443) for 15 minutes at 4°C. The permeabilized cells were then incubated with 5% bovine serum albumin (HiMedia MB083) solution for 1 hour at 37°C, followed by overnight incubation with primary antibodies:  $\gamma$ -H2AX (1:200, rabbit, Cell signalling 9718), Phospho-ATM (Ser1981) (1:100, rabbit, Cell Signalling 5883), Phospho-ATR (Ser428)(1:50, rabbit, Cell Signalling

2853), Phospho-Chk2 (Thr68) (1:100, rabbit, Cell Signalling 2197), RPA32/RPA2 (1:200, mouse, Abcam ab2175), HP-1 alpha (goat, 1:100, Abcam 77256), Ku80 (rabbit, 1:200, Cell Signalling 2180) and pBRCA1 (rabbit, 1:50, Cell Signalling 9009). The coverslips were then washed with PBS three times for 5 minutes each and were incubated with the secondary antibodies: FITC-conjugated anti-goat (1:200, Abcam 6737), anti-rabbit Alexa488 conjugated (1:100, ThermoFischer scientific A11034) in a moist chamber at room temperature for 1 hour. Unbound antibody was removed by washing with PBS subsequent to which the cells were mounted in VECTASHIELD mounting media (Vector Labs H1000), counterstained with DAPI (0.5ug/ml; Sigma-Aldrich 96542). The cells were then visualized under Zeiss LSM 780 Meta Confocal Microscope. Image J software was used for quantitation of HP-1 alpha intensity and FociCounter software was used for counting the number of foci/cell.

### 3.2.3 Comet assay

0.1 million cells were harvested in cold condition at different time points after radiation: 2, 4, 6, 8, 24, 48 hours as well as the non-irradiated and RR cells, washed with cold PBS and re-suspended in 10µl of PBS. The alkaline comet assay was performed as described by Singh *et al*[250]. These cells were then mixed with 90 µl of low-melting point agarose or LMPA (0.5%, 37°C), spread onto the slides pre-coated with 1% normal melting point agarose or NMPA placing the coverslip onto slide resting on ice packs allowing the agarose layer to harden (~5 to 10 minutes). The coverslips were then removed and the slides were incubated in freshly prepared lysis solution (2.5M NaCl, 100mM EDTA, 10mM Tris, 1% Triton X-100 and 10% DMSO) for 2 hours in dark at 4°C. The slides were then removed from the lysis solution and placed in the reservoir tank filled with freshly made pH>13 electrophoresis buffer (300mM NaOH and 1mM EDTA) for 20 minutes to allow for unwinding of the DNA and the expression of alkali-labile damage. The slides were then electrophoresed at 24 volts (~0.74 V/cm) for 30 minutes, adjusting the current to 300 milliamperes by raising or lowering

the buffer level. The slides were then thrice coated with neutralization buffer (0.4 M Tris-HCl pH 7.5) for 5 minutes each. Slides were then stained with DAPI solution (1 µg/ml), visualized under upright microscope (Zeiss, Axioimager Z1).

The neutral comet assay was performed as described by Olive *et al* [251] with minor modifications. Briefly, 750 µl of 1% low-melting-point agarose was added to the cell suspension. The contents were pipetted onto a slide, precoated with 1% normal agarose, covered with coverglass, and allowed to gel for 20 min. Slides were then immersed in warm lysing solution (30 mmol/L EDTA, 1% Triton X-100, pH 8.3) for 4 h at 37°C with coverglass on. Following lysis and removal of the coverglass, slides were rinsed 3 times in TBE buffer (90 mmol/L Tris, 90 mmol/L boric acid, 2 mmol/L EDTA, pH 8.5) and were electrophoresed at 0.66 V/cm for 25 min at room temperature. After rinsing 3 times in MilliQ water slides were stained with DAPI solution (1 µg/ml).

The percentage DNA in tail was determined using CometScore software for at least 100 cells from each time point.

### **3.2.4 Histone acid extraction**

Four million cells were harvested, washed twice with ice cold PBS and then re-suspended in Triton Extraction Buffer (250mM sucrose, 50mM Tris-HCl, pH 7.5, 25mM KCl, 5mM MgCl<sub>2</sub>, 50mM NaHSO<sub>3</sub>, 45mM sodium butyrate, 0.2mM phenylmethylsulfonyl fluoride, 2mM ethylenediaminetetraacetic acid, 2mM ethylene glycol tetraacetic acid, 1mM sodium orthovanadate, 10mM sodium fluoride, 10mM β-glycerophosphate, 10mM 2-mercaptoethanol and 0.2% Triton X-100) at a cell density of 10<sup>7</sup> cells/ml. Subsequently the cells were lysed on ice for 10 minutes with gentle vortexing. The suspension was then centrifuged at 2000rpm for 10 minutes at 4°C. The supernatant was transferred to another tube and the nuclear pellet was then washed again with half the volume of lysis buffer to

remove any debris. Further the pellet was re-suspended in 6 times volume of 0.2M H<sub>2</sub>SO<sub>4</sub> (approximately 300-400 µl) and extracted in the acid by vigorous vortexing at 4°C. The samples were then centrifuged at 16,100g for 20 minutes at 4°C, supernatant was collected and chilled acetone (4 vol) of the supernatant was added. Next day, the pellet was washed with 50mM HCl in acetone, with acetone and subsequently the pellet was vacuum dried in speed back, dissolved the pellet in β-mercaptoethanol (0.1%) in water. The samples were loaded onto 18% acrylamide and histones were quantified after silver staining and Image J analysis.

### 3.2.5 Western blot analysis

Equal amount of histones were loaded onto 18% SDS-polyacrylamide gel and transferred onto the nitrocellulose membrane at 300mM for 3 hours at 4°C. The membranes were stained with fast green to visualize the transferred histones, washed with TBS containing 0.1% Tween-20 (Sigma-Aldrich 9416) and blocked with 5% bovine serum albumin (HiMedia MB083) for an hour at room temperature. The membranes were then incubated overnight with primary antibodies: Phospho-Chk2 (Thr68) (1:100, rabbit, Cell Signalling 2197), Phospho-Chk1 (Ser345) (1:1000, rabbit, Cell Signalling 2348), Ku80 (1:1000, rabbit, Cell Signalling 2180), pBRCA1 (Ser1524) (1:1000, rabbit, Cell Signalling 9009), total BRCA1 (1:800, rabbit, Cell Signalling 9010), β-actin (1:5000, Sigma-Aldrich A5316), H3K4me<sub>2</sub>, H3K27me<sub>2</sub>, H3K9me<sub>2</sub>, H3K36me<sub>2</sub>, H3K79me<sub>2</sub> and total H3 (1:1000, rabbit, Cell Signalling 9847) at 4°C on shaking. The membranes were then washed with TBST (3 times, 10 minutes each) and incubated with secondary antibodies: anti-rabbit HRP labelled (1:2500, Cell Signalling 7074) and anti-mouse HRP labelled (1:2500, Cell Signalling 7076) for 1 hour at room temperature. The membranes were then washed to remove the secondary antibody with TBST thrice for 15 minutes each and were subsequently was visualized with Takara chemiluminescence HRP substrate (catalogue number T7101A).

### 3.2.6 RNA isolation, cDNA synthesis and Quantitative real-time RT-PCR

Total RNA was extracted from parent and radiation resistant cells by Trizol reagent (Invitrogen) based methods and later resolved on 1.2% agarose gel to confirm the integrity of the RNA. First strand cDNA synthesis was performed using Superscript III kit (Invitrogen) using equal concentration of RNA and semi-quantitative evaluative PCR for *GAPDH*, *SETMAR*, *NSD1*, *EZH2*, *Dot1L* and *Suv39h2* was performed to check the cDNA integrity, optimum primer concentrations and melt curve analysis was performed to check the primer dimer or non-specific amplifications. Real-time PCR was carried out using KAPA master mix (KAPA SYBR® FAST Universal qPCR kit) in 5µl volume in triplicate on Light cycler 480 (Roche, Mannheim, Germany) machine. All the experiments were repeated thrice independently. The data was normalized with internal reference *GAPDH*, and analyzed by using delta-delta Ct method described previously [247]. The details of all the primers used for expression analysis have been provided in Annexure I.

### 3.2.7 Cloning of shRNAs against SETMAR in pLKO.1-Tet-On knockdown

The oligo sequences for SETMAR available at The RNAi Consortium shRNA Library were ordered and reconstituted in 1X Tris-EDTA to 100mM. Equal concentration of the primers (20µM) in 50µl volume were used for annealing in 1X NEB buffer 2 (containing 50mM NaCl, 10mM Tris-HCl, 10mM MgCl<sub>2</sub> and 1mM DTT) at 95°C for 5 minutes, 70°C for 10 minutes followed by incubation at room temperature for 2 hours. Simultaneously, the vector pLKO.1-Tet-On was digested with EcoRI+ AgeI and gel-purified using gel extraction kit-MACHEREY-NAGEL (Ref 740609.50). Ligation reaction was set up as: 1µl of annealed oligos, 1µl of gel-purified digested pLKO-Tet-On (10-20 ng), 1µl of 10X ligase buffer (NEB# M0202S, 0.5µl of T4 DNA ligase (NEB#M0202S) and 6µl of ddH<sub>2</sub>O overnight at 16°C. The ligated mixture was transformed in Stb3 E.coli competent cells with 4 ul of the

total ligation reaction volume incubated for 20-30 minutes in ice, heat shock for 45 seconds at 42°C, followed by growth in SOC medium. The colonies were then grown in LB+ Ampicillin media and the positive colonies (XhoI digested colonies giving band of ~200bp) were sequenced using H1 primer for confirming the insertion of shRNAs into the vector.

### **3.2.8 Site-Directed mutagenesis (SDM) and cloning of mutant/wild type H3.3 in pBABE vector**

The mutation at the H3.3 was performed using QuikChange II Site-Directed Mutagenesis Kit instruction manual (Agilent Catalog #200523). For conducting SDM, H3.3 was amplified from H3.3- pTZ57R/T (kind gift from Dr. Sanjay Gupta, ACTREC, India) using forward primer which had a mutation base change from AA to GC at 109,110 position in the presence of Pfu ultra HF DNA Polymerase. Mutagenic Primer Design:

The mutagenic oligonucleotide primers used was designed as per the following guidelines:

- ◆ Both mutagenic primers must contain the desired mutation and anneal to the same sequence on opposite strands of the plasmid.
- ◆ Primers should be between 25 and 45 bases in length, with a melting temperature (T<sub>m</sub>) of ≥78°C. Primers longer than 45 bases may be used, but using longer primers increases the likelihood of secondary structure formation, which may affect the efficiency of the mutagenesis reaction.

The following formula is commonly used for estimating the T<sub>m</sub> of primers:

$$T_m = 81.5 + 0.41(\%GC) (675/N) \% \text{ mismatch}$$

For calculating T<sub>m</sub>:

- N is the primer length in bases.
- values for %GC and % mismatch are whole numbers

For calculating  $T_m$  for primers intended to introduce insertions or deletions, use this modified version of the above formula:

$$81.5 + 0.41(\%GC) (675/ ) T_m = - N$$

where N does not include the bases which are being inserted or deleted.

◆ The desired mutation (deletion or insertion) should be in the middle of the primer with ~10–15 bases of correct sequence on both sides.

◆ The primers optimally should have a minimum GC content of 40% and should terminate in one or more C or G bases.

#### Additional Primer Considerations

◆ The mutagenesis protocol uses 125 ng of each oligonucleotide primer. To convert nanograms to picomoles of oligo, use the following equation:

$$\begin{aligned} X \text{ pmoles of oligos} &= \frac{\text{ng of oligos}}{330 * \text{no of bases in oligo}} \\ &= 12.6 \text{ pmole} \end{aligned}$$

◆ Primers need not be 5' phosphorylated but must be purified either by fast polynucleotide liquid chromatography (FPLC) or by polyacrylamide gel electrophoresis (PAGE). Failure to purify the primers results in a significant decrease in mutation efficiency.

◆ It is important to keep primer concentration in excess. Varying the amount of template while keeping the concentration of the primer constantly in excess.

The PCR reaction set up was as follows:

Control reaction: 5  $\mu$ l of 10 $\times$  reaction buffer 2  $\mu$ l (10 ng) of pWhitescript 4.5-kb control plasmid (5ng/ $\mu$ l) 1.25  $\mu$ l (125ng) of oligonucleotide control primer #1 [34-mer (100 ng/ $\mu$ l)] 1.25  $\mu$ l (125ng) of oligonucleotide control primer #2 [34-mer (100 ng/ $\mu$ l)] 1  $\mu$ l of dNTP mix

3  $\mu$ l of QuikSolution reagent 36.5  $\mu$ l of double-distilled water (ddH<sub>2</sub>O) to a final volume of 50  $\mu$ l. Then add 1  $\mu$ l of PfuUltra HF DNA polymerase (2.5 U/ $\mu$ l)

Sample reaction(s): 5  $\mu$ l of 10 $\times$  reaction buffer, 10 ng of dsDNA template, 125 ng of forward primer #1, 125 ng of reverse primer #2, 1  $\mu$ l of dNTP mix, 3  $\mu$ l of QuikSolution ddH<sub>2</sub>O to a final volume of 50  $\mu$ l and then 1  $\mu$ l of Pfu Ultra HF DNA polymerase (2.5 U/ $\mu$ l) was added.

The PCR conditions are as follows:

**Table 3.1: Cycling Parameters for the QuikChange II XL Method.**

Segment	Cycles	Temperature	Time
1	1	95°C.	1 min
2	18	95°C.	50 sec
		60°C.	50 sec
		68°C.	1 min/kb
3	1	68°C.	7 minutes

The PCR amplified product was digested using the Dpn1 endonucleases which is specific for methylated and hemimethylated DNA to digest the parent DNA template. The nicked vector DNA incorporating the desired mutation was transformed into ultra-competent E. coli DH5 $\alpha$  cells. The plasmids were isolated were sequenced using pBABE reverse primer.

### 3.2.9 Cloning of wild type H3.3 and H3.3K36A mutant in retroviral vector pBABE

#### 3.2.9.1 PCR Gene Specific Amplification of H3.3 from TA vector

We amplified our gene H3.3 using M13 primers that flank the TA cloning vector pTZ57R/T (Annexure I) using the following reaction conditions.

**Table 3.2: PCR reaction mixture for H3.3 amplification.**

Reagents	Stock	Final	For 20ul
Taq Buffer	10X	1X	2ul

Taq Polymerase	5U	1U	0.2ul
Forward Primer	10mM	15 picomoles	1.0ul
Reverse Primer	10mM	15 picomoles	1.0ul
MgCl <sub>2</sub>	25mM	2mM	0.2ul
dNTP's	0.2mM	0.2mM	0.5ul
Template	100-200 ng/ul		1-2ul
Distilled Water			13.6ul
Total			20ul

**Table 3.3: Optimised PCR Conditions**

Step	Temperature	Time
Initial Denaturation	95°C	3 mins
Denaturation	95°C	30 sec
Annealing	55°C	30 sec
Extension	72°C	20 sec (35 cycles)
Final extension	72°C	5mins
Hold	4°C	∞

The PCR products were run on 1.8% agarose gel containing 2ul of 0.5ug/ml of EtBr and gel extracted using extraction kit- MACHERY-NAGEL (REF 740609.50).

pBABE is a retroviral expression vector of 5.2kb is an expression vector optimized for higher expression in mammalian cells. The MCS is in between the immediate early promoter of CMV and the YFP coding sequence. The restriction enzyme sites chosen from the MCS for inserting H3.3 were EcoR1 and BamH1. The gel purified PCR product and pBABE vector were double digested with BamHI (NEB, R3136S) and EcoRI (NEB, R0104S) incubated overnight at 37°C. The enzymes were then inactivated by heating to 65°C for 10mins. After running digested products on gel, band was eluted and purified using PCR clean-up gel extraction kit- MACHERY-NAGEL (Ref. 740609.50) as per the kit instructions.

### 3.2.9.2 Ligation

The digested vector and insert were added to ligation mix in 1:4 and 1:6 molar ratios. The amount of insert to be added per 50ng of vector was calculated by using following formula.

$$\text{Insert mass in ng} = \left( \frac{\text{ng of vector} \times \text{kb size of insert}}{\text{kb size of vector}} \right) \times \text{molar ratio of } \left( \frac{\text{insert}}{\text{vector}} \right)$$

3.2.9.3 *Transformation:* The protocol is as follows:

- 1) Competent cells DH5 $\alpha$  were thawed on ice and 2 $\mu$ l of DNA of interest was added into the cells.
- 2) The cells were kept on ice.
- 3) Cells were immediately given heat shock at 42°C for exactly 90 seconds.
- 4) After heat shock cells were again quickly kept on ice for about 5min.
- 5) Luria broth of 800 $\mu$ l was added in the tube having cells and kept at 37°C for 1 hour on shaker.
- 6) Cells were centrifuged at 5,000rpm for 5min. Supernatant was discarded leaving 100 $\mu$ l behind and pellet was re-suspended in rest of supernatant.
- 7) Cells were spread onto the plate containing 100 $\mu$ g/ml ampicillin.
- 8) Plates were kept at 37°C incubator overnight for about 15 hours.
- 9) Next day the colonies were allowed to grow in 5ml of luria broth media.

The plasmid DNA was the extracted using MACHERY-NAGEL mini-prep kit (Ref. 740499.50).

To confirm the insertion of gene into the vector, PCR was done using gene as well as vector specific primers from the isolated plasmids. The PCR conditions used were same as described previously. The PCR positive colonies were then confirmed using Sanger sequencing.

Plasmid extracted from the ligated colonies – 1 $\mu$ l (300ng)

Primer (H3.3 Fwd) – 1 $\mu$ l (5pmols)

### **3.2.10 Retrovirus and lentivirus production, infection and drug selection**

293FT cells were seeded in 6 well plates one day prior to transfection and each shRNA constructs including the scrambled (4 $\mu$ g each) or pBABE-H3.3K36A and pBABE-H3.3K36 with pPAX or pAmpho (1.5 $\mu$ g) and pVSVG (150ng) helper vectors were transfected using Lipofectamine 3000 reagent (Invitrogen L3000008) as per manufacturer's protocol. Viral supernatant was collected after 48 and 72 hours of transfection, filtered (with 0.45 $\mu$ M filter) and infected the U87MG and SF268 cells seeded at 0.4 million density in six well plate with one ml of the virus supernatant (1:2 dilution) and 8 $\mu$ g/ml of polybrene (Sigma-Aldrich) for seven hours. Cells were selected in 2 $\mu$ g/ml of puromycin (Sigma-Aldrich P8833).

### **3.2.11 Transfection of NHEJ and HR vectors**

4.5 $\mu$ g of HR vector and 1.5 $\mu$ g of NHEJ vector were first incubated overnight with I-SceI endonuclease enzyme (NEB catalogue number R0694S) to linearize the vectors. The linearized vectors were then purified using PCR clean-up gel extraction kit- MACHERY-NAGEL (Ref. 740609.50) as per the kit instructions. 0.5million U87MG and SF268 parent as well as RR cells were seeded in a 6-well plate 12 hours prior to transfection. The transfection mixture was as follows: 4.5 $\mu$ g of linearized HR vector/ 1.5 $\mu$ g of linearized NHEJ vector + 0.5  $\mu$ g of TdRed expressing plasmid +2.5  $\mu$ l of X-treme GENE HP DNA Transfection Reagent (Roche Diagnostics catalogue number 06366244001) mixed in 200  $\mu$ l of plain DMEM and incubated at room temperature for 30 minutes. The transfection mixture was then added on top of the cells containing 1ml of DMEM+10% FBS using cut tips and incubated for 72hours. The cells were then visualized under the florescent microscope for GFP positive cells and percentage of GFP, Red and dual positive cells were determined on FACS Aria, BD Biosciences. The analysis of the flow data was performed using FlowJo software.

### **3.3 Results**

#### **3.3.1 Re-appearance of $\gamma$ -H2AX observed in radiation resistant cells**

Since the aim of this study is to understand the regulation of DNA damage repair in radiation resistant cells, we started by examining the earliest indicator of DNA damage that is the phosphorylation of H2AX. We first examined the kinetics of H2AX phosphorylation at different time points post radiation treatment in the parent population until the formation of MNGCs. As shown in figure 3.2A and C, maximum number of cells with foci was seen in 2 and 4 hours post radiation in SF268 and U87MG, respectively. The resolution of  $\gamma$ -H2AX foci occurred in 24 and 48 hours in these cell lines. To further evaluate the amount of DNA damage in these cells we performed neutral as well as alkaline comet assay which showed maximum damage as represented by the percentage DNA in tail was observed at 2 hours in SF268 and at 4 hours in U87MG with subsequent decrease in the later time points (Figure 3.2A-D) consistent with the phosphorylation of H2AX, However, unexpectedly, there was re-appearance of the phospho-H2AX in the MNGCs indicating the induction of DNA damage in these cells 8-12 days post radiation. Similar results were seen with alkaline comet assay indicating presence of DNA damage other than DSBs, where the radiation resistant cells had higher damage compared to the parent non-irradiated cells confirming the generation of secondary DNA breaks.

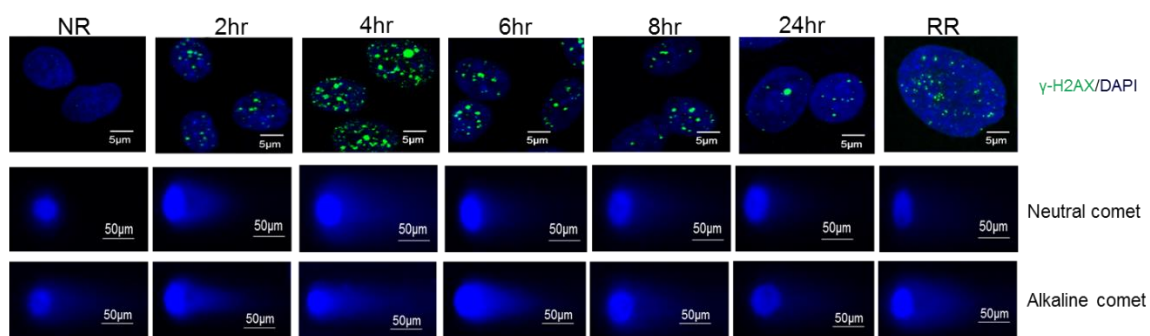
#### **3.3.2 Phosphorylation of H2AX in the resistant cells can be mediated either by ATM or ATR**

Re-appearance of gamma-H2AX we also examined in the MNGCs generated in the primary cultures from the patient samples. Similar to the resistant cells from cell lines, radiation resistant cells from primary cultures also displayed phospho-H2AX demonstrating that

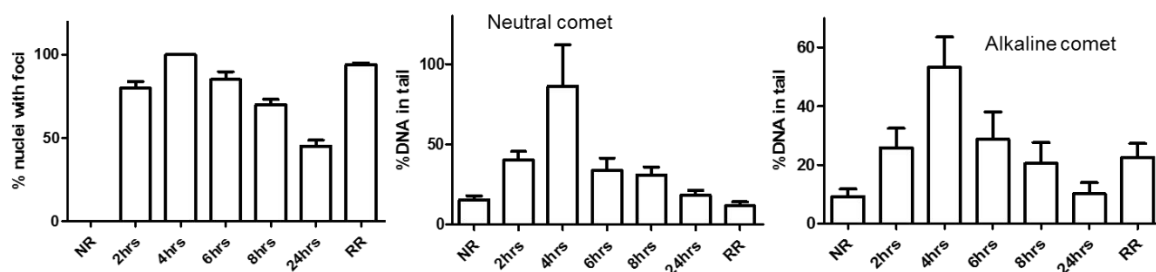
activation of DNA damage repair response in the glioma residual cells is not a cell line artefact (Figure 3.3A).

The phosphorylation at serine139 of H2AX is brought about by ATM or ATR, depending upon the type of damage induced, thus their recruitment was determined in the radiation resistant cells generated from cell lines and patient samples. Surprisingly, only 5 out of 10 patient samples shown in the figure 3.3A displayed pATM foci in the radiation resistant cells while the remaining samples recruited ATR at the break sites.

**A** U87MG



**B**



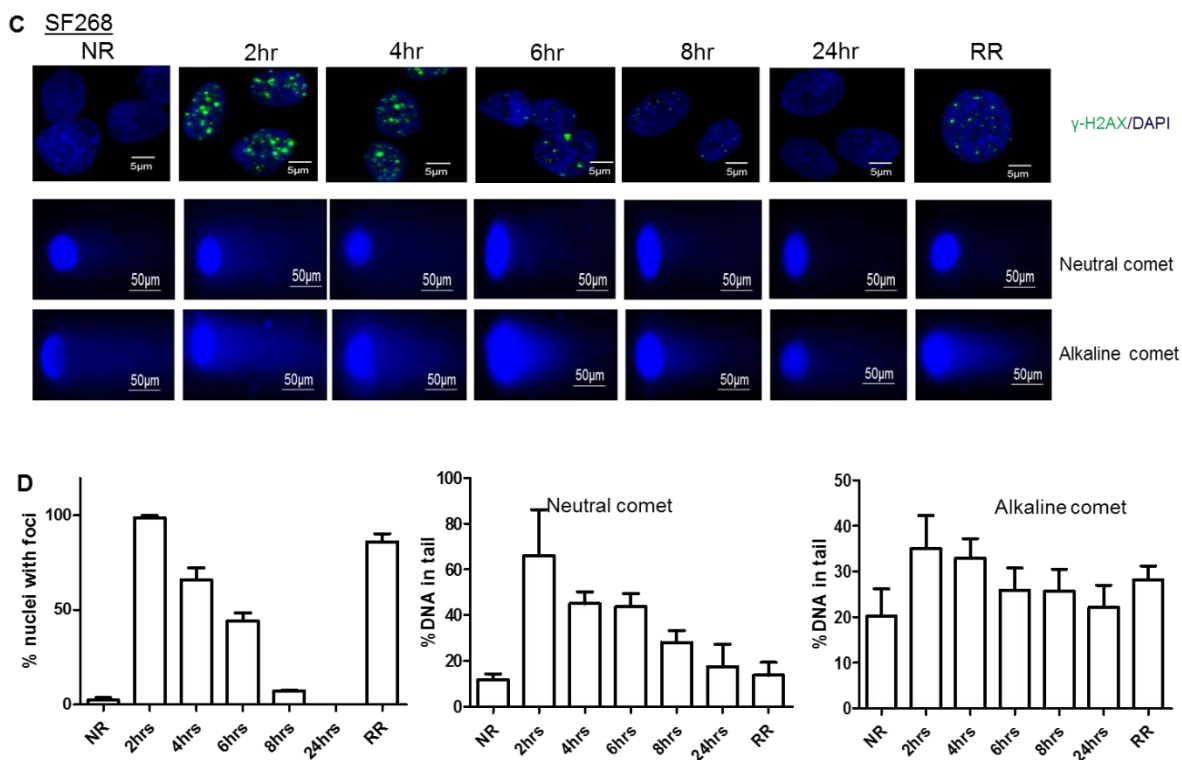
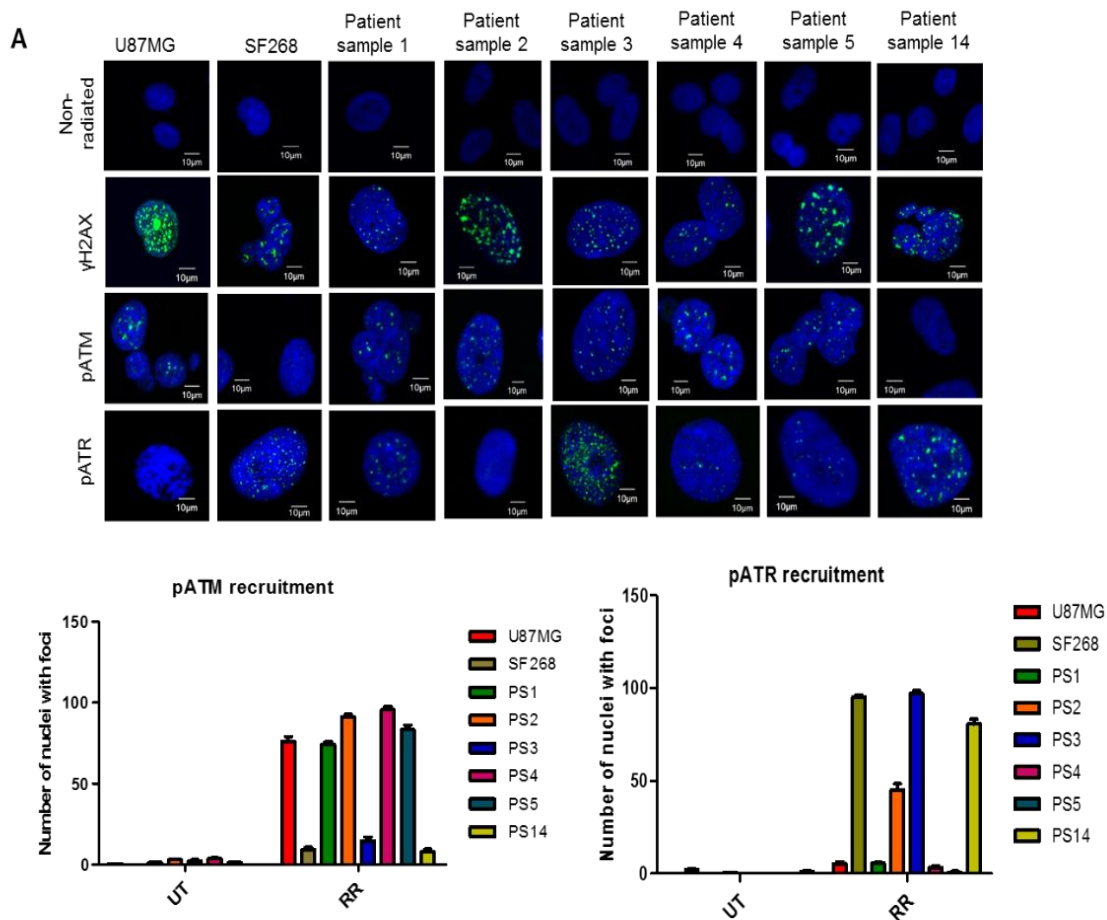


**Figure 3.2: Re-appearance of phosphorylated H2AX in the radiation resistant cell possessing higher damage compared to the parent cells.** A and C) Immunofluorescence images for  $\gamma$ H2AX (green) nuclei counterstained with DAPI (blue) in U87MG and SF268 cell lines at different time intervals after radiation. Representative images for neutral and alkaline comet assay are shown for different time points. Scale bar-5 $\mu$ m for immunofluorescence, 50  $\mu$ m comet images. B and D) Bar graph depicts the percentage of nuclei with foci for N= 50 cells, quantitation of neutral and alkaline comet assay. Percentage DNA in comet tail as calculated using CometScore for N=100 is shown. NR-non-irradiated and RR-radiation resistant cells.

Additionally, 3 of the patient samples activated both the sensory kinases, however, at variable levels. Accordingly, the activation of downstream checkpoint kinases (Chk1 and Chk2) also varied in the resistant cells. The samples that recruited ATM activated Chk2 while the samples (SF268, patient samples 1, 3 and 14) that recruited ATR activated Chk1 (Figure 3.3A and B). Notably, RR cells from SF268, patient sample 1 and 3 showed RPA32 cluster

formation depicting the coating of single strand breaks by RPA32 protein (Figure 3.3C).

Thus, these RR cells displayed heterogeneity in the repair pathways.



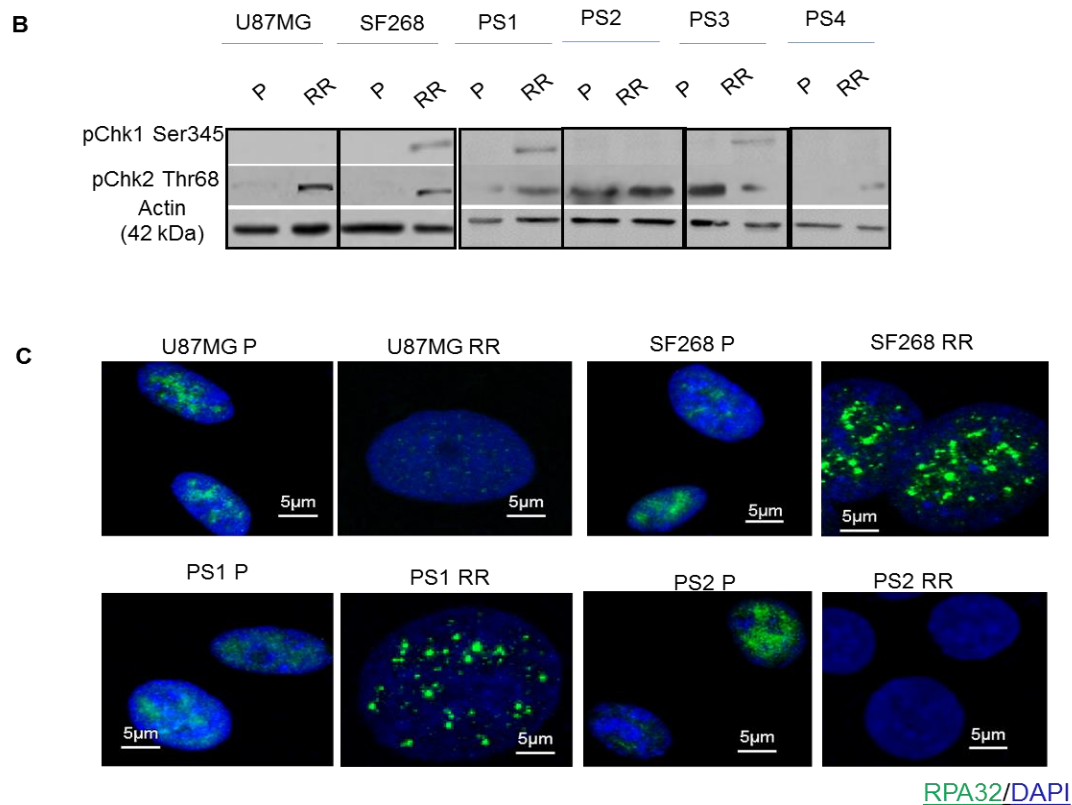


**Figure 3.3: Differential recruitment of sensory kinases in the RR cells.** A) Immunofluorescence images depicting the recruitment of pATM and pATR (green; nuclei-DAPI) in RR cells. Bar graph represents quantitation of the percentage of nuclei with foci formed by these proteins, where N=50. B) Expression levels of pChk1 and pChk2 in different RR samples is shown. C) RPA32 staining (green) counterstained with DAPI in RR and parent cells of cell lines and 2 patient samples are represented. Scale bar-5 $\mu$ m.

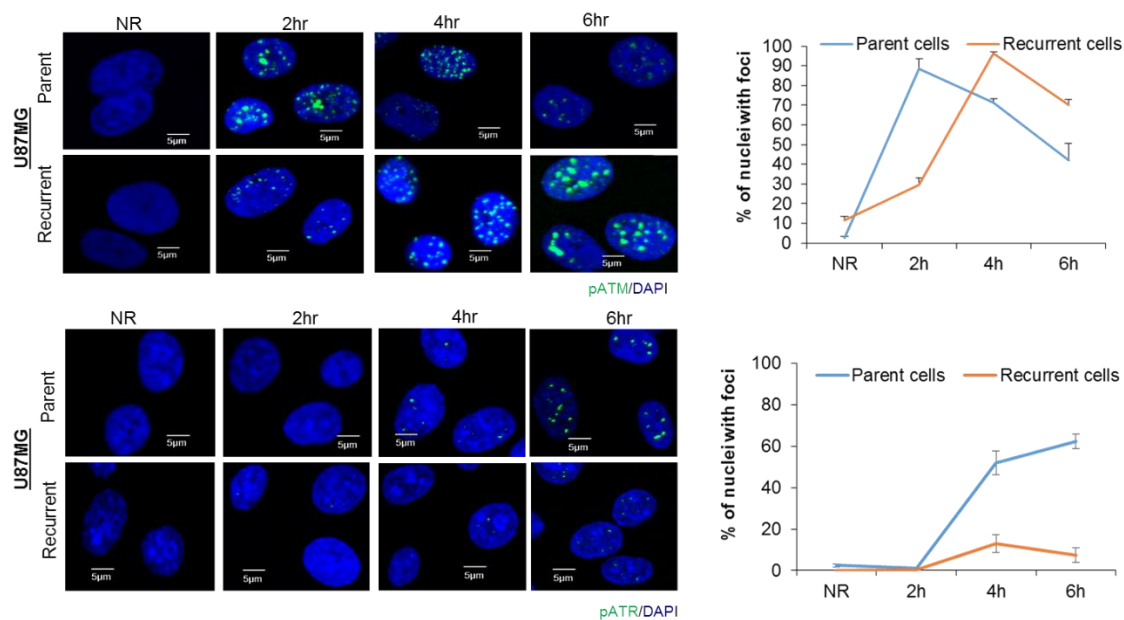
### 3.3.3 Recurrent cells display altered ATM/ATR recruitment kinetics

Importantly, the recurrent cells generated from the resistant cells showed altered activation of ATM kinase compared to the parent cells upon exposure to lethal dose of radiation. As shown in figure 3.4, the U87MG recurrent cells recruited ATM at different time points at a rate different to that of parent cells while the SF268 recurrent cells revealed little induction in the pATM levels after radiation as compared to parent cells. Instead, SF268 cells showed

enhanced recruitment of pATR within 4hours at the DSB sites, demonstrating the shift in the preference of sensory kinase from parent to recurrent cells.

### 3.3.4 Recurrent cells generated from radiation resistant cells show variable sensitivity towards ATM inhibitor

As shown in figure 3.4, the recurrent cells generated from U87MG and SF268 cells exhibited altered recruitment kinetics of ATM upon exposure to the lethal dose of radiation. We then questioned whether the altered kinetics had any influence on the radiation sensitivity of the recurrent cells generated from cell lines and patient samples as compared to the parent cells. As shown before, the recurrent cells generated from SF268, patient sample 1, 2 and 3 had higher clonogenic capacity at low doses of radiation while U87MG recurrent cell showed sensitivity towards low dose of radiation as compared to the parent cells. Upon inhibition with 10 $\mu$ M of ATM kinase inhibitor KU55933, we observed that the clonogenic ability of the



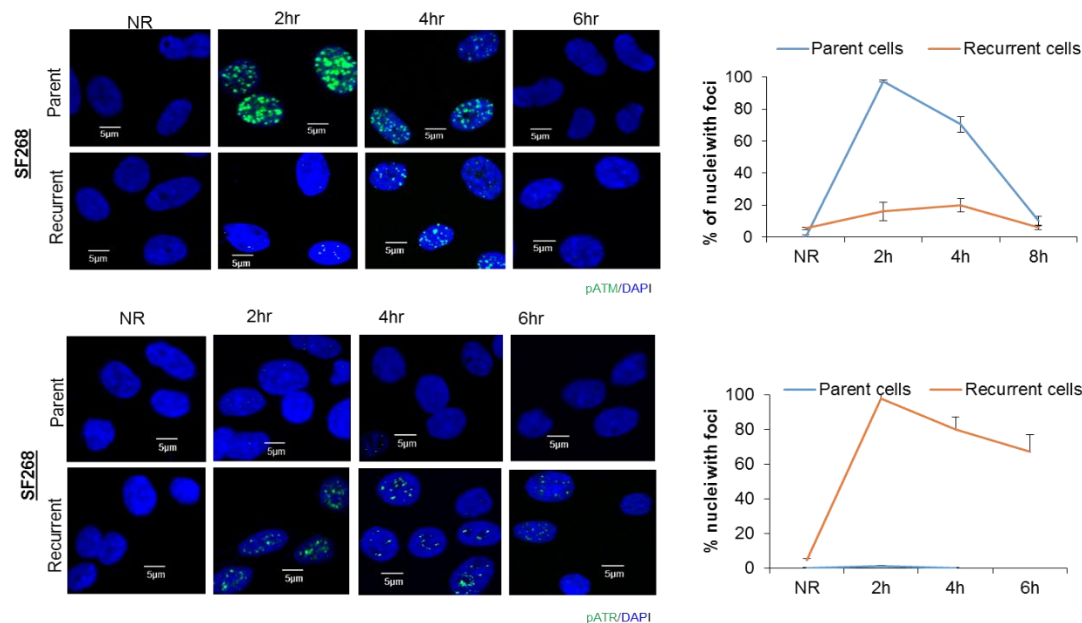


**Figure 3.4: Recruitment kinetics of pATM and pATR vary in recurrent cells as compared to parent cells.** Representative immunofluorescence images depicting recruitment of both sensory kinases ATM and ATR (green, counterstained with DAPI) in recurrent and parent cells upon exposure to lethal dose of radiation. Line graph shows the quantitation from three independent experiments. Scale bar- 5µm.

recurrent cells were reduced in U87MG and patient sample 2 as compared to the parent cells at different doses of radiation. However, recurrent cells from SF268 and patient samples 1 and 3 showed higher survival capacity as compared to the parent cells as seen in lower doses of radiation (Figure 3.5). These observations demonstrate the variable response of ATM inhibition on the survival of different recurrent cells. Since the cells with higher clonogenic ability showed recruitment of pATR, hence might be contributing to their enhanced clonogenic capacity after radiation.

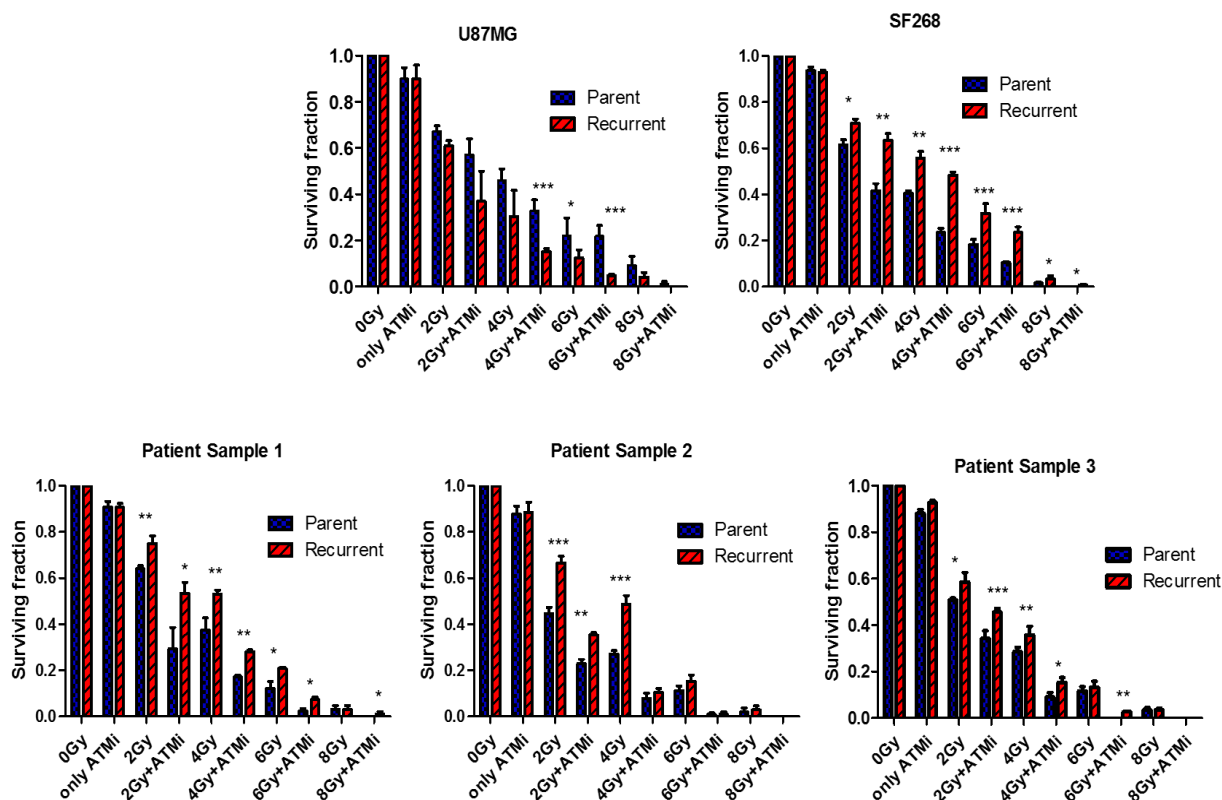


**Figure 3.5: Clonogenic assay with inhibitor alone or in combination with KU55933 in the parent and recurrent cells.**

### 3.3.5 Radiation resistant cells prefer NHEJ pathway repair over HR pathway

As mentioned earlier, the radiation resistant cells generated after 8-12 days post radiation show high levels of  $\gamma$ -H2AX foci early in the non-proliferative phase mediated by ATM or ATR. We then wanted to examine the preference of DSB repair pathway in these cells which can either be brought about by Non homologous end joining (NHEJ) or homologous end joining (HR). For this, we performed immunofluorescence and western blot with NHEJ protein Ku80 and HR protein pBRCA1. We found that there was significantly higher expression and recruitment of Ku80 as compared to pBRCA1 (Figure 3.6A and B). However, the recruitment of repair

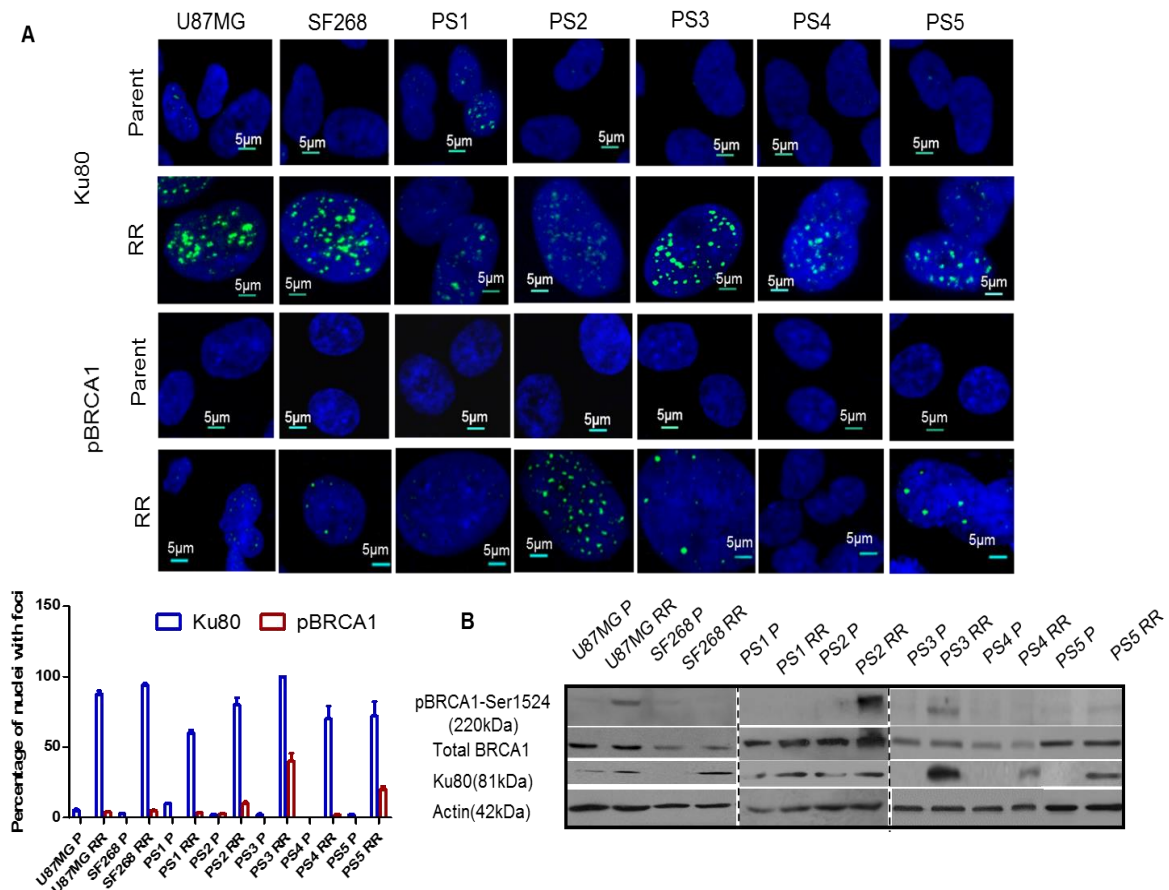


**Figure 3.6: Higher recruitment and expression of Ku80 in RR cells.** A) and B) Immunofluorescence images and western blots showing recruitment and expression of pBRCA1 and Ku80 (green, nuclei-DAPI) in different RR cells. Scale bar- 5µm.

proteins is only suggestive of favouring of NHEJ pathway. Thus, to ascertain whether higher recruitment translated into higher NHEJ repair efficiency in RR cells, we measured the efficiency of both the pathways using an *in vivo* fluorescent assays with GFP gene interrupted by an intron (GFP-Pem1), an adenoviral exon flanked by two HindIII and two inverted I-SceI sites. The digestion of NHEJ-I construct with I-SceI enzyme generated incompatible ends similar to the ends generated by radiation, followed by repair reconstructs the GFP gene. Similarly, the HR reporter construct consists of two defective copies of GFP-Pem1 with the first copy containing the sites for I-SceI and the repair of the cleaved I-SceI ends indicates HR repair. First, we transfected the linearized reporter constructs of NHEJ and HR and the

ratio of GFP positive cells from each other vectors was determined for calculating the repair efficiencies. Notably, we observed that the RR cells showed enhanced NHEJ repair compared to the HR when calculated from the ratio of GFP positive cells for NHEJ and HR vectors (U87MG-6%/1%= 6 and SF268 -7%/1.5%= 4.66) as shown in figure 3.7A. To rule out the possibility of different transfection efficiencies of the RR cells, these were then co-transfected with TdRed expressing plasmid along with the repair vectors. The percentage of cells expressing both red and green fluorescence were then determined and the ratio of GFP+ and TdRed+ cells in parent and RR cells transfected with NHEJ and HR vectors was used to measure the efficiency of NHEJ or HR repair. Consequently, we observed that the RR cells even though were present arrested in different cell cycle phases as shown in figure 2.11, showed higher NHEJ repair efficiency (repair efficiency: U87MG parent vs RR cells=1.7±0.6 vs 2.61±0.5 and SF268 parent vs RR cells =1.59±0.2 vs 2.38±0.6). These results suggest that the RR cells prefer error-prone NHEJ over HR pathway to repair their DNA.

To investigate the dependency of RR cells on NHEJ pathway for their survival, we incubated the residual resistant cells with NHEJ inhibitor NU7026 and determined their clonogenic capacity. We observed that indeed the survival capacity of RR cells was significantly diminished, preventing the formation of recurrent cells (Figure 3.7C), thus highlighting the importance of NHEJ pathway in facilitating the survival of RR cells.

### **3.3.6 Radiation resistant cells display altered chromatin architecture**

The chromatin including the organization and histone modifications are known to regulate the recruitment of various transcription factors as well as DNA repair proteins thus influencing the choice of repair pathway and the efficiency of repair. Therefore, we wanted to understand

the role of chromatin in regulating DNA repair in the radiation resistant cells (RR). First the RR

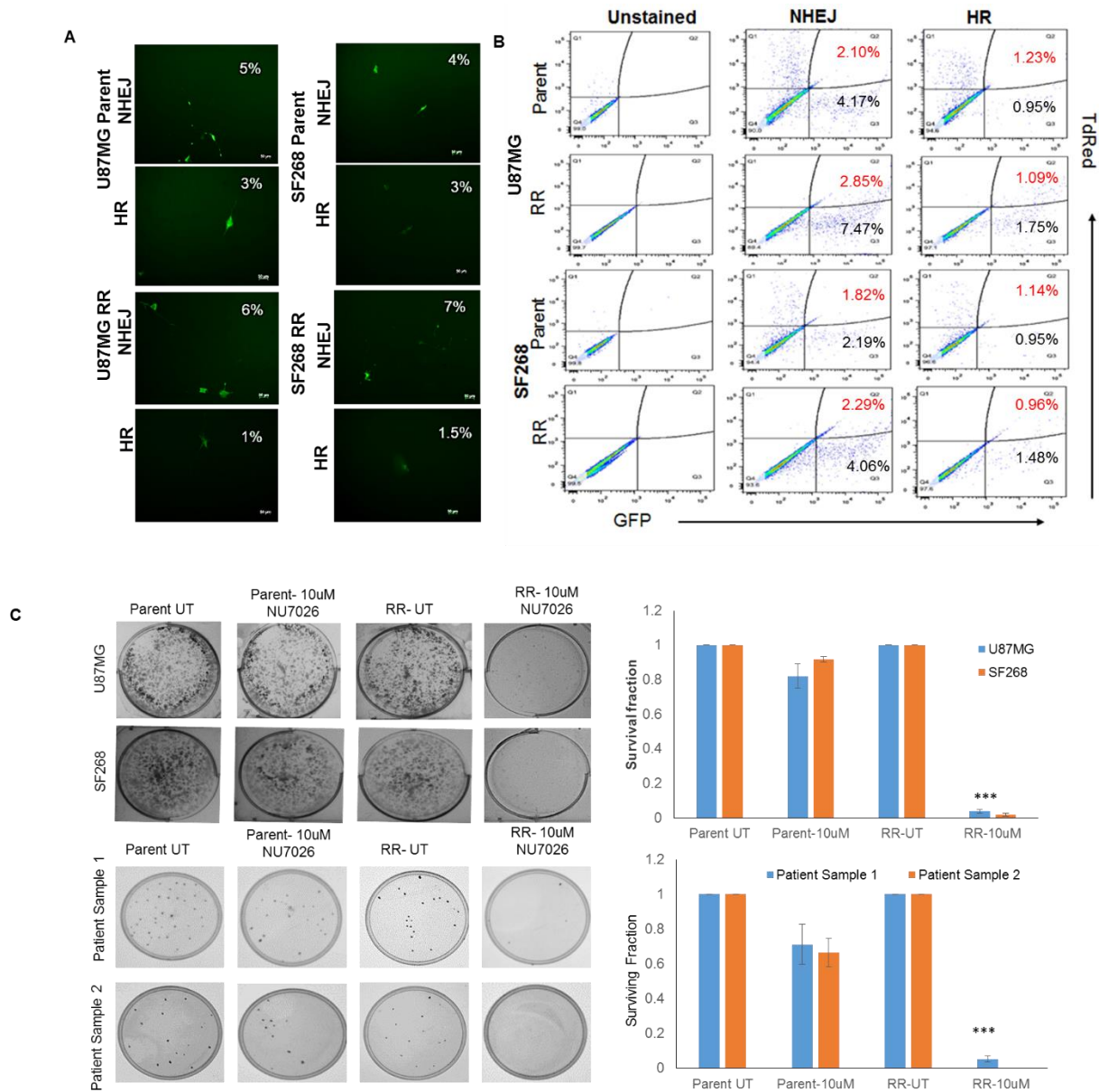


**Figure 3.7: RR cells show higher NHEJ repair efficiency as compared to HR.** A) Representative images of parent and RR cells transfected with NHEJ and HR vectors. B) Scatter plot showing the expression of GFP indicating NHEJ and HR repair efficiencies along with transfection control plasmid expressing TdRed. C) Clonogenic assay of parent and RR cells after incubation with 10µm of NHEJ repair inhibitor NU7026.

cells generated from the parent cells were examined for over-all chromatin changes. We found that the RR cells displayed a more relaxed chromatin architecture as compared to the parent cells when examined under transmission electron microscope (Figure 3.8A). This data is suggestive of RR cells having more euchromatinized DNA. To confirm this observation, we performed immunostaining with HP-1 alpha (Heterochromatin Protein-1 alpha) which is known to bind heterochromatin or more compact chromatin. As seen in the confocal images and the quantitation that HP-1 alpha staining showed significant reduction in HP-1 alpha expression confirming more open chromatin organization compared to the parent cells in RR population (Figure 3.8B).

### **3.3.7 Radiation resistant cells show over-expression of H3K36me2 and H3K4me2 modifications concomitant with the increase in its methyltransferases**

The histone methylation is known to regulate the chromatin architecture as well as the double strand break repair response. Thus, we examined the expression levels of histone methylations namely H3K4me2, H3K79me2, H3K9me2, H3K27me2 and H3K36me2 reported in literature to be associated with DNA repair response [237] in the RR cells from the two GBM cell lines U87MG and SF268. We found two histone modifications- H3K36me2 and H3K4me2 to be up-regulated in both the cells lines (Figure 3.9A). These histone marks are also known to be involved in mediating euchromatinization and aiding in better DDR response [248, 249]. Additionally, we observed lower expression of H3K9me2 marks a known histone mark that interacts with HP-1 to induce heterochromatin. Therefore, low expression of H3K9me2 is consistent with lower HP-1 recruitment. (Figure 3.9A). Furthermore, there was also a decreased expression of Suv39h2 a methyltransferase that transfers a methyl group to H3K9 explaining the decrease in H3K9me2 mark (Figure 3.9B).

Furthermore, we observed loss of H3K27me2 and H3K79me2 modifications in U87MG RR cells while SF268 RR cells showed similar levels of H3K27me2 and higher levels of H3K79me2 as compared to the parent cells (Figure 3.9A). The enzyme Dot1L was found to be up-regulated in RR cells from both the cell lines while down-regulation of EZH2 was seen, the transcript levels not corroborating with their modification H3K79me2 and H3K27me2, respectively (Figure 3.9B).

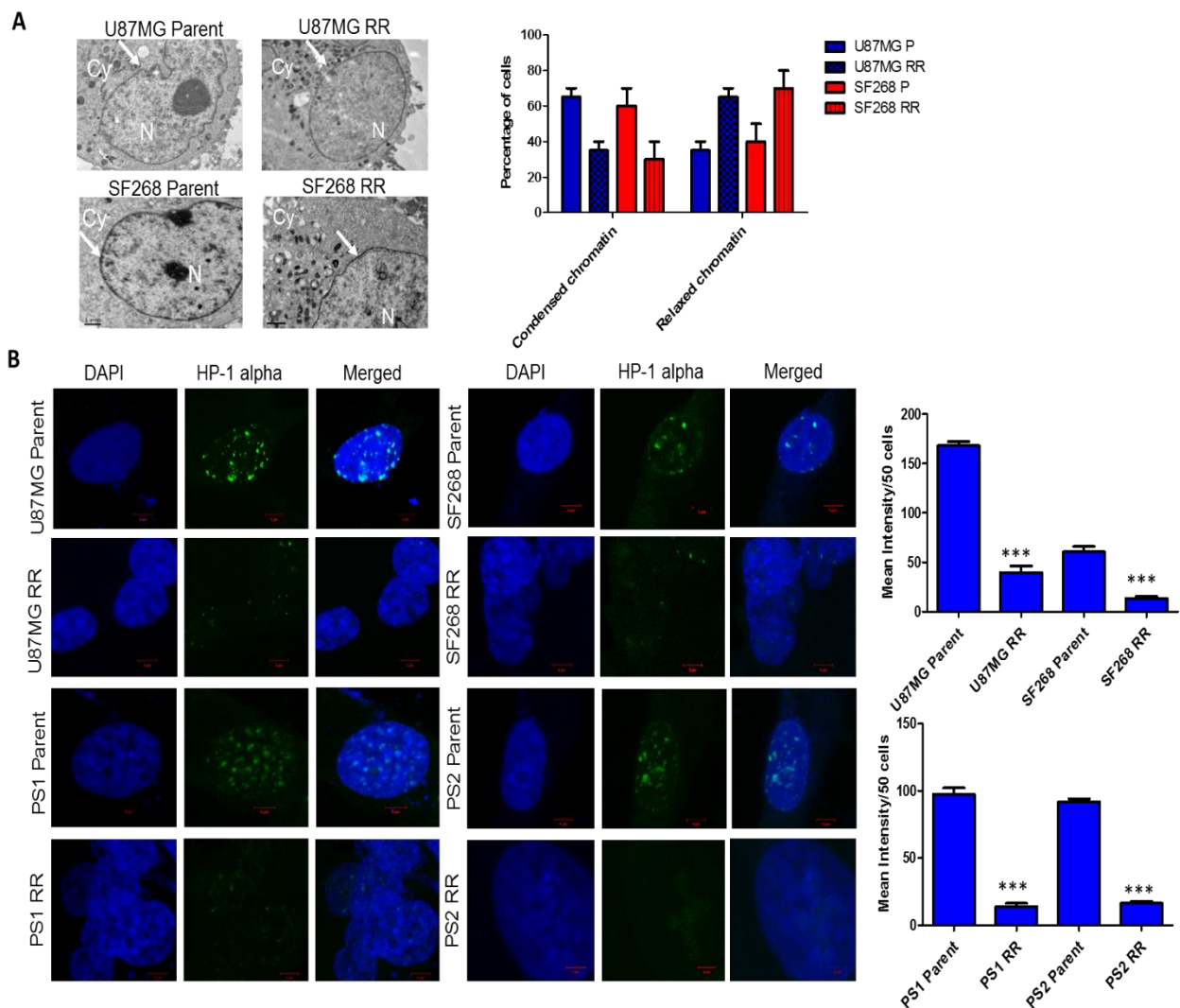


**Figure 3.8: Global architectural analysis reveals euchromatinization in the RR cells. A)**

Representative electron microscopy images of parent and radiation resistant (RR) cells from cell lines. White arrows indicate the nuclei margin. Quantitative data for the cells with

condensed or relaxed chromatin is also shown as bar graph. N=10 and the experiment was performed in duplicate. B) Representative confocal images depicting the expression levels of HP-1 alpha protein (green –pan staining and also clusters) counterstained with DAPI in parent and resistant cells (RR). Average intensity per 50 cells as measured by Image J is represented in the bar graph. Scale bar- 5µm and \*\*\* depicts  $p < 0.001$ . Results are representative of three independent experiments.

Because of consistent findings with H3K36me2 and H3K4me2 in the RR cells of cell lines, we expanded our screen to examine these modifications in the RR cells generated from primary cultures derived from patient samples. As shown in Figure 3.9C, 6 out of the 8 patient samples showed higher expression of H3K36me2 (fold change ranging from 1.4 to 10.8) while di-methylation of H3K4 was observed to be up-regulated in 4/8 samples (fold change ranging from 1.8 to 15.5).

The transfer of a methyl group from S-adenosine methionine to the histone N-terminal lysine residues are brought about by several of the SET and non-SET domain containing methyltransferases. Thus, we checked for the expression of SETMAR and NSD1 methyltransferases known to modify H3K36 and H3K4 di-methylations. We observed that the transcript levels of one of the methyltransferases SETMAR also known as Metnase to be up-regulated in 7/10 RR cells (including the cell lines), co-relating with the expression of H3K36me2 (Figure 3.9C) while NSD1 showed up-regulation only in 2/10 samples with most of the samples having lower NSD1 transcript levels as compared to the parent cells (Figure 3.9D).

Overall, we observed 70% percent of the samples over-expressed SETMAR transcripts and H3K36me2 in the RR cells. These data intrigued us to investigate the role of

SETMAR and H3K36me2 in RR cells. For this, we adopted two strategies: 1) knockdown of SETMAR specifically in the RR cells and 2) mutation of lysine 36 residue to alanine in H3.3.

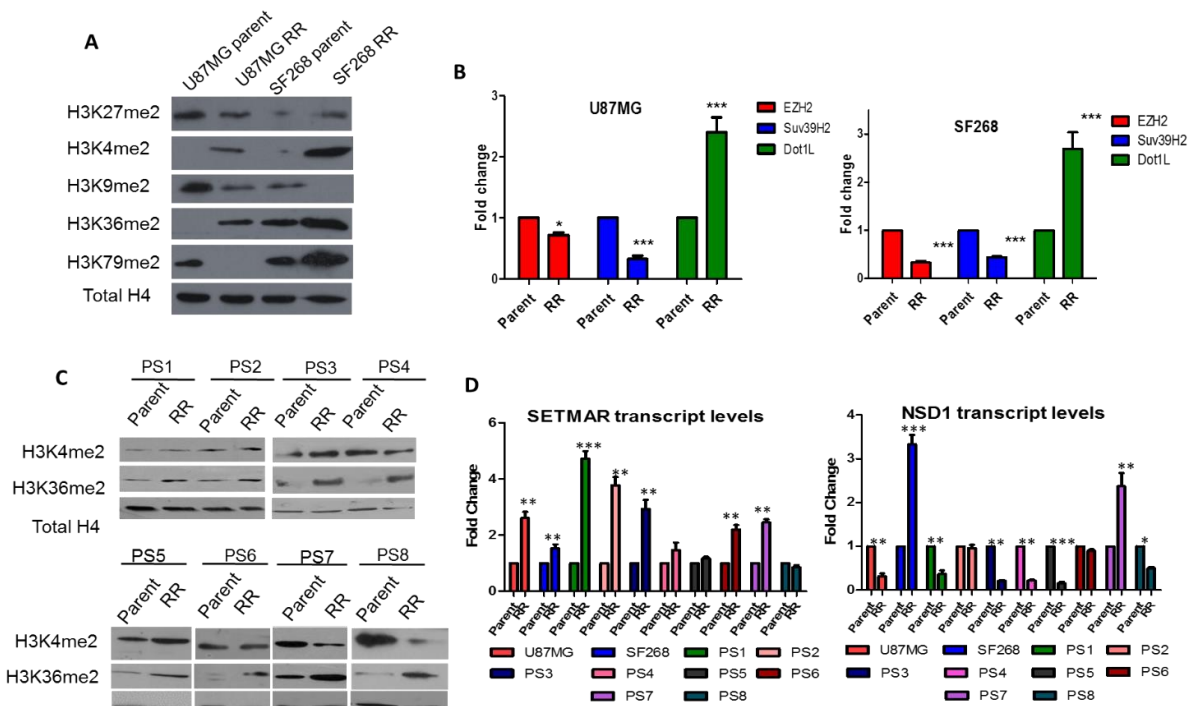


**Figure 3.9: Increased levels of H3K36me2 and SETMAR observed in majority of the GBM resistant cells.** A) Western blot analysis for di-methylation of H3K27, H3K4, H3K9, H3K36 and H3K79 in the acid extracted histone samples from parent and radiation resistant cells (RR) of U87MG and SF268 cell lines. Total H4 was used as a loading control. B) Transcript levels of Suv39H2, EZH2 and Dot1L in the RR cells from the two cell lines are shown as bar graph. C) H3K4me2 and H3K36me2 expression levels in RR cells generated from patient samples. D) Transcript levels of histone methyltransferases SETMAR and NSD1 in RR cells normalized to that in the parent cells. GAPDH was used as an internal reference. \*\*\* depicts p-value<0.001, \*\* indicates p-value <0.01 and \* for p-value<0.05. PS1,2,3,4,5,6,7,8 -patient samples 1,2,3,4,5,6,7,8.

### 3.3.8 SETMAR is required for proliferation of RR cells

Because SETMAR is a methyltransferase required for normal functioning of the cells to delineate its role specifically in RR population, we wanted the knockdown of SETMAR only during the RR phase of cell. For this we generated 2 shRNA constructs targeting SETMAR and a control scrambled shRNA under Tet- inducible system (Figure 3.10A and B representing chromatogram for shRNA1) and established cell lines expressing inducible SETMAR shRNAs. Upon induction with doxycycline, sh1 showed 70-76% and 82-90% reduction in the transcript levels of SETMAR in parent and RR cells, respectively while sh2 showed 40-50% reduction in both parent and RR cells (Figure 3.11A). To begin with, we first determined the growth potential of the parent and RR cells expressing both the shRNA constructs and compared it to the scrambled shRNA. As shown in figure 3.11B, sh1 displaying a greater knockdown of SETMAR induced cell death of about 95% RR cells and the few cells (5%) became senescent as they showed positivity for  $\beta$ -galactosidase staining. The cells that remained senescent for as long as 40 days with reversing back from senescence.

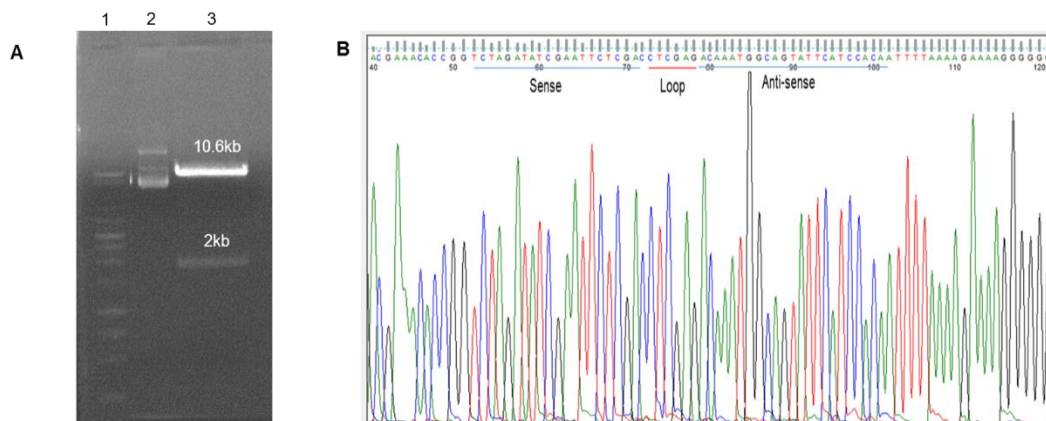


**Figure 3.10: Cloning of shRNAs against SETMAR in pLKO.1-tet.** A) Double digestion of pLKO.1-tet puro with EcoRI and AgeI. 1- 1kb ladder, 2-undigested pLKO.1 vector, 3- EcoRI and AgeI digested vector. B) Chromatogram depicting the shRNA1 inserted into the pLKO.1 vector.

RR cells expressing sh2 similar to the sh1, initially did show decrease in the cell number, however the cells that survived regained their growth capacity similar to the scrambled shRNA cells (Figure 3.11B). Interestingly, none of these shRNA constructs altered the growth pattern of parent cells but only hampered the proliferation potential of RR cells, highlighting an important role that SETMAR plays in the RR cells.

We then wanted to see if the effects seen by the knockdown of SETMAR are mediated via H3K36me2. We checked for H3K36me2 mark in the cells showing SETMAR knockdown and found significant reduction in H3K36me2 marks in the cells expressing shRNA1 against SETMAR (Figure 3.11C). A report from Fnu *et al* in 2011 suggested a link between SETMAR mediated H3K36me2 modification and DSB repair via NHEJ pathway [250]. As demonstrated previously, we also observed NHEJ pathway preference in RR cells, we asked whether SETMAR is involved in aiding NHEJ pathway repair. For this, we examined the recruitment of NHEJ protein Ku80 in the RR cells in a SETMAR knockdown background. We observed that upon shRNA-mediated silencing, there is a significant reduction in the Ku80 recruitment (Figure 3.11D), suggesting SETMAR mediated NHEJ repair driving the growth of RR cells.

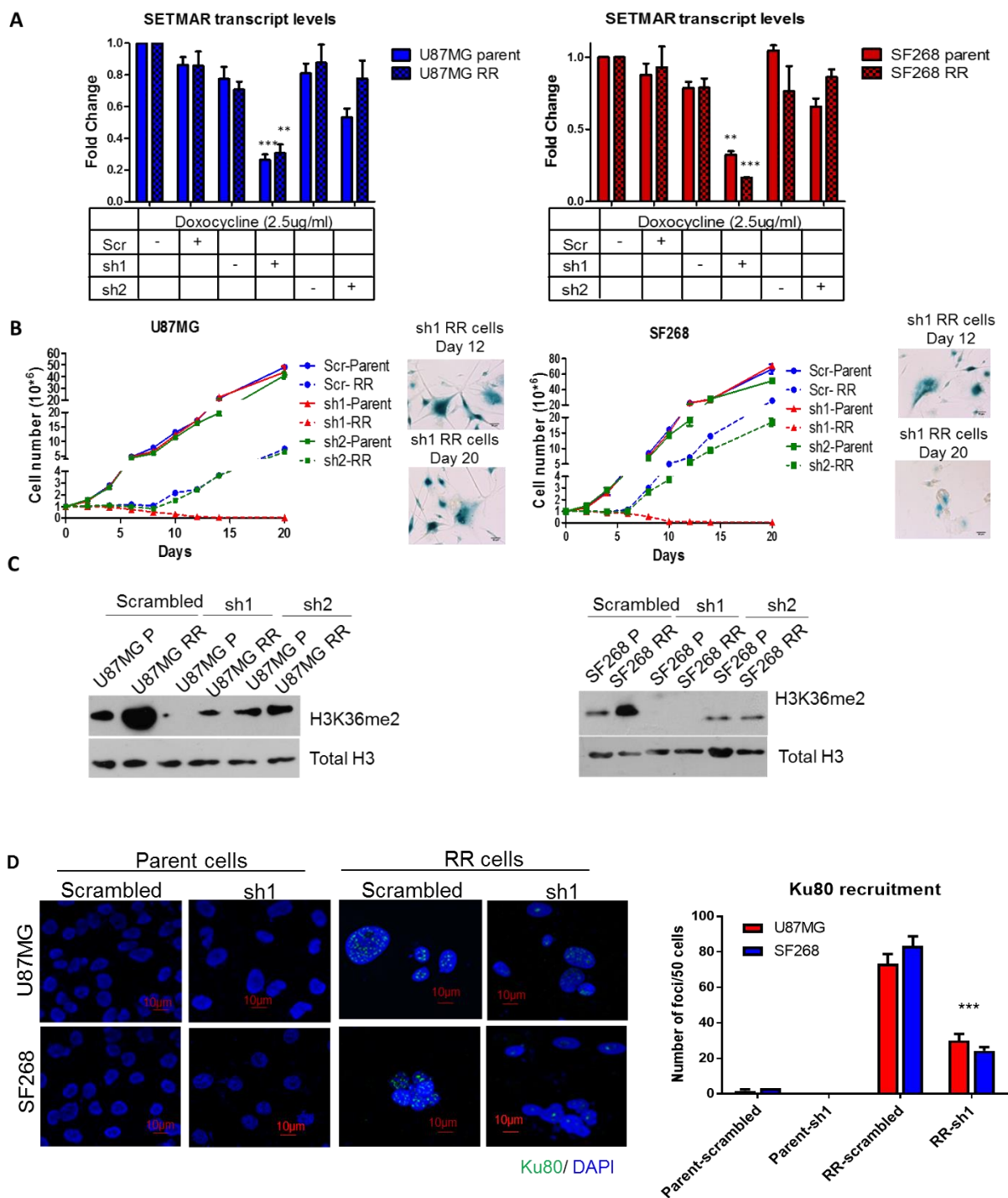


**Figure 3.11: SETMAR is required for proliferation, H3K36me2 and recruitment of Ku80 in RR cells.** A) Transcript levels of SETMAR in cells expressing scrambled shRNA and shRNAs against SETMAR -sh1 and sh2 with and without doxycycline induction. B) Growth curve of cells expressing SETMAR shRNAs (after induction) in RR and parent cells. Right panel shows representative images of the  $\beta$ -galactosidase staining in the RR cells after

12 and 20 days after knockdown. Scale bar-50µm. C) Western blot showing the expression of H3K36me2 in parent and RR cells of both U87MG and SF268 cell lines expressing scrambled shRNA and sh1. D) Recruitment of Ku80 in the knockdown parent and RR cells. Quantitation of the same is shown as bar graph, N=100 cells. Scale bar-10µm.

### 3.3.9 H3K36me2 is required for retention of Ku80 and mediates the survival of RR cells

To address the importance of over-expressed di-methylated H3K36 in RR cells, we cloned the wild type H3.3K36 and mutant H3.3K36A in the retroviral vector pBABE-puro (Figure 3.12).

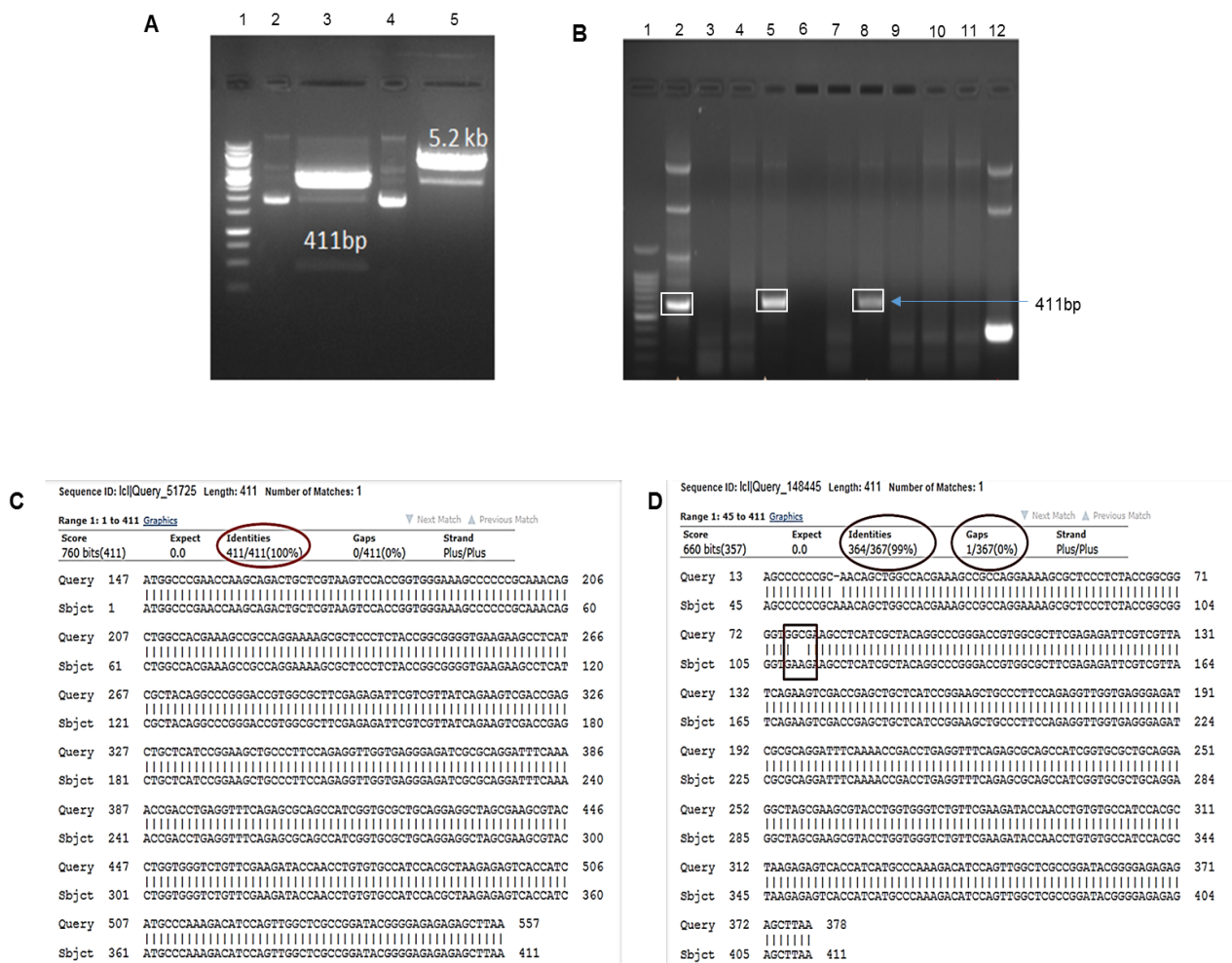


**Figure 3.12: Cloning of wild type and K36A H3.3 in pBABE vector.** A) Double digestion of pBABE- puro and pTZ57R/T containing H3.3 with EcoRI and BamHI. 1- 1kb ladder, 2-

undigested pTZ57R/T vector, 3- double digested pTZ57R/T vector, 4- undigested pBABE vector, 4- double digested pBABE vector, 3- undigested vector. C) and D) Nucleotide blast results depicting the percentage sequence match from the wild type H3.3 and H3K36A (GC>AA) cloned into the pBABE vector.

We then generated stable U87MG and SF268 cells harbouring mutation at the lysine 36 residue of H3.3 and cells with un-altered H3.3. Overexpression was confirmed by checking for the transcripts of H3.3 in 293FT, U87MG and SF268 cells (Figure 3.13). To begin with, the expression of H3K36me2 in the mutant and wild type expressing parent and RR cells was checked in the acid extracted histones. Indeed, we observed that RR cells of expressing mutant

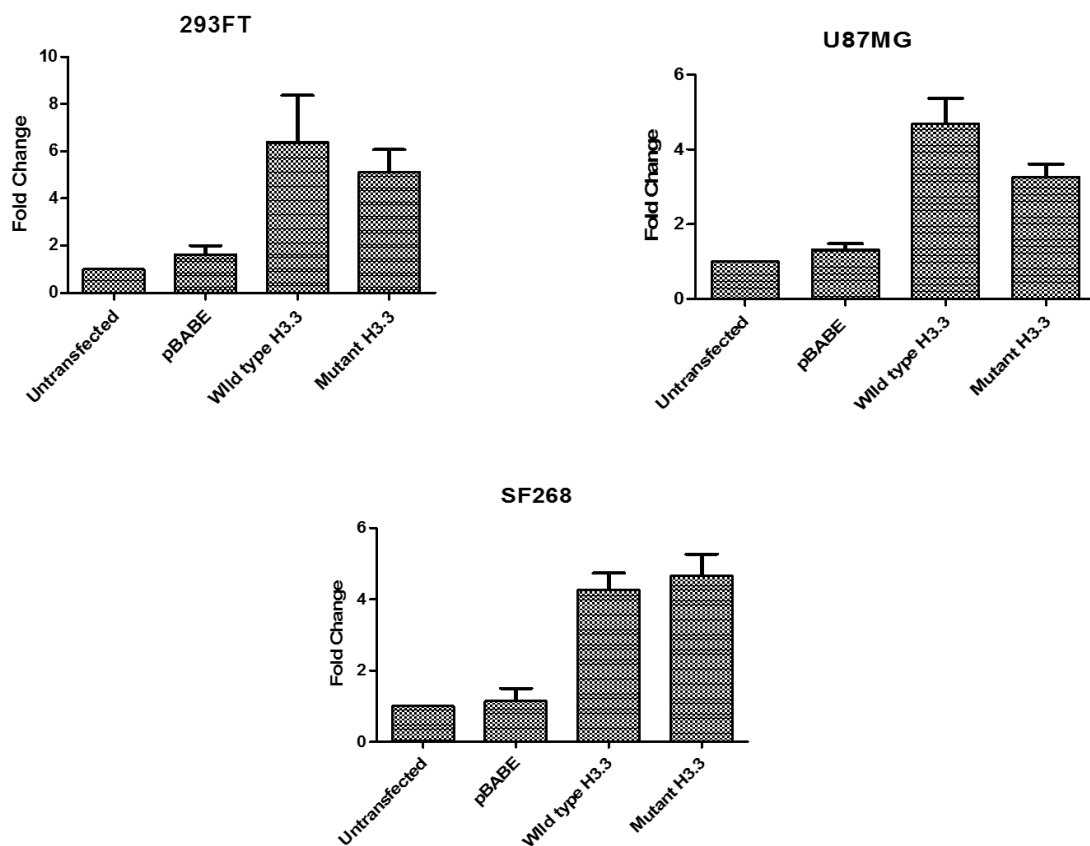


**Figure 3.13: Higher transcript levels of H3.3 was observed in 293FT, U87MG and SF268 cells as determined by real time PCR.**

H3K36 showed none or very faint levels of H3K36me<sub>2</sub>, confirming that most of the endogenous wild type H3.3 is replaced by mutant H3K36A (Figure 3.14A). Incorporation of the mutated histones was also confirmed with the immunofluorescence for H3K36me<sub>2</sub>. Similar to the western blots, U87MG H3.3 mutant showed no expression of the modification while SF268 cells did exhibit marginal expression of H3K36 di-methylation in the nucleus (Figure 3.14B). Several of these histone methylations are reported to regulate the cell proliferation and

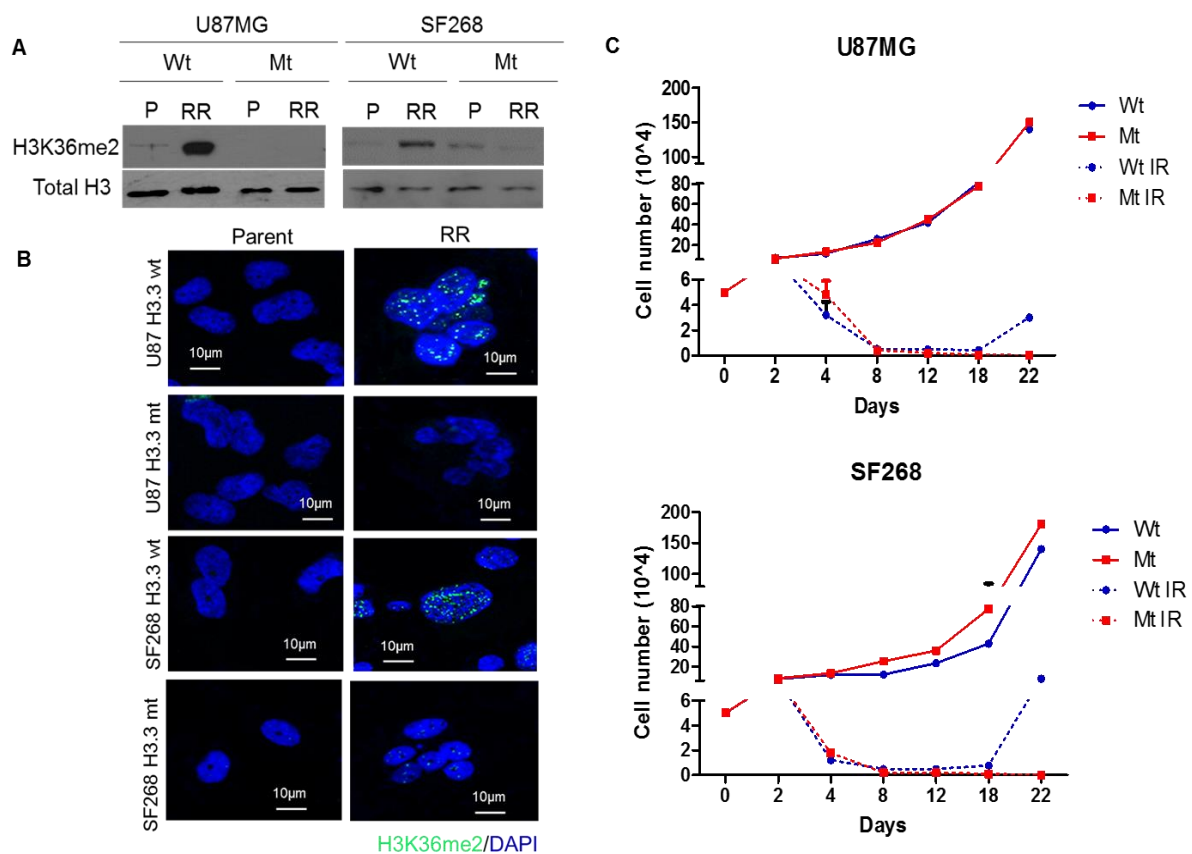


**Figure 3.14: H3.3 mutant cells demonstrate reduced survival capability compared to the wild type H3.3 expressing cells.** A and B) Expression and recruitment of H3K36me<sub>2</sub> in H3.3 wild type and mutant expressing U87MG and SF268 cells lines are shown. Scale bar

10 $\mu$ m. C) Growth curve of these cells at different time points after exposure to lethal dose of radiation is shown as line graph.

growth, lack of which can lead to the cell cycle defects. Thus, we first examined the growth kinetics of the non-irradiated and irradiated wild and mutant H3.3 expressing cells. As shown in Figure 3.14C, loss of lysine 36 residue did not alter the growth rate of non-irradiated cells however, post irradiation continuous cell death was observed, that is there were no radiation resistant cells formed.

Since the loss of H3K36me2 prevented the survival of the RR cells, we further examined the influence of histone amino acid change on the NHEJ and HR repair responses. For this, we checked for the recruitment and expression of Ku80 and pBRCA1 proteins expressing wild type and mutant H3.3 by immunofluorescence and western blot at different time intervals post irradiation. Interestingly, within 6-14 hours after radiation treatment, expression of NHEJ protein Ku80 and HR protein pBRCA1 was observed in both the cells expressing wild type H3.3 and mutant H3.3, and there was recruitment to the sites of DSB as well at initial time points (6 -14 hours) as these cells progressed from G1 to S and G2-M phases of the cell cycle. However, a significant increase in the expression and recruitment of Ku80 was observed in H3.3 wild type cells while a substantial amount of reduction in the recruitment of Ku80 was observed in the H3.3 mutant cells as compared to the cells expressing wild type H3.3 at later time points (24-48 hours). The difference in the recruitment was most prominent in the RR population as shown in figure 3.15, 3.16A and B.

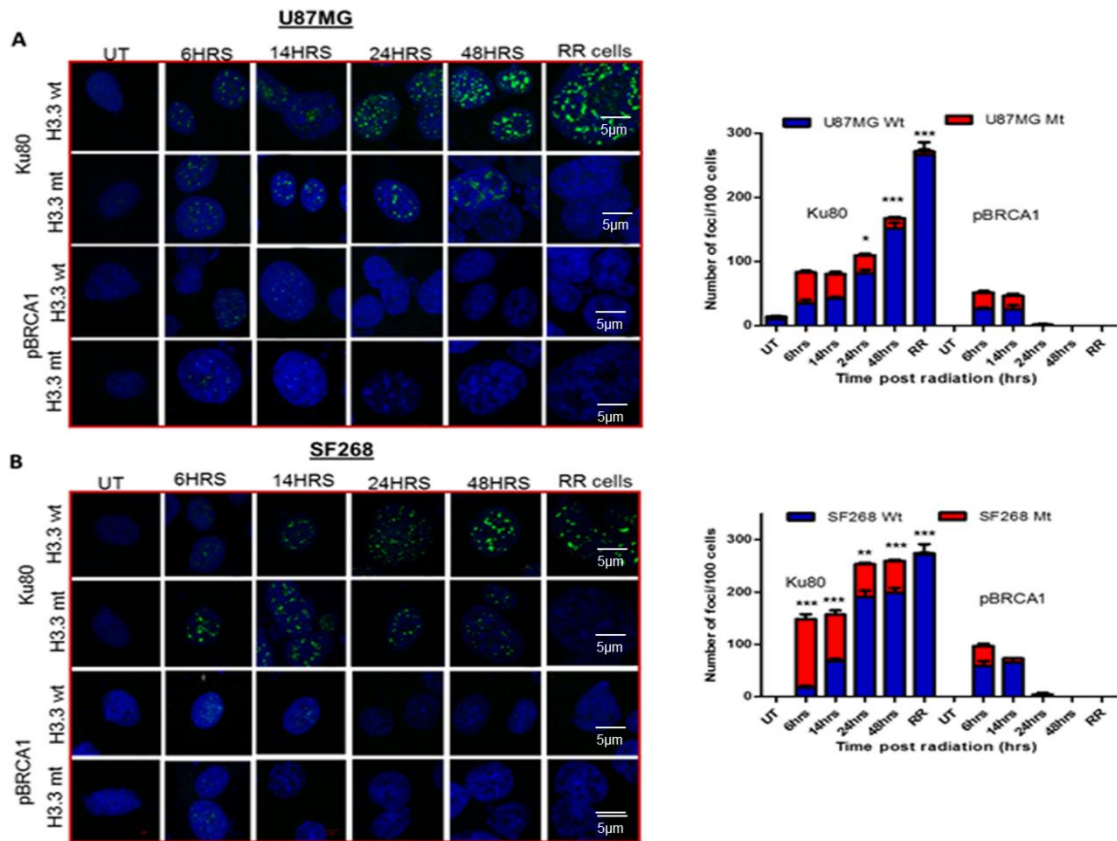


**Figure 3.15: Recruitment kinetics of Ku80 in H3.3 mutant cells vary from that of the wild type H3.3 expressing cells.** A and B) Representative images depicting the recruitment of Ku80 and pBRCA1 in H3.3 wild type and mutant expressing U87MG and SF268 cells lines are shown. Bar graph depicts the number of foci as counted in 100 cells. Scale bar- 5µm. Results are representative of three independent experiments. \*\*\* depicts p-value<0.001, \*\* indicates p-value <0.01 and \* for p-value<0.05.

Notably, we also observed decrease in the expression of Ku80 in H3.3 mutant expressing cells. To rule out the possibility of decreased expression leading to reduced recruitment of Ku80, we quantitated the western blot expression and immunofluorescence images. Even though very low levels of Ku80 protein was still being expressed in the mutant RR cells, there was absolutely no recruitment of Ku80 was seen in the mutant H3.3

expressing RR cells, suggesting that apart from recruitment, H3K36me2 may be involved in regulating the expression of the Ku80 as well, however requires further investigation.

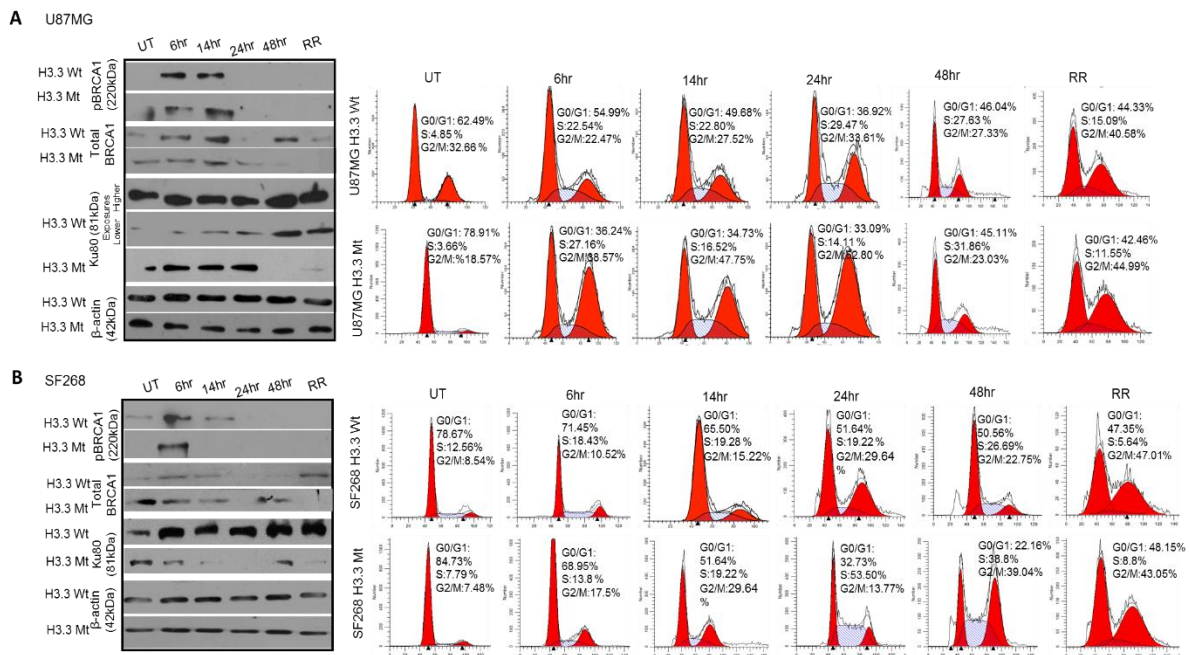


**Figure 3.16: Expression levels of Ku80 in H3.3 mutant cells vary from that of the wild type H3.3 expressing cells.** A and B) Shows western blot analysis for the Ku80, total BRCA1 and pBRCA1 as well as the cell cycle distribution in H3.3 wild type and mutant expressing U87MG and SF268 cells lines at different time points after radiation exposure.

Furthermore, to our surprise even though substantial percentage of the cells were present in S and G2-M phases, the expression of total BRCA1 and pBRCA1 was perturbed in the later time points post radiation in the wild type expressing cells. Moreover, in spite of similar distribution of cells in S and G2-M population in both wild type and mutant expressing cells, change (loss) in the expression of total BRCA1 was observed in the cells harbouring mutant H3.3 (Figure 3.16). This could possibly be due to the continuous apoptosis occurring in the mutant cells or due to its regulation via H3K36me2, however requires additional confirmatory experiments.

### **3.4 Discussion**

Glioblastoma (GBM) is the most frequent, highly infiltrative type of primary brain tumour arising from glial cells and associated with poor prognosis. Despite of increase in the understanding of this disease and the advancements in the treatment regime, the cure still eludes the GBM patients. DNA repair components have been reported to be altered (over-expressed and mutated) in various cancer cells. Cancers harbouring alterations in the repair proteins in turn modulate the efficacy of chemotherapeutic drugs and radiotherapy, playing an important role in imparting resistance to the cancer therapy. One of the most common DNA repair protein known to impart resistance phenotype to the cancers include the over-expression of MGMT in colon cancer [251, 252], melanoma [253, 254], pancreatic carcinoma [255], lung cancer [256] and gliomas [257]. Thus, a number of therapeutic methods have been initiated to inhibit MGMT and increase the efficiency of drug responses in the clinical scenario. The functions of these DNA repair proteins are in turn controlled by epigenetic processes including DNA methylation and histone modification. Thus, this study was envisaged to investigate the role of DNA repair proteins and its regulation by histone methylation.

For this, we studied the radiation resistant (RR) cells generated from parent cultures of cell lines and patient samples after subjecting them to radiation as previously reported [116]. The parent cells immediately after radiation showed increased levels of phospho-H2AX and recruited pATM, initiating DNA repair and subsequently resolving the damaged DNA. Interestingly, at later time point after 6-10 days post radiation, these cells revealed enhanced damage indicated by alkaline comet assay and  $\gamma$ H2AX and activating either ATM-Chk2 or ATR-Chk1-RPA32 repair axis, however a cross-talk between these axes was also observed in different patient samples. Similar to the RR cells, the recurrent cells from these RR cells also displayed variations in the recruitment choices of ATM and ATR and hence,

the recurrent cells differed on their response towards ATM inhibitor along with radiation compared to the parent cells. Thus, the RR cells alter the activation of DDR components, extrapolating it to the recurrent cells and thus, increasing the heterogeneity of the repair response. The results demonstrate that even though all the samples were subjected to their lethal dose of radiation, the remaining RR cells so formed generate variable levels of single strand breaks/ DNA overhangs. Further studies on the DNA ends processivity will be required to understand the possible reasons for difference in the recruitment of sensory kinases.

Furthermore, upon electron microscopic examination of the RR cells, we observed a global change in the organization of the chromatin compared to the parent cells. This observation was further confirmed by the decrease in the overall expression of HP-1 alpha in the RR cells when compared with the expression in parent cells. Several reports have suggested that the formation of heterochromatin architecture inhibits the DNA repair processes [258, 259] and a global de-compaction of the chromatin occurs possibly aided by loss of HP-1 alpha, making the damaged sites accessible to DNA repair proteins.

Notably, these RR cells show higher recruitment of NHEJ protein Ku80 as compared to HR protein pBRCA1, repairing the lesions induced by lethal dose of radiation. Furthermore, these cell exhibit higher levels of H3K36 and H3K4 di-methylation along with over-expression of Metnase enzyme known to di- methylate H3 at both 36 and 4 lysine residues, compared to the parent cells. High expression of H3K36me2 has been previously shown to initiate oncogenic programming influencing myeloma pathogenesis [260] and is associated with poorly differentiated histologic grade of Squamous Cell Carcinoma of the Head and Neck [261]. Furthermore, Metnase/ SETMAR is overexpressed in acute leukaemia cells compared to the normal hematopoietic progenitors, mediating resistance to the DNA damaging drug etoposide [262]. Similar to leukemic cells, expression of SETMAR also

conferred breast cancer cells resistant phenotype against adriamycin [263]. Additionally, the SET-domain of SETMAR mediates di-methylation of H3K36 adjacent the site of DSBs, stabilizing and retaining the Ku and MRN complex at the DNA breaks. This further leads to enhanced DSB repair via non-homologous end joining pathway (NHEJ) [250]. Based on these reports and our results, we questioned whether the H3K36me2 over-expression was mediated by SETMAR. Upon shRNA mediated knockdown of SETMAR in RR cells, we observed that a significant reduction in the H3K36me2 expression. However, a complete loss of H3K36me2 was not seen since the fewer transcripts of SETMAR were still present. The presence of additional methyltransferases contributing to the di-methylation of H3K36 also cannot be ruled out. Importantly, upon knockdown of SETMAR in RR cells, the resistant cells could not regain their growth potential after the non-proliferative phase, rather displayed a senescent phenotype as seen by  $\beta$ -galactosidase staining. However, no such defect in the cell proliferation was seen in the parent samples. This suggests that the silencing of the SETMAR displayed a greater effect on the RR cells which probably rely on its expression for the cell growth. Williamson et al also observed that the anti-proliferative effect of ciprofloxacin mediated inhibition of SETMAR varied in different cancer cells possibly due to varying expression of the enzyme [264]. Furthermore, we observed that the SETMAR knockdown led to the reduction in Ku80 foci in the RR cells demonstrating that H3K36me2 induced by SETMAR facilitated NHEJ repair in the resistant cells during their non-proliferative phase. Similar to the knockdown, loss of H3K36me2 due to mutation at lysine 36 residue completely abolished the growth capacity of resistant cells, preventing their maintenance. Importantly, loss of this modification prevented persistent recruitment or retention Ku80 protein at the DSB site as well as its expression suggesting that the presence of H3K36me2 is required as a substrate for efficient assembly or retention of NHEJ repair factors and thus, loss of this modification could not provide adequate time for the cells to

repair, eventually underwent cell death. To our surprise, loss of total BRCA1 protein was observed in the H3.3 mutant expressing cells as compared to the wild type cells. In this context, thus further experiments will be necessary to help in understanding the regulation of DDR pathway in the cells having high H3K36me2.

The di-methylation is known to occur at both H3.2 and H3.3 lysine 36 residues with higher abundance of H3.3K36me2 relative to H3.2K36me2 reported in the neuronal cells and also during postnatal development of mouse brain neurons have shown to accumulation more of H3.3 than H3.2 [265, 266]. Furthermore, the analysis of the GBM tissues from The Cancer Genome Atlas revealed 18% over-expression of H3.3 genes as compared to H3.2 genes. The complete loss of H3K36me2, thus indicates towards more incorporation of H3.3 into the GBM cells, however a quantitative mass spectrometry approach will be required to validate these observations.

Taken together, ours is the first study demonstrating the multistep process of survival in the radiation resistant GBM cells. We show that these cells preferentially undergo repair by activating ATM/ATR and NHEJ pathway. We observe that regulation of NHEJ pathway occurs at the level of chromatin by the SETMAR-mediated H3K36me2. We also show that specific targeting of SETMAR in the resistant cells can prevent the formation of recurrent cells.

**Chapter 4**

***Summary and Conclusion***

## 4.1 Summary

Glioblastoma is the most fatal type of primary brain tumour associated with worst prognosis. The principal cause of the poor prognosis is majorly due to presence of highly treatment refractory GBM cells. Current understanding of resistance mechanisms predominantly directed towards temozolomide resistance, are based on studies on naïve primary GBM tissues and/or *in vivo* orthotropic models. However, the bulk GBM tumours consist of multiple clones, each eliciting a heterogeneous response to therapy. Additionally, monitoring of the resistant cells is not possible with the current *in vivo* models. Thus, in this thesis an *in vitro* model was established from 20 naïve primary GBM tissues to understand the radiation resistance in GBM cells. Using this model, we obtained a population of cell that is innately resistant to a single lethal dose of radiation. We observed the following:

1. The innately resistant cells (RR) underwent a non-proliferative phase lasting for almost a week after radiation, arrested in different cell cycle phases and predominantly expressing inhibitory phosphorylation of Cdk1(tyrosine 15).
2. Morphologically, these cells displayed multinucleated and giant cells (MNGCs) phenotype. The percentage of multinucleated and giant cells varied in different patient samples and cell lines.
3. Pre-existing large cells from the parent samples did not possess survival capacity. This demonstrated that the multinucleated and giant cells enriched in resistant cells were induced post radiation exposure and were not the pre-existing cells from parent population.
4. Unlike other reports, the resistant cells (MNGCs) showed no apoptosis but over-expressed pro-survival genes including BIRC3, Bcl-xL and pAKT. They underwent a transient senescent phase as seen by  $\beta$ -galactosidase assay however, eventually could

undergo atypical cytokinesis as seen by presence of multiple spindle poles to regain growth forming recurrent cells.

5. To understand the importance of the resistant cells associated characteristics in patient survival we performed correlating analysis with the radio-pathological parameters and resistance associated markers including the day of required for emergence of RR cells ( $D_{rr}$ ), percentage of multinucleated cells, percentage of giant cells, length of non-proliferative phase and total days taken to form recurrent population ( $D_r$ ), for 20 patient samples. We observed that tumour volume showed a significant positive correlation with length of non-proliferation phase ( $r=0.758$ ,  $p=0.007$ ) and percentage of giant cells ( $r=0.682$ ,  $p=0.021$ ) indicating that larger tumours have higher number of resistant cells (Figure 3.6D-F). Individually, percentage of giant cells influenced the clinical outcome with a marginal significance. However, patients with lower tumour volume and lower percentage of giant cells had better prognosis (15.33 months, 95% CI: 14.04-16.64) as compared to the patients with higher tumour volume and higher percentage of giant cells (6 months, 95% CI: 2.159-9.841).
6. The multinucleated and giant cells enriched in resistant cells were formed predominantly by cell- cell fusion process, however occurrence of endo-replication in small percentage of cells could not be ruled out.
7. We show that these cells can be targeted either by using Wee1 kinase inhibitor by inducing mitosis prematurely or by inhibiting cytokinesis using Wiskostatin to prevent recurrent cell population.

Since the resistant cells escaped the lethal dose of radiation, this thesis aimed to identify various survival mechanisms contributing to their survival. Therapy is primarily governed by the DNA repair which in turn is influenced by chromatin architecture of the cell.

Hence, the role of double strand break repair along with the chromatin- histone methylation was investigated in these resistant cells.

1. The radiation resistance cells formed after a week of radiation, displayed high levels of  $\gamma$ H2AX foci mediated by either ATM or ATR sensory kinases. Depending upon the kinase (ATM or ATR) activated in the cells either Chk2 or Chk1-RPA32 respectively are activated as downstream effector proteins.
2. Irrespective of the upstream sensor kinase activation and cell cycle phase, resistant cells showed higher expression and recruitment of NHEJ repair protein Ku80 and showed higher NHEJ repair efficiency when compared with the HR. Accordingly resistant cells incubated with NHEJ inhibitor showed significantly reduction in their survival capacity.
3. In addition, the resistant cells displayed more open chromatin architecture as seen by loss of HP-1 alpha. Resistant cells showed high levels of H3K36me2 modification and over-expression of methyltransferase SETMAR
4. To understand the role of H3K36me2 and SETMAR over-expression in resistant cells, we mutated H3.3 at lysine 36 position and generated inducible knockdown constructs against SETMAR.
5. Mutation at lysine 36 position led to reduction in the recruitment of Ku80 proteins and abrogation of radiation resistant (RR) cell formation.
6. Inducible knockdown of SETMAR led to a significant decrease in the H3K36 dimethylation resulting in decrease expression and recruitment of Ku80 proteins in the resistant cells. The resistant cells expressing shRNA1 against SETMAR displayed an irreversible senescence, altering the growth potential of resistant cells.

Furthermore, our model system also enables us to generate and thus characterize the recurrent cells formed from the radiation resistant cells.

1. Recurrent cells had similar morphology when compared with the parent cells however they showed higher resistance index at lower doses of radiation except for the recurrent cells from U87MG cell line. The recurrent cells also showed variable rate of proliferation among different samples.
2. The recurrent cells showed higher expression of Survivin transcripts and higher levels of pERK1/2 as compared to the parent cells, although as with the proliferation and resistant phenotype disparity across recurrent cells was observed.
3. Additionally, the recurrent cells generated from cell lines and patient samples varied in their recruitment of ATM and ATR sensory kinases and thus, displayed altered sensitivity towards ATM inhibitor KU55933 when compared with the parent cells.
4. Irrespective of the biological dissimilarity, Raman spectroscopic analysis of the recurrent and parent cells led to a distinct classification parent and recurrent cells based on PCA and PCA-LDA. Spectroscopically, higher lipid related spectral peaks were observed in recurrent population.
5. Importantly, Raman spectral analysis led to classification of an independent set of naïve primary glioblastoma tumour tissues into non-responders and responders groups.

## **4.2 Conclusion**

Overall, the major part of the study involves the establishment of the *in vitro* radiation model and characterization of the innately resistant cells where we identified multiple mechanisms involving a rare process of cell-cell fusion, gene and protein expression changes and altered DNA double strand break repair pathway facilitated by histone methylation to be important RR cell survival and their escape from the radiation stress. Furthermore, a preliminary study on recurrent samples generated *in vitro* as well as primary tissues using Raman spectroscopy

demonstrated potential of the spectral features of recurrent cells to be used in predicting therapy response in GBM

Future studies on identifying molecular players involved in cell-cell fusion as well as the regulation of NHEJ repair would help in better understanding of the survival strategies adopted by these resistant GBM cells. Establishment of *in vivo* radiation resistant orthotopic mouse model has already been undertaken in the laboratory to identify the innately resistant cells. These studies will further enable in the development of therapeutic strategies that will improve the GBM patient outcome.

## *References*

1. Ferlay, J., et al., *Estimates of worldwide burden of cancer in 2008: GLOBOCAN 2008*. Int J Cancer, 2010. 127(12): p. 2893-917.
2. Schwartzbaum, J.A., et al., *Epidemiology and molecular pathology of glioma*. Nat Clin Pract Neurol, 2006. 2(9): p. 494-503; quiz 1 p following 516.
3. Louis, D.N., et al., *The 2007 WHO classification of tumours of the central nervous system*. Acta Neuropathol, 2007. 114(2): p. 97-109.
4. Adamson, C., et al., *Glioblastoma multiforme: a review of where we have been and where we are going*. Expert Opin Investig Drugs, 2009. 18(8): p. 1061-83.
5. Porter, K.R., et al., *Prevalence estimates for primary brain tumors in the United States by age, gender, behavior, and histology*. Neuro Oncol, 2010. 12(6): p. 520-7.
6. Ohgaki, H. and P. Kleihues, *Population-based studies on incidence, survival rates, and genetic alterations in astrocytic and oligodendroglial gliomas*. J Neuropathol Exp Neurol, 2005. 64(6): p. 479-89.
7. P, S., et al., *High Grade Gliomas: Newer Horizon-New Hope* International Journal of Science and Research 2015. 4(6): p. 4.
8. Munshi, A. and R. Jalali, *Therapy for glioma: Indian perspective*. Indian J Cancer, 2009. 46(2): p. 127-31.
9. Kim, J.E. and M. Lim, *The role of checkpoints in the treatment of GBM*. J Neurooncol, 2015.
10. Hottinger, A.F. and Y. Khakoo, *Update on the management of familial central nervous system tumor syndromes*. Curr Neurol Neurosci Rep, 2007. 7(3): p. 200-7.
11. Kinnersley, B., et al., *Genome-wide association study identifies multiple susceptibility loci for glioma*. Nat Commun, 2015. 6: p. 8559.
12. Weller, M., et al., *EANO guideline for the diagnosis and treatment of anaplastic gliomas and glioblastoma*. Lancet Oncol, 2014. 15(9): p. e395-403.
13. Kao, H.W., et al., *Advanced MR imaging of gliomas: an update*. Biomed Res Int, 2013. 2013: p. 970586.
14. Li, W.B., et al., *MRI manifestations correlate with survival of glioblastoma multiforme patients*. Cancer Biol Med, 2012. 9(2): p. 120-3.
15. Jain, R., et al., *Outcome prediction in patients with glioblastoma by using imaging, clinical, and genomic biomarkers: focus on the nonenhancing component of the tumor*. Radiology, 2014. 272(2): p. 484-93.
16. Wangaryattawanich, P., et al., *Multicenter imaging outcomes study of The Cancer Genome Atlas glioblastoma patient cohort: imaging predictors of overall and progression-free survival*. Neuro-Oncology, 2015.
17. Stupp, R., et al., *Radiotherapy plus concomitant and adjuvant temozolomide for glioblastoma*. N Engl J Med, 2005. 352(10): p. 987-96.
18. Hegi, M.E., et al., *MGMT gene silencing and benefit from temozolomide in glioblastoma*. N Engl J Med, 2005. 352(10): p. 997-1003.
19. Verhaak, R.G., et al., *Integrated genomic analysis identifies clinically relevant subtypes of glioblastoma characterized by abnormalities in PDGFRA, IDH1, EGFR, and NF1*. Cancer Cell, 2010. 17(1): p. 98-110.
20. Noushmehr, H., et al., *Identification of a CpG island methylator phenotype that defines a distinct subgroup of glioma*. Cancer Cell, 2010. 17(5): p. 510-22.
21. Gilbert, M.R., et al., *A randomized trial of bevacizumab for newly diagnosed glioblastoma*. N Engl J Med, 2014. 370(8): p. 699-708.
22. Weller, M. and W.K. Yung, *Angiogenesis inhibition for glioblastoma at the edge: beyond AVAGlio and RTOG 0825*. Neuro Oncol, 2013. 15(8): p. 971.
23. McDermott, M.W., P.K. Sneed, and P.H. Gutin, *Interstitial brachytherapy for malignant brain tumors*. Semin Surg Oncol, 1998. 14(1): p. 79-87.

24. Chakravarti, A., et al., *The epidermal growth factor receptor pathway mediates resistance to sequential administration of radiation and chemotherapy in primary human glioblastoma cells in a RAS-dependent manner.* *Cancer Res*, 2002. 62(15): p. 4307-15.
25. Chakravarti, A., et al., *Survivin enhances radiation resistance in primary human glioblastoma cells via caspase-independent mechanisms.* *Oncogene*, 2004. 23(45): p. 7494-506.
26. Kitange, G.J., et al., *Induction of MGMT expression is associated with temozolomide resistance in glioblastoma xenografts.* *Neuro Oncol*, 2009. 11(3): p. 281-91.
27. Ye, F., et al., *Protective properties of radio-chemoresistant glioblastoma stem cell clones are associated with metabolic adaptation to reduced glucose dependence.* *PLoS One*, 2013. 8(11): p. e80397.
28. Ichimura, K., et al., *Molecular pathogenesis of astrocytic tumours.* *J Neurooncol*, 2004. 70(2): p. 137-60.
29. Chen, J., R.M. McKay, and L.F. Parada, *Malignant glioma: lessons from genomics, mouse models, and stem cells.* *Cell*, 2012. 149(1): p. 36-47.
30. Joung, J.G., et al., *Genomic Characterization and Comparison of Multi-Regional and Pooled Tumor Biopsy Specimens.* *PLoS One*, 2016. 11(3): p. e0152574.
31. Meyer, M., et al., *Single cell-derived clonal analysis of human glioblastoma links functional and genomic heterogeneity.* *Proc Natl Acad Sci U S A*, 2015. 112(3): p. 851-6.
32. Galli, R., et al., *Isolation and characterization of tumorigenic, stem-like neural precursors from human glioblastoma.* *Cancer Res*, 2004. 64(19): p. 7011-21.
33. Bao, S., et al., *Glioma stem cells promote radioresistance by preferential activation of the DNA damage response.* *Nature*, 2006. 444(7120): p. 756-60.
34. Madhusudan, S. and M.R. Middleton, *The emerging role of DNA repair proteins as predictive, prognostic and therapeutic targets in cancer.* *Cancer Treat Rev*, 2005. 31(8): p. 603-17.
35. Bartkova, J., et al., *DNA damage response as a candidate anti-cancer barrier in early human tumorigenesis.* *Nature*, 2005. 434(7035): p. 864-70.
36. Gorgoulis, V.G., et al., *Activation of the DNA damage checkpoint and genomic instability in human precancerous lesions.* *Nature*, 2005. 434(7035): p. 907-13.
37. Bartkova, J., et al., *Oncogene-induced senescence is part of the tumorigenesis barrier imposed by DNA damage checkpoints.* *Nature*, 2006. 444(7119): p. 633-7.
38. Di Micco, R., et al., *Oncogene-induced senescence is a DNA damage response triggered by DNA hyper-replication.* *Nature*, 2006. 444(7119): p. 638-42.
39. Park, T.J., et al., *Methylation of O(6)-methylguanine-DNA methyltransferase gene is associated significantly with K-ras mutation, lymph node invasion, tumor staging, and disease free survival in patients with gastric carcinoma.* *Cancer*, 2001. 92(11): p. 2760-8.
40. Hayashi, H., et al., *Inactivation of O6-methylguanine-DNA methyltransferase in human lung adenocarcinoma relates to high-grade histology and worse prognosis among smokers.* *Jpn J Cancer Res*, 2002. 93(2): p. 184-9.
41. Hiraga, J., et al., *Promoter hypermethylation of the DNA-repair gene O6-methylguanine-DNA methyltransferase and p53 mutation in diffuse large B-cell lymphoma.* *Int J Hematol*, 2006. 84(3): p. 248-55.
42. Esteller, M., et al., *Inactivation of the DNA-repair gene MGMT and the clinical response of gliomas to alkylating agents.* *N Engl J Med*, 2000. 343(19): p. 1350-4.
43. Son, B.H., et al., *Significance of mismatch repair protein expression in the chemotherapeutic response of sporadic invasive ductal carcinoma of the breast.* *Breast J*, 2004. 10(1): p. 20-6.
44. Catto, J.W., et al., *Differential expression of hMLH1 and hMSH2 is related to bladder cancer grade, stage and prognosis but not microsatellite instability.* *Int J Cancer*, 2003. 105(4): p. 484-90.

45. Pearl, L.H., et al., *Therapeutic opportunities within the DNA damage response*. *Nat Rev Cancer*, 2015. 15(3): p. 166-80.
46. Mao, G., et al., *Preferential loss of mismatch repair function in refractory and relapsed acute myeloid leukemia: potential contribution to AML progression*. *Cell Res*, 2008. 18(2): p. 281-9.
47. Casorelli, I., M.T. Russo, and M. Bignami, *Role of mismatch repair and MGMT in response to anticancer therapies*. *Anticancer Agents Med Chem*, 2008. 8(4): p. 368-80.
48. Shrivastav, M., L.P. De Haro, and J.A. Nickoloff, *Regulation of DNA double-strand break repair pathway choice*. *Cell Res*, 2008. 18(1): p. 134-47.
49. Fojo, T., *Cancer, DNA repair mechanisms, and resistance to chemotherapy*. *J Natl Cancer Inst*, 2001. 93(19): p. 1434-6.
50. Jackson, S.P., *Sensing and repairing DNA double-strand breaks*. *Carcinogenesis*, 2002. 23(5): p. 687-96.
51. Podhorecka, M., A. Skladanowski, and P. Bozko, *H2AX Phosphorylation: Its Role in DNA Damage Response and Cancer Therapy*. *J Nucleic Acids*, 2010. 2010.
52. Lee, J.H. and T.T. Paull, *Activation and regulation of ATM kinase activity in response to DNA double-strand breaks*. *Oncogene*, 2007. 26(56): p. 7741-8.
53. Annovazzi, L., et al., *The DNA damage/repair cascade in glioblastoma cell lines after chemotherapeutic agent treatment*. *Int J Oncol*, 2015. 46(6): p. 2299-308.
54. Cancer Genome Atlas Research, N., *Comprehensive genomic characterization of squamous cell lung cancers*. *Nature*, 2012. 489(7417): p. 519-25.
55. Cancer Genome Atlas, N., *Comprehensive molecular characterization of human colon and rectal cancer*. *Nature*, 2012. 487(7407): p. 330-7.
56. Cancer Genome Atlas, N., *Comprehensive molecular portraits of human breast tumours*. *Nature*, 2012. 490(7418): p. 61-70.
57. Bea, S., et al., *Landscape of somatic mutations and clonal evolution in mantle cell lymphoma*. *Proc Natl Acad Sci U S A*, 2013. 110(45): p. 18250-5.
58. Landau, D.A. and C.J. Wu, *Chronic lymphocytic leukemia: molecular heterogeneity revealed by high-throughput genomics*. *Genome Med*, 2013. 5(5): p. 47.
59. Squatrito, M., et al., *Loss of ATM/Chk2/p53 pathway components accelerates tumor development and contributes to radiation resistance in gliomas*. *Cancer Cell*, 2010. 18(6): p. 619-29.
60. Carruthers, R., et al., *Abrogation of radioresistance in glioblastoma stem-like cells by inhibition of ATM kinase*. *Mol Oncol*, 2015. 9(1): p. 192-203.
61. Brown, E.J. and D. Baltimore, *ATR disruption leads to chromosomal fragmentation and early embryonic lethality*. *Genes Dev*, 2000. 14(4): p. 397-402.
62. de Klein, A., et al., *Targeted disruption of the cell-cycle checkpoint gene ATR leads to early embryonic lethality in mice*. *Curr Biol*, 2000. 10(8): p. 479-82.
63. Gilad, O., et al., *Combining ATR suppression with oncogenic Ras synergistically increases genomic instability, causing synthetic lethality or tumorigenesis in a dosage-dependent manner*. *Cancer Res*, 2010. 70(23): p. 9693-702.
64. Murga, M., et al., *A mouse model of ATR-Seckel shows embryonic replicative stress and accelerated aging*. *Nat Genet*, 2009. 41(8): p. 891-8.
65. Schoppy, D.W., et al., *Oncogenic stress sensitizes murine cancers to hypomorphic suppression of ATR*. *J Clin Invest*, 2012. 122(1): p. 241-52.
66. van Gent, D.C., J.H. Hoeijmakers, and R. Kanaar, *Chromosomal stability and the DNA double-stranded break connection*. *Nat Rev Genet*, 2001. 2(3): p. 196-206.
67. Symington, L.S. and J. Gautier, *Double-strand break end resection and repair pathway choice*. *Annu Rev Genet*, 2011. 45: p. 247-71.
68. Lieber, M.R., *The mechanism of double-strand DNA break repair by the nonhomologous DNA end-joining pathway*. *Annu Rev Biochem*, 2010. 79: p. 181-211.

69. Burma, S., B.P. Chen, and D.J. Chen, *Role of non-homologous end joining (NHEJ) in maintaining genomic integrity*. DNA Repair (Amst), 2006. 5(9-10): p. 1042-8.
70. Gu, Y., et al., *Growth retardation and leaky SCID phenotype of Ku70-deficient mice*. Immunity, 1997. 7(5): p. 653-65.
71. Someya, M., et al., *The association of DNA-dependent protein kinase activity with chromosomal instability and risk of cancer*. Carcinogenesis, 2006. 27(1): p. 117-22.
72. Peng, G. and S.Y. Lin, *Exploiting the homologous recombination DNA repair network for targeted cancer therapy*. World J Clin Oncol, 2011. 2(2): p. 73-9.
73. Kelley, M.R. and M.L. Fishel, *DNA repair proteins as molecular targets for cancer therapeutics*. Anticancer Agents Med Chem, 2008. 8(4): p. 417-25.
74. Gao, Y., et al., *Interplay of p53 and DNA-repair protein XRCC4 in tumorigenesis, genomic stability and development*. Nature, 2000. 404(6780): p. 897-900.
75. Barnes, D.E., et al., *Targeted disruption of the gene encoding DNA ligase IV leads to lethality in embryonic mice*. Curr Biol, 1998. 8(25): p. 1395-8.
76. Gao, Y., et al., *A critical role for DNA end-joining proteins in both lymphogenesis and neurogenesis*. Cell, 1998. 95(7): p. 891-902.
77. Frank, K.M., et al., *DNA ligase IV deficiency in mice leads to defective neurogenesis and embryonic lethality via the p53 pathway*. Mol Cell, 2000. 5(6): p. 993-1002.
78. Willmore, E., et al., *A novel DNA-dependent protein kinase inhibitor, NU7026, potentiates the cytotoxicity of topoisomerase II poisons used in the treatment of leukemia*. Blood, 2004. 103(12): p. 4659-65.
79. O'Connor, M.J., N.M. Martin, and G.C. Smith, *Targeted cancer therapies based on the inhibition of DNA strand break repair*. Oncogene, 2007. 26(56): p. 7816-24.
80. Shinohara, E.T., et al., *DNA-dependent protein kinase is a molecular target for the development of noncytotoxic radiation-sensitizing drugs*. Cancer Res, 2005. 65(12): p. 4987-92.
81. Li, X. and W.D. Heyer, *Homologous recombination in DNA repair and DNA damage tolerance*. Cell Res, 2008. 18(1): p. 99-113.
82. Lim, D.S. and P. Hasty, *A mutation in mouse rad51 results in an early embryonic lethal that is suppressed by a mutation in p53*. Mol Cell Biol, 1996. 16(12): p. 7133-43.
83. Tsuzuki, T., et al., *Targeted disruption of the Rad51 gene leads to lethality in embryonic mice*. Proc Natl Acad Sci U S A, 1996. 93(13): p. 6236-40.
84. Sonoda, E., et al., *Rad51-deficient vertebrate cells accumulate chromosomal breaks prior to cell death*. EMBO J, 1998. 17(2): p. 598-608.
85. De Silva, I.U., et al., *Defects in interstrand cross-link uncoupling do not account for the extreme sensitivity of ERCC1 and XPF cells to cisplatin*. Nucleic Acids Res, 2002. 30(17): p. 3848-56.
86. Lundin, C., et al., *Different roles for nonhomologous end joining and homologous recombination following replication arrest in mammalian cells*. Mol Cell Biol, 2002. 22(16): p. 5869-78.
87. Chen, P.L., et al., *The BRC repeats in BRCA2 are critical for RAD51 binding and resistance to methyl methanesulfonate treatment*. Proc Natl Acad Sci U S A, 1998. 95(9): p. 5287-92.
88. Alsop, K., et al., *BRCA mutation frequency and patterns of treatment response in BRCA mutation-positive women with ovarian cancer: a report from the Australian Ovarian Cancer Study Group*. J Clin Oncol, 2012. 30(21): p. 2654-63.
89. Lim, Y.C., et al., *A role for homologous recombination and abnormal cell-cycle progression in radioresistance of glioma-initiating cells*. Mol Cancer Ther, 2012. 11(9): p. 1863-72.
90. Lim, Y.C., et al., *Increased sensitivity to ionizing radiation by targeting the homologous recombination pathway in glioma initiating cells*. Mol Oncol, 2014. 8(8): p. 1603-15.
91. Long, C., et al., *Promoter hypermethylation of the RUNX3 gene in esophageal squamous cell carcinoma*. Cancer Invest, 2007. 25(8): p. 685-90.

92. Akiyama, Y., et al., *GATA-4 and GATA-5 transcription factor genes and potential downstream antitumor target genes are epigenetically silenced in colorectal and gastric cancer*. *Mol Cell Biol*, 2003. 23(23): p. 8429-39.
93. Dobrovic, A. and D. Simpfendorfer, *Methylation of the BRCA1 gene in sporadic breast cancer*. *Cancer Res*, 1997. 57(16): p. 3347-50.
94. Lee, M.N., et al., *Epigenetic inactivation of the chromosomal stability control genes BRCA1, BRCA2, and XRCC5 in non-small cell lung cancer*. *Clin Cancer Res*, 2007. 13(3): p. 832-8.
95. Lahtz, C. and G.P. Pfeifer, *Epigenetic changes of DNA repair genes in cancer*. *J Mol Cell Biol*, 2011. 3(1): p. 51-8.
96. Chodaparambil, J.V., et al., *Nucleosome structure and function*. Ernst Schering Res Found Workshop, 2006(57): p. 29-46.
97. van Attikum, H. and S.M. Gasser, *The histone code at DNA breaks: a guide to repair?* *Nat Rev Mol Cell Biol*, 2005. 6(10): p. 757-65.
98. Sukanuma, T. and J.L. Workman, *Signals and combinatorial functions of histone modifications*. *Annu Rev Biochem*, 2011. 80: p. 473-99.
99. Fraga, M.F., et al., *Loss of acetylation at Lys16 and trimethylation at Lys20 of histone H4 is a common hallmark of human cancer*. *Nat Genet*, 2005. 37(4): p. 391-400.
100. Song, J., et al., *Increased expression of histone deacetylase 2 is found in human gastric cancer*. *APMIS*, 2005. 113(4): p. 264-8.
101. Yang, X.J., *The diverse superfamily of lysine acetyltransferases and their roles in leukemia and other diseases*. *Nucleic Acids Res*, 2004. 32(3): p. 959-76.
102. Kouzarides, T., *Histone methylation in transcriptional control*. *Curr Opin Genet Dev*, 2002. 12(2): p. 198-209.
103. Peterson, C.L. and M.A. Laniel, *Histones and histone modifications*. *Curr Biol*, 2004. 14(14): p. R546-51.
104. Martin, C. and Y. Zhang, *The diverse functions of histone lysine methylation*. *Nat Rev Mol Cell Biol*, 2005. 6(11): p. 838-49.
105. Fischle, W., et al., *Molecular basis for the discrimination of repressive methyl-lysine marks in histone H3 by Polycomb and HP1 chromodomains*. *Genes Dev*, 2003. 17(15): p. 1870-81.
106. Ayoub, N., et al., *HP1-beta mobilization promotes chromatin changes that initiate the DNA damage response*. *Nature*, 2008. 453(7195): p. 682-6.
107. Ayrappetov, M.K., et al., *DNA double-strand breaks promote methylation of histone H3 on lysine 9 and transient formation of repressive chromatin*. *Proc Natl Acad Sci U S A*, 2014. 111(25): p. 9169-74.
108. Sun, Y., X. Jiang, and B.D. Price, *Tip60: connecting chromatin to DNA damage signaling*. *Cell Cycle*, 2010. 9(5): p. 930-6.
109. Sun, Y., et al., *Histone H3 methylation links DNA damage detection to activation of the tumour suppressor Tip60*. *Nat Cell Biol*, 2009. 11(11): p. 1376-82.
110. Wu, W., et al., *Interaction of BARD1 and HP1 Is Required for BRCA1 Retention at Sites of DNA Damage*. *Cancer Res*, 2015. 75(7): p. 1311-21.
111. Botuyan, M.V., et al., *Structural basis for the methylation state-specific recognition of histone H4-K20 by 53BP1 and Crb2 in DNA repair*. *Cell*, 2006. 127(7): p. 1361-73.
112. Albert, M. and K. Helin, *Histone methyltransferases in cancer*. *Semin Cell Dev Biol*, 2010. 21(2): p. 209-20.
113. Yoo, K.H. and L. Hennighausen, *EZH2 methyltransferase and H3K27 methylation in breast cancer*. *Int J Biol Sci*, 2012. 8(1): p. 59-65.
114. Zeidler, M., et al., *The Polycomb group protein EZH2 impairs DNA repair in breast epithelial cells*. *Neoplasia*, 2005. 7(11): p. 1011-9.
115. Berens, M.E. and A. Giese, *"...those left behind." Biology and oncology of invasive glioma cells*. *Neoplasia*, 1999. 1(3): p. 208-19.

116. Kaur, E., et al., *Radiation-induced homotypic cell fusions of innately resistant glioblastoma cells mediate their sustained survival and recurrence*. *Carcinogenesis*, 2015. 36(6): p. 685-95.
117. Giannini, C., et al., *Patient tumor EGFR and PDGFRA gene amplifications retained in an invasive intracranial xenograft model of glioblastoma multiforme*. *Neuro Oncol*, 2005. 7(2): p. 164-76.
118. Mathieu, V., et al., *Combining bevacizumab with temozolomide increases the antitumor efficacy of temozolomide in a human glioblastoma orthotopic xenograft model*. *Neoplasia*, 2008. 10(12): p. 1383-92.
119. Nanni, S., et al., *Epithelial-restricted gene profile of primary cultures from human prostate tumors: a molecular approach to predict clinical behavior of prostate cancer*. *Mol Cancer Res*, 2006. 4(2): p. 79-92.
120. Dahlberg, W.K., et al., *Radiosensitivity in vitro of human soft tissue sarcoma cell lines and skin fibroblasts derived from the same patients*. *Int J Radiat Biol*, 1993. 63(2): p. 191-8.
121. Laks, D.R., et al., *Neurosphere formation is an independent predictor of clinical outcome in malignant glioma*. *Stem Cells*, 2009. 27(4): p. 980-7.
122. Crystal, A.S., et al., *Patient-derived models of acquired resistance can identify effective drug combinations for cancer*. *Science*, 2014. 346(6216): p. 1480-6.
123. Douglas-Jones, A.G. and W.T. Barr, *Breast carcinoma with tumor giant cells. Report of a case with fine needle aspiration cytology*. *Acta Cytol*, 1989. 33(1): p. 109-14.
124. Jones, M.A., R.H. Young, and R.E. Scully, *Endometrial adenocarcinoma with a component of giant cell carcinoma*. *Int J Gynecol Pathol*, 1991. 10(3): p. 260-70.
125. Kawano, H., et al., *Immunohistochemical study of giant cell in glioblastoma*. *Clin Neuropathol*, 1995. 14(2): p. 118-23.
126. Parwani, A.V., M. Herawi, and J.I. Epstein, *Pleomorphic giant cell adenocarcinoma of the prostate: report of 6 cases*. *Am J Surg Pathol*, 2006. 30(10): p. 1254-9.
127. Moore, J.G. and T. Bocklage, *Fine-needle aspiration biopsy of large-cell undifferentiated carcinoma of the salivary glands: presentation of two cases, literature review, and differential cytodiagnosis of high-grade salivary gland malignancies*. *Diagn Cytopathol*, 1998. 19(1): p. 44-50.
128. Sneige, N., et al., *Chemotherapy-induced histologic changes in mastectomy specimens and their potential significance*. *Breast*, 2001. 10(6): p. 492-500.
129. Ariizumi, T., et al., *Multinucleation followed by an acytokinetic cell division in myxofibrosarcoma with giant cell proliferation*. *J Exp Clin Cancer Res*, 2009. 28: p. 44.
130. Weihua, Z., et al., *Formation of solid tumors by a single multinucleated cancer cell*. *Cancer*, 2011. 117(17): p. 4092-9.
131. Geigl, J.B., et al., *Defining 'chromosomal instability'*. *Trends Genet*, 2008. 24(2): p. 64-9.
132. Holland, A.J. and D.W. Cleveland, *Boveri revisited: chromosomal instability, aneuploidy and tumorigenesis*. *Nat Rev Mol Cell Biol*, 2009. 10(7): p. 478-87.
133. Krajcovic, M. and M. Overholtzer, *Mechanisms of ploidy increase in human cancers: a new role for cell cannibalism*. *Cancer Res*, 2012. 72(7): p. 1596-601.
134. Brodbeck, W.G. and J.M. Anderson, *Giant cell formation and function*. *Curr Opin Hematol*, 2009. 16(1): p. 53-7.
135. Duelli, D.M., et al., *A primate virus generates transformed human cells by fusion*. *J Cell Biol*, 2005. 171(3): p. 493-503.
136. Hosaka, M., et al., *Giant cell formation through fusion of cells derived from a human giant cell tumor of tendon sheath*. *J Orthop Sci*, 2004. 9(6): p. 581-4.
137. Nishimura, M., et al., *Cytological properties of stromal cells derived from giant cell tumor of bone (GCTSC) which can induce osteoclast formation of human blood monocytes without cell to cell contact*. *J Orthop Res*, 2005. 23(5): p. 979-87.

138. Eom, Y.W., et al., *Two distinct modes of cell death induced by doxorubicin: apoptosis and cell death through mitotic catastrophe accompanied by senescence-like phenotype*. *Oncogene*, 2005. 24(30): p. 4765-77.
139. Erenpreisa, J., M. Kalejs, and M.S. Cragg, *Mitotic catastrophe and endomitosis in tumour cells: an evolutionary key to a molecular solution*. *Cell Biol Int*, 2005. 29(12): p. 1012-8.
140. Erenpreisa, J., et al., *Segregation of genomes in polyploid tumour cells following mitotic catastrophe*. *Cell Biol Int*, 2005. 29(12): p. 1005-11.
141. Zhang, S., et al., *Generation of cancer stem-like cells through the formation of polyploid giant cancer cells*. *Oncogene*, 2013.
142. Barok, M., et al., *Trastuzumab-DM1 causes tumour growth inhibition by mitotic catastrophe in trastuzumab-resistant breast cancer cells in vivo*. *Breast Cancer Res*, 2011. 13(2): p. R46.
143. Malpica, A., et al., *Grading ovarian serous carcinoma using a two-tier system*. *Am J Surg Pathol*, 2004. 28(4): p. 496-504.
144. Kumar V, A.A., Fausto N, Aster JC, *Robbins and Cotran Pathologic Basis of Disease 8th edn Chapter 7: Neoplasia ed. 2010, 8th edn, Chapter 7:Neoplasia: Elsevier: New York, USA*
145. Coppe, J.P., et al., *The senescence-associated secretory phenotype: the dark side of tumor suppression*. *Annu Rev Pathol*, 2010. 5: p. 99-118.
146. Young, A.R. and M. Narita, *SASP reflects senescence*. *EMBO Rep*, 2009. 10(3): p. 228-30.
147. Shay, J.W. and I.B. Roninson, *Hallmarks of senescence in carcinogenesis and cancer therapy*. *Oncogene*, 2004. 23(16): p. 2919-33.
148. Fumagalli, M. and F. d'Adda di Fagagna, *SASPense and DDRama in cancer and ageing*. *Nat Cell Biol*, 2009. 11(8): p. 921-3.
149. Tribius, S., A. Pidel, and D. Casper, *ATM protein expression correlates with radioresistance in primary glioblastoma cells in culture*. *Int J Radiat Oncol Biol Phys*, 2001. 50(2): p. 511-23.
150. Iliadis, G., et al., *Volumetric and MGMT parameters in glioblastoma patients: survival analysis*. *BMC Cancer*, 2012. 12: p. 3.
151. Ganem, N.J., Z. Storchova, and D. Pellman, *Tetraploidy, aneuploidy and cancer*. *Curr Opin Genet Dev*, 2007. 17(2): p. 157-62.
152. Larkins, B.A., et al., *Investigating the hows and whys of DNA endoreduplication*. *J Exp Bot*, 2001. 52(355): p. 183-92.
153. Gal, H. and V. Krizhanovskiy, *Cell fusion induced senescence*. *Aging (Albany NY)*, 2014. 6(5): p. 353-4.
154. Zhou, X., et al., *Cell Fusion Connects Oncogenesis with Tumor Evolution*. *Am J Pathol*, 2015. 185(7): p. 2049-60.
155. Bastida-Ruiz, D., K. Van Hoesen, and M. Cohen, *The Dark Side of Cell Fusion*. *Int J Mol Sci*, 2016. 17(5).
156. Robinson, J.P., et al., *Akt signaling is required for glioblastoma maintenance in vivo*. *Am J Cancer Res*, 2011. 1(2): p. 155-167.
157. Qian, J., et al., *Synergy between phosphatidylinositol 3-kinase/Akt pathway and Bcl-xL in the control of apoptosis in adenocarcinoma cells of the lung*. *Mol Cancer Ther*, 2009. 8(1): p. 101-9.
158. Sherr, C.J. and J.M. Roberts, *CDK inhibitors: positive and negative regulators of G1-phase progression*. *Genes Dev*, 1999. 13(12): p. 1501-12.
159. Charrier-Savournin, F.B., et al., *p21-Mediated nuclear retention of cyclin B1-Cdk1 in response to genotoxic stress*. *Mol Biol Cell*, 2004. 15(9): p. 3965-76.
160. Romanov, V.S., et al., *p21(Waf1) is required for cellular senescence but not for cell cycle arrest induced by the HDAC inhibitor sodium butyrate*. *Cell Cycle*, 2010. 9(19): p. 3945-55.
161. Wang, Q., et al., *Survivin and escaping in therapy-induced cellular senescence*. *Int J Cancer*, 2011. 128(7): p. 1546-58.

162. Hirai, H., et al., *MK-1775, a small molecule Wee1 inhibitor, enhances anti-tumor efficacy of various DNA-damaging agents, including 5-fluorouracil*. *Cancer Biol Ther*, 2010. 9(7): p. 514-22.
163. Bompard, G., G. Rabeharivelo, and N. Morin, *Inhibition of cytokinesis by wiskostatin does not rely on N-WASP/Arp2/3 complex pathway*. *BMC Cell Biol*, 2008. 9: p. 42.
164. Fujiwara, T., et al., *Cytokinesis failure generating tetraploids promotes tumorigenesis in p53-null cells*. *Nature*, 2005. 437(7061): p. 1043-7.
165. He, X., et al., *Cell fusion between gastric epithelial cells and mesenchymal stem cells results in epithelial-to-mesenchymal transition and malignant transformation*. *BMC Cancer*, 2015. 15: p. 24.
166. Chuprin, A., et al., *Cell fusion induced by ERVWE1 or measles virus causes cellular senescence*. *Genes Dev*, 2013. 27(21): p. 2356-66.
167. Rodier, F. and J. Campisi, *Four faces of cellular senescence*. *J Cell Biol*, 2011. 192(4): p. 547-56.
168. Sausville, E.A., et al., *Phase I trial of 72-hour continuous infusion UCN-01 in patients with refractory neoplasms*. *J Clin Oncol*, 2001. 19(8): p. 2319-33.
169. Inda, M.M., R. Bonavia, and J. Seoane, *Glioblastoma multiforme: a look inside its heterogeneous nature*. *Cancers (Basel)*, 2014. 6(1): p. 226-39.
170. Sun, S., et al., *Protein alterations associated with temozolomide resistance in subclones of human glioblastoma cell lines*. *J Neurooncol*, 2012. 107(1): p. 89-100.
171. Hirschmann-Jax, C., et al., *A distinct "side population" of cells with high drug efflux capacity in human tumor cells*. *Proc Natl Acad Sci U S A*, 2004. 101(39): p. 14228-33.
172. Zeppernick, F., et al., *Stem Cell Marker CD133 Affects Clinical Outcome in Glioma Patients*. *Clinical Cancer Research*, 2008. 14(1): p. 123-129.
173. Ryzhikova, E., et al., *Raman spectroscopy of blood serum for Alzheimer's disease diagnostics: specificity relative to other types of dementia*. *J Biophotonics*, 2014. 9999(9999).
174. Ellis, D.I., et al., *Illuminating disease and enlightening biomedicine: Raman spectroscopy as a diagnostic tool*. *Analyst*, 2013. 138(14): p. 3871-84.
175. Sahu, A., et al., *Serum based diagnosis of asthma using Raman spectroscopy: an early phase pilot study*. *PLoS One*, 2013. 8(11): p. e78921.
176. Chang, V.T., et al., *Quantitative physiology of the precancerous cervix in vivo through optical spectroscopy*. *Neoplasia*, 2009. 11(4): p. 325-32.
177. Yamazaki, H., et al., *The diagnosis of lung cancer using 1064-nm excited near-infrared multichannel Raman spectroscopy*. *Radiat Med*, 2003. 21(1): p. 1-6.
178. Li, S., et al., *Identification and characterization of colorectal cancer using Raman spectroscopy and feature selection techniques*. *Opt Express*, 2014. 22(21): p. 25895-908.
179. Singh, S.P., et al., *In vivo Raman spectroscopic identification of premalignant lesions in oral buccal mucosa*. *J Biomed Opt*, 2012. 17(10): p. 105002.
180. Zhou, Y., et al., *Human brain cancer studied by resonance Raman spectroscopy*. *J Biomed Opt*, 2012. 17(11): p. 116021.
181. Evers, D., et al., *Optical spectroscopy: current advances and future applications in cancer diagnostics and therapy*. *Future Oncol*, 2012. 8(3): p. 307-20.
182. Mizuno, A., et al., *Near-infrared FT-Raman spectra of the rat brain tissues*. *Neurosci Lett*, 1992. 141(1): p. 47-52.
183. Mizuno, A., et al., *Near-infrared Fourier transform Raman spectroscopic study of human brain tissues and tumours*. *Journal of Raman Spectroscopy*, 1994. 25(1).
184. Beljebbar, A., et al., *Ex vivo and in vivo diagnosis of C6 glioblastoma development by Raman spectroscopy coupled to a microprobe*. *Anal Bioanal Chem*, 2010. 398(1): p. 477-87.
185. Koljenovic, S., et al., *Discriminating vital tumor from necrotic tissue in human glioblastoma tissue samples by Raman spectroscopy*. *Lab Invest*, 2002. 82(10): p. 1265-77.

186. Ji, M., et al., *Rapid, label-free detection of brain tumors with stimulated Raman scattering microscopy*. *Sci Transl Med*, 2013. 5(201): p. 201ra119.
187. Jermyn, M., et al., *Intraoperative brain cancer detection with Raman spectroscopy in humans*. *Sci Transl Med*, 2015. 7(274): p. 274ra19.
188. Harder, S.J., et al., *A Raman spectroscopic study of cell response to clinical doses of ionizing radiation*. *Appl Spectrosc*, 2015. 69(2): p. 193-204.
189. Devpura, S., et al., *Vision 20/20: the role of Raman spectroscopy in early stage cancer detection and feasibility for application in radiation therapy response assessment*. *Med Phys*, 2014. 41(5): p. 050901.
190. Vidyasagar, M.S., et al., *Prediction of radiotherapy response in cervix cancer by Raman spectroscopy: a pilot study*. *Biopolymers*, 2008. 89(6): p. 530-7.
191. Shaikh, R., M.S. Vidyasagar, and C.M. Krishna, *Raman Spectroscopy of Tissues Collected at Different Fractions of Radiation Therapy: Response Assessment to Radiotherapy in Cervix Cancers* *Journal of Innovative Optical Health Sciences* 2013. 06(02): p. 8.
192. Yasser, M., et al., *Raman spectroscopic study of radioresistant oral cancer sublines established by fractionated ionizing radiation*. *PLoS One*, 2014. 9(5): p. e97777.
193. Sahu, A., et al., *Recurrence prediction in oral cancers: a serum Raman spectroscopy study*. *Analyst*, 2015. 140(7): p. 2294-301.
194. Trapnell, C., et al., *Differential gene and transcript expression analysis of RNA-seq experiments with TopHat and Cufflinks*. *Nat Protoc*, 2012. 7(3): p. 562-78.
195. Crow, P., et al., *The use of Raman spectroscopy to differentiate between different prostatic adenocarcinoma cell lines*. *Br J Cancer*, 2005. 92(12): p. 2166-70.
196. Ghanate, A.D., et al., *Comparative evaluation of spectroscopic models using different multivariate statistical tools in a multicancer scenario*. *J Biomed Opt*, 2011. 16(2): p. 025003.
197. Parker, F.S., *Applications of infrared, Raman, and resonance Raman spectroscopy in biochemistry*. 1983: Springer Science & Business Media.
198. Movasaghi, Z., S. Rehman, and I.U. Rehman, *Raman Spectroscopy of Biological Tissues*. *Applied Spectroscopy Reviews*, 2007. 42(5): p. 493-541.
199. Schröder, R., K. Feisel, and R.-I. Ernestus, *Ki-67 Labeling is Correlated with the Time to Recurrence in Primary Glioblastomas*. *Journal of Neuro-Oncology*, 2002. 56(2): p. 127-132.
200. Xie, D., et al., *Expression of cytoplasmic and nuclear Survivin in primary and secondary human glioblastoma*. *Br J Cancer*, 2006. 94(1): p. 108-14.
201. Chakravarti, A., et al., *Quantitatively determined survivin expression levels are of prognostic value in human gliomas*. *J Clin Oncol*, 2002. 20(4): p. 1063-8.
202. Stone, N., et al., *Raman spectroscopy for identification of epithelial cancers*. *Faraday Discussions*, 2004. 126(0): p. 141-157.
203. Stone, N., et al., *Near-infrared Raman spectroscopy for the classification of epithelial pre-cancers and cancers*. *Journal of Raman Spectroscopy*, 2002. 33(7): p. 564-573.
204. Kalkanis, S.N., et al., *Raman spectroscopy to distinguish grey matter, necrosis, and glioblastoma multiforme in frozen tissue sections*. *Journal of Neuro-Oncology*, 2014. 116(3): p. 477-485.
205. Kunjachan, S., et al., *Multidrug resistance: Physiological principles and nanomedical solutions*. *Adv Drug Deliv Rev*, 2013. 65(13-14): p. 1852-65.
206. Gelsomino, G., et al., *Omega 3 fatty acids chemosensitize multidrug resistant colon cancer cells by down-regulating cholesterol synthesis and altering detergent resistant membranes composition*. *Mol Cancer*, 2013. 12: p. 137.
207. Todor, I.N., N.Y. Lukyanova, and V.F. Chekhun, *The lipid content of cisplatin- and doxorubicin-resistant MCF-7 human breast cancer cells*. *Exp Oncol*, 2012. 34(2): p. 97-100.
208. Liu, Y.Y., et al., *A role for ceramide in driving cancer cell resistance to doxorubicin*. *FASEB J*, 2008. 22(7): p. 2541-51.

209. Liu, Y.Y., R.A. Hill, and Y.T. Li, *Ceramide glycosylation catalyzed by glucosylceramide synthase and cancer drug resistance*. *Adv Cancer Res*, 2013. 117: p. 59-89.
210. Walid, M.S., *Prognostic factors for long-term survival after glioblastoma*. *Perm J*, 2008. 12(4): p. 45-8.
211. Sahu, A., et al., *Raman spectroscopy and cytopathology of oral exfoliated cells for oral cancer diagnosis*. *Analytical Methods*, 2015. 7(18): p. 7548-7559.
212. Rubina S., et al., *Raman spectroscopic study on classification of cervical cell specimens*. *Vibrational Spectroscopy*, 2013. 68: p. 115-121.
213. Krishna M.C., et al., *Micro-Raman spectroscopy of mixed cancer cell populations*. *Vibrational Spectroscopy*, 2005. 38(1-2): p. 95-100.
214. Murali Krishna, C., et al., *Characterisation of uterine sarcoma cell lines exhibiting MDR phenotype by vibrational spectroscopy*. *Biochim Biophys Acta*, 2005. 1726(2): p. 160-7.
215. Chapman, J.R., M.R. Taylor, and S.J. Boulton, *Playing the end game: DNA double-strand break repair pathway choice*. *Mol Cell*, 2012. 47(4): p. 497-510.
216. Mehta, A. and J.E. Haber, *Sources of DNA double-strand breaks and models of recombinational DNA repair*. *Cold Spring Harb Perspect Biol*, 2014. 6(9): p. a016428.
217. Cornforth, M.N., *Radiation-Induced Damage and the Formation of Chromosomal Aberrations*, in *DNA Damage and Repair: Volume 2: DNA Repair in Higher Eukaryotes*, J.A. Nickoloff and M.F. Hoekstra, Editors. 1998, Humana Press: Totowa, NJ. p. 559-585.
218. Jackson, S.P. and J. Bartek, *The DNA-damage response in human biology and disease*. *Nature*, 2009. 461(7267): p. 1071-8.
219. McKinnon, P.J., *DNA repair deficiency and neurological disease*. *Nat Rev Neurosci*, 2009. 10(2): p. 100-12.
220. San Filippo, J., P. Sung, and H. Klein, *Mechanism of eukaryotic homologous recombination*. *Annu Rev Biochem*, 2008. 77: p. 229-57.
221. Rogakou, E.P., et al., *DNA double-stranded breaks induce histone H2AX phosphorylation on serine 139*. *J Biol Chem*, 1998. 273(10): p. 5858-68.
222. Lukas, J., C. Lukas, and J. Bartek, *More than just a focus: The chromatin response to DNA damage and its role in genome integrity maintenance*. *Nat Cell Biol*, 2011. 13(10): p. 1161-9.
223. Burma, S., et al., *ATM phosphorylates histone H2AX in response to DNA double-strand breaks*. *J Biol Chem*, 2001. 276(45): p. 42462-7.
224. Stiff, T., et al., *ATM and DNA-PK function redundantly to phosphorylate H2AX after exposure to ionizing radiation*. *Cancer Res*, 2004. 64(7): p. 2390-6.
225. Ward, I.M. and J. Chen, *Histone H2AX is phosphorylated in an ATR-dependent manner in response to replicational stress*. *J Biol Chem*, 2001. 276(51): p. 47759-62.
226. Harper, J.W. and S.J. Elledge, *The DNA damage response: ten years after*. *Mol Cell*, 2007. 28(5): p. 739-45.
227. Meek, K., V. Dang, and S.P. Lees-Miller, *DNA-PK: the means to justify the ends?* *Adv Immunol*, 2008. 99: p. 33-58.
228. Cimprich, K.A. and D. Cortez, *ATR: an essential regulator of genome integrity*. *Nat Rev Mol Cell Biol*, 2008. 9(8): p. 616-27.
229. Ward, I.M., et al., *Accumulation of checkpoint protein 53BP1 at DNA breaks involves its binding to phosphorylated histone H2AX*. *J Biol Chem*, 2003. 278(22): p. 19579-82.
230. Celeste, A., et al., *Histone H2AX phosphorylation is dispensable for the initial recognition of DNA breaks*. *Nat Cell Biol*, 2003. 5(7): p. 675-9.
231. Paull, T.T., et al., *A critical role for histone H2AX in recruitment of repair factors to nuclear foci after DNA damage*. *Curr Biol*, 2000. 10(15): p. 886-95.
232. Ahn, J.Y., et al., *Threonine 68 phosphorylation by ataxia telangiectasia mutated is required for efficient activation of Chk2 in response to ionizing radiation*. *Cancer Res*, 2000. 60(21): p. 5934-6.

233. Smith, J., et al., *The ATM-Chk2 and ATR-Chk1 pathways in DNA damage signaling and cancer*. Adv Cancer Res, 2010. 108: p. 73-112.
234. Bensimon, A., R. Aebbersold, and Y. Shiloh, *Beyond ATM: the protein kinase landscape of the DNA damage response*. FEBS Lett, 2011. 585(11): p. 1625-39.
235. Hartley, K.O., et al., *DNA-dependent protein kinase catalytic subunit: a relative of phosphatidylinositol 3-kinase and the ataxia telangiectasia gene product*. Cell, 1995. 82(5): p. 849-56.
236. Gottlieb, T.M. and S.P. Jackson, *The DNA-dependent protein kinase: requirement for DNA ends and association with Ku antigen*. Cell, 1993. 72(1): p. 131-42.
237. Hunt, C.R., et al., *Histone modifications and DNA double-strand break repair after exposure to ionizing radiations*. Radiat Res, 2013. 179(4): p. 383-92.
238. Huyen, Y., et al., *Methylated lysine 79 of histone H3 targets 53BP1 to DNA double-strand breaks*. Nature, 2004. 432(7015): p. 406-11.
239. Pei, H., et al., *MMSET regulates histone H4K20 methylation and 53BP1 accumulation at DNA damage sites*. Nature, 2011. 470(7332): p. 124-8.
240. Conrad, T. and A. Akhtar, *Dosage compensation in Drosophila melanogaster: epigenetic fine-tuning of chromosome-wide transcription*. Nat Rev Genet, 2011. 13(2): p. 123-34.
241. Feil, R. and M.F. Fraga, *Epigenetics and the environment: emerging patterns and implications*. Nat Rev Genet, 2011. 13(2): p. 97-109.
242. Nguyen, A.T. and Y. Zhang, *The diverse functions of Dot1 and H3K79 methylation*. Genes Dev, 2011. 25(13): p. 1345-58.
243. Ferrari, K.J., et al., *Polycomb-dependent H3K27me1 and H3K27me2 regulate active transcription and enhancer fidelity*. Mol Cell, 2014. 53(1): p. 49-62.
244. Nakayama, J., et al., *Role of histone H3 lysine 9 methylation in epigenetic control of heterochromatin assembly*. Science, 2001. 292(5514): p. 110-3.
245. Peng, J.C. and G.H. Karpen, *Heterochromatic genome stability requires regulators of histone H3 K9 methylation*. PLoS Genet, 2009. 5(3): p. e1000435.
246. Leroy, G., et al., *A quantitative atlas of histone modification signatures from human cancer cells*. Epigenetics Chromatin, 2013. 6(1): p. 20.
247. Livak, K.J. and T.D. Schmittgen, *Analysis of relative gene expression data using real-time quantitative PCR and the 2(-Delta Delta C(T)) Method*. Methods, 2001. 25(4): p. 402-8.
248. Wagner, E.J. and P.B. Carpenter, *Understanding the language of Lys36 methylation at histone H3*. Nat Rev Mol Cell Biol, 2012. 13(2): p. 115-26.
249. Zhang, X., H. Wen, and X. Shi, *Lysine methylation: beyond histones*. Acta Biochim Biophys Sin (Shanghai), 2012. 44(1): p. 14-27.
250. Fnu, S., et al., *Methylation of histone H3 lysine 36 enhances DNA repair by nonhomologous end-joining*. Proc Natl Acad Sci U S A, 2011. 108(2): p. 540-5.
251. Zaidi, N.H., L. Liu, and S.L. Gerson, *Quantitative immunohistochemical estimates of O6-alkylguanine-DNA alkyltransferase expression in normal and malignant human colon*. Clin Cancer Res, 1996. 2(3): p. 577-84.
252. Redmond, S.M., et al., *Assessment of P-glycoprotein, glutathione-based detoxifying enzymes and O6-alkylguanine-DNA alkyltransferase as potential indicators of constitutive drug resistance in human colorectal tumors*. Cancer Res, 1991. 51(8): p. 2092-7.
253. Moriwaki, S., et al., *O6-alkylguanine-DNA alkyltransferase activity in human malignant melanoma*. J Dermatol Sci, 1992. 4(1): p. 6-10.
254. Lee, S.M., et al., *Immunohistological examination of the inter- and intracellular distribution of O6-alkylguanine DNA-alkyltransferase in human liver and melanoma*. Br J Cancer, 1992. 66(2): p. 355-60.
255. Kokkinakis, D.M., et al., *Role of O6-methylguanine-DNA methyltransferase in the resistance of pancreatic tumors to DNA alkylating agents*. Cancer Res, 1997. 57(23): p. 5360-8.

256. Citron, M., et al., *O6-methylguanine-DNA methyltransferase in human normal and malignant lung tissues*. *Cancer Invest*, 1993. 11(3): p. 258-63.
257. Bobola, M.S., et al., *O6-Methylguanine-DNA methyltransferase in pediatric primary brain tumors: relation to patient and tumor characteristics*. *Clin Cancer Res*, 2001. 7(3): p. 613-9.
258. Kruhlak, M.J., et al., *Changes in chromatin structure and mobility in living cells at sites of DNA double-strand breaks*. *J Cell Biol*, 2006. 172(6): p. 823-34.
259. Murga, M., et al., *Global chromatin compaction limits the strength of the DNA damage response*. *J Cell Biol*, 2007. 178(7): p. 1101-8.
260. Kuo, A.J., et al., *NSD2 links dimethylation of histone H3 at lysine 36 to oncogenic programming*. *Mol Cell*, 2011. 44(4): p. 609-20.
261. Saloura, V., et al., *WHSC1 promotes oncogenesis through regulation of NIMA-related kinase-7 in squamous cell carcinoma of the head and neck*. *Mol Cancer Res*, 2015. 13(2): p. 293-304.
262. Wray, J., et al., *Metnase mediates chromosome decatenation in acute leukemia cells*. *Blood*, 2009. 114(9): p. 1852-8.
263. Wray, J., et al., *Metnase mediates resistance to topoisomerase II inhibitors in breast cancer cells*. *PLoS One*, 2009. 4(4): p. e5323.
264. Williamson, E.A., et al., *Targeting the transposase domain of the DNA repair component Metnase to enhance chemotherapy*. *Cancer Res*, 2012. 72(23): p. 6200-8.
265. Pina, B. and P. Suau, *Changes in histones H2A and H3 variant composition in differentiating and mature rat brain cortical neurons*. *Dev Biol*, 1987. 123(1): p. 51-8.
266. Garcia, B.A., J. Shabanowitz, and D.F. Hunt, *Characterization of histones and their post-translational modifications by mass spectrometry*. *Curr Opin Chem Biol*, 2007. 11(1): p. 66-73.

*Appendix*

**Appendix I**

<b>Gene name</b>	<b>Sequence</b>	
P21	Forward	GACACCACTGGAGGGTGACT
	Reverse	ACAGGTCCACATGGTCTTCC
BAX	Forward	GCTGGACATTGGACTTCCTC
	Reverse	CAGCCCATCTTCTTCCAGAT
GAPDH	Forward	ACCCACTCCTCCACCTTTGA
	Reverse	CTGTTGCTGTAGCCAAATTCGT
BIRC3	Forward	TATGTGGGTAACAGTGATGA
	Reverse	GAAACCACTTGGCATGTTGA
BIRC4	Forward	GCCCAGTGTTTCTTCTGCTTCA
	Reverse	GCACTTCTCCGCAGTTTCCTC
SURVIVIN	Forward	TCCACTGCCCACTGAGAAC
	Reverse	TGGCTCCCAGCCTTCCA
Bcl-xL	Forward	GATCCCCATGGCAGCAGTAAAGCAAG
	Reverse	CCCCATCCCGGAAGAGTTCATTC ACT
IL-8	Forward	CAGTTTTGCCAAGGAGTGCT
	Reverse	TTGGGGTGGAAAGGTTTGG A
SCF	Forward	TGGGATCTCGTCAACCTTCT
	Reverse	GCAGAATCAGACCGAAAAGC
GM-SCF	Forward	CATCACCGTGGTTGAGAGC
	Reverse	AATTGTAGTGTGCCACCTCTC
IL-6	Forward	AATGAAAAGGCCCCCAAGGTAGTTATCC
	Reverse	GTCGTTTCCGCAACAAGTCCTCTTC
NSD1	Forward	AAGGAAGCGAAAACGACA
	Reverse	CGGGATCGTGTTCTACAC
Dot1L	Forward	GATGCCTACAGATCCCCTCA
	Reverse	GGCGTCTTCTCCTTCTCCT
SETMAR	Forward	GAAAGGGCCCAATTCTTCTC
	Reverse	AGCATTTTCTGCATCCTGCT
Suv39H2	Forward	CGGTGAGAATGACTTCAGCA
	Reverse	CTCACAGGTGTGGCATTAC
EZH2	Forward	TTCATGCAACACCCAACACT
	Reverse	CTCCCTCCAAATGCTGGTAA
H3.3_SDM	Forward	CTACCGGCGGGGTGGC GAAGCCTC ATCGCT
	Reverse	AGCGATGAGGCTTCGCCACCCCGCCGGTAG
H3.3_PCR	Forward	ATGGCCC GAACCAAGCAGACTGCT
	Reverse	AGCCA ACTGGATGTCTTTGG
H3.3_qPCR	Forward	AGGAAAAGCGCTCCCTCTAC
Sh1SETMAR	Forward	CCGGTCTAGATATCGAATTCTCGACCTCGAGACAA ATGGCAGTATTCATCCACAATTTTTG
	Reverse	AATTCAAAAATTGTGGATGAATACTGCCATTTGTCT

		CGAGGTCGAGAATTCGATATCTG
Sh2SETMAR	Forward	CCGGTTCTACGGTCGTTTGACATTTCTCGAGAAATG TCGAACGACCGTAGAATTTTGTG
	Reverse	AATTCAAAAATTCTACGGTCGTTTCGACATTTCTCGA GAAATGTCGAACGACCGTAGAA
Scrambled shRNA	Forward	CCGGTAGTCTGTAGCTAGCTACTAAAGTTCTCTTAG TCTGTAGCTAGCTACTATTTTGTG
	Reverse	AATTCAAAAATAGTCTGTAGCTAGCTACTAAGAGA ACTTTAGTCTGTAGCTAGCTAGAA
H1	Forward	TTTCCCAGAACACATAGCGA
pBABE	Forward	CTTTATCCAGCCCTCAC
	Reverse	ACCCTAACTGACACACATTCC